Fall 2014

Alternative tile intake design for intensively managed agro-ecosystems

William Dirk Ettema
University of Iowa

ALTERNATIVE TILE INTAKE DESIGN FOR INTENSIVELY MANAGED AGRO-ECOSYSTEMS

by

William Dirk Ettema

A thesis submitted in partial fulfillment
of the requirements for the Master of
Science degree in Civil and Environmental Engineering (Hydraulics)
in the Graduate College of
The University of Iowa

December 2014

Thesis Supervisors: Professor Athanasios N. Papanicolaou
Assistant Research Professor Christopher G. Wilson

Graduate College
The University of Iowa
Iowa City, Iowa

CERTIFICATE OF APPROVAL

MASTER'S THESIS

This is to certify that the Master's thesis of

William Dirk Ettema

has been approved by the Examining Committee
for the thesis requirement for the Master of Science
degree in Civil and Environmental Engineering (Hydraulics) at the
December 2014 graduation.

Thesis Committee:

Athanasios N. Papanicolaou, Thesis Supervisor

Christopher G. Wilson, Co-Advisor

Marian Muste

Jerald L. Schnoor

To my grandparents Joan and Trevor McIntosh,
my oma and opa Tine and Wiebe (Vic) Ettema,
and all of my family in New Zealand.

It is not the mountain we conquer, but ourselves.

Edmund Hillary

ACKNOWLEDGMENTS

I would like to express my thanks and appreciation to my advisors Dr. Thanos Papanicolaou and Dr. Christopher Wilson for challenging and guiding me in this research.

Thanks to my committee members, Dr. Marian Muste and Dr. Jerald Schnoor for their helpful comments and suggestions.

So many thanks go to my father Dr. Robert Ettema, my mother Susan Ettema, my brothers Alexander and Edward, my sister Jennifer, and of course Taryn Tigges for all of their love and support.

ABSTRACT

The overarching objective of this study is to assess the effectiveness and performance of ATIs. In doing so, this research provides a fundamental understanding of the flow and sediment propagation through a different combination of porous media (pea gravel and woodchips). The research hypothesizes that the theory of advection and diffusion describes the migration of flow and identifies a myriad of depositional networks of sediment. A key hypothesis of the study is that global and local pressure differentiation affects the flow pathways and distribution with intimate effects of sediment trapping efficiency and distribution within the permeameter. A significant goal of this study is to decompose the key mechanisms that affect this migration of sediment under a fixed value for the head and incoming concentration. The nature of the study is experimental and is supported by limited numerical and field analysis. Although the experimental setup is site specific to the conditions encountered in the study location, it offers a generic way of examining flow and sediment intrusion within a permeable bed. The study in that sense hypothesizes that the intrusion by Einstein is valid and it shows the change in the hydraulic gradient that occurs during an event and during a sequence of events. A secondary goal of this research is to understand the cyclicity in the migration of sediment in a sequence of different events, where the initial conditions of each run constitutes the outcome of the final result of the previous runs. The nature of those experiments is to mimic the occurrence of sequential events in nature, although the continuous examined in the laboratory as reflective of conditions representing extreme runs. This research also treats the hydraulic conductivity as a dynamic entity to reflect the effect of localized clogging on the propagation of flow. The experimental design of this research considers a series of experimental runs to address the aforementioned objectives of this research and test the posed hypothesis.

PUBLIC ABSTRACT

The overall goal of this study is to demonstrate the effectiveness of an alternative tile intake (ATI) at reducing runoff, and sediment loads produced by heavy rainfall in intensively managed agricultural fields within the Clear Creek watershed in Iowa. An ATI is a best management practice (BMP) consisting of a 3-foot pea gravel layer atop a 1-foot layer of wood chips.

Gravel intakes have been shown to be highly efficient at trapping sediment and sediment-bound particulates, like phosphorus, by enhancing settling through ponding and filtration, while the addition of the wood chips is to facilitate denitrification, similar to a bioreactor. Additionally, these intakes can help reduce the flow rate of runoff into the subsurface tile drain network relative to conventional intakes. The primary method focus of this study was to model the intake design with a physical model in a laboratory to quantify the saturated hydraulic conductivity and filter efficiency of different combinations of pea gravel and wood chips. However, this study also conducted a study of prototype ATIs installed at a field site in the Clear Creek watershed. Due to drought conditions, only limited observations and data were obtained from the field site.

Replacing much of the field study, the Water Erosion Prediction Project (WEPP), a watershed modeling software, was used to simulate the field conditions at the site for calculating runoff volumes and sediment loads to the intake for rainfall events of different magnitude. A three-part control volume was conceptualized, consisting of the contributing hillslope, the ATI, and the subsurface pipe below the ATI.

TABLE OF CONTENTS

LIST OF TABLES ix

LIST OF FIGURES x

LIST OF SYMBOLS xiv

CHAPTER 1. INTRODUCTION 1
1.1 Motivation 1
1.2 Objectives 2
1.3 Background 4
1.3.1 Soil Erosion and Nutrient Loss 4
1.3.2 Tile Drainage 6
1.4 ATI Performance Under Sediment Loading 7

CHAPTER 2. FIELD MONITORING AND NUMERICAL SIMULATIONS 11
2.1 A Three-part Control Volume Approach 11
2.2 Field Work 12
2.3 Numerical Watershed Modeling with WEPP 21
2.4 Depth of Ponding at the ATI 25
2.5 Suspended Sediment Concentration and Mass Loading Rate 31
2.6 Input to Laboratory Experiments. 33

CHAPTER 3. EXPERIMENTAL SETUP 35
3.1 Facilities and Instrumentation 35
3.1.1 Overview of Physical Model 35
3.2 Functioning of Experiment Setup 37
3.3 Data and Observation Acquisition 39
3.3.1 Experiment Procedure for the Constant Head Experiments 40
3.3.2 Experiment Procedure for the Sediment Trapping Experiments 43

CHAPTER 4. LABORATORY RESULTS 51
4.1 Introduction 51
4.2 Clear-water Flow Experiments 53
4.2.1 Constant Head Tests 53
4.2.2 Flow-Rate Tests 58
4.2.3 Reynolds Number and Friction Factor 61
4.3 Sediment-laden Flow Experiments 64
4.3.1 Head Box Water Level During Partial Clogging 65
4.3.2 Partial Clogging Effects Observed with the Piezometers 74
4.3.3 Hydraulic Gradient 79
4.3.4 Hydraulic Conductivity 81
4.3.5 Inflow-Outflow Hydrographs from Experimental Runs 85
4.3.6 Mechanisms of Clogging 86
4.3.7 Sediment Deposits by Layer 89

CHAPTER 5. CONCLUSIONS 124
5.1 Brief Summary 124
5.2 Conclusions 124

5.3 Recommendations for Future Research.....128
REFERENCES 130

LIST OF TABLES

Table 2-1. Input Parameters to WEPP. 22

Table 2-2. Sediment concentration statistics estimated from the 100-year continuous simulation using WEPP....24

Table 2-3. WEPP Watershed Model with Impoundment. 28

Table 2-4. Ranges of sediment concentration for verification of computations using WEPP results....33

Table 2-5. Experiments to test single and dual media combinations with sediment loading and runoff specific to the initial field site conditions simulated with WEPP. All values reflect amounts used in the physical model. 34

Table 4-1. Clear-water values of hydraulic conductivity, K, and the equivalent hydraulic conductivity in the vertical (z) direction, which accounts different strata. 56

Table 4-2. Summary of flow rates measured using the bucket method. 60

Table 4-3. Calculated superficial velocity, v_s, modified friction factor, f_k, and modified Reynolds number, Re_*. 62

Table 4-4. Variables for the experimental runs. Note: at the beginning of each run, $Q_{in} = Q_{out}$. 66

Table 4-5. The average rate of head increase in the head box. The sediment concentration used was approximately 17 g/L. 67

Table 4-6. The total pressure difference in each piezometer for each run. 76

Table 4-7. The average rate of pressure increase (cm of water per minute) determined for each piezometer during the runs. 77

Table 4-8. Average values of pressure difference between neighboring piezometers. 79

Table 4-9. Summary of results. 86

Table 4-10. Average rate of water level increase for each type of bucket lid orifice. 89

Table 4-11. The mass of sediment accumulated in the permeameter (kg) and the filter efficiency (%). 90

LIST OF FIGURES

Figure 1.1. Total phosphorus transported in the Mississippi river basin. Courtesy of USGS (2009). 5

Figure 1.2. Total nitrogen transported in the Mississippi river basin. Courtesy of USGS (2009)....6

Figure 1.3. Ponding around a conventional tile intake, namely the orange slotted pipe at the Clear Creek, IA demonstration site. 8

Figure 1.4. Much reduced ponding at an installed ATI at the same site (The orange stand pipe indicates the ATI position). 8

Figure 1.5. Vertical cross-section of an ATI....9

Figure 2.1. Three segment approach of analysis....12

Figure 2.2. Locations of the three ATIs and associated control intakes downslope of the ATIs. All intakes are installed within water and sediment control basins. Source: NRCS (2010). 13

Figure 2.3. Side-view of the layout between the ATI and Control intakes (not to scale). 15

Figure 2.4. The monitored ATI in the Clear Creek watershed and its contributing hillslope. Downslope is the location of the control. 16

Figure 2.5. Rainfall amounts measured with the tipping bucket on June 24, 2013. A total of 2 inches of rain fell in 15 hours. 17

Figure 2.6. Water depth as measured by pressure transducer in the sampling port. Peaks correspond to rainfall in Figure 2.3. Max depth of 4.5 cm; pipe diameter is 12.7 cm; about 35.4% of the depth, so not pressurized flow, but indicative of clogging. 17

Figure 2.7. (a) Rill flow downslope; (b) ponding at a control intake. 18

Figure 2.8. Recent photographs (February 2013) show one of the installed ATI prototypes has retained its structure and function; where (a) shows the entire ATI; and (b) shows the pea gravel surface un-affected by siltation. 19

Figure 2.9. (a) ATI surface (July 2013); (b) further silted and vegetated over ATI surface (October 2013). 20

Figure 2.10. Screen capture of the WEPP interface. (Source: USDA, 2010)....22

Figure 2.11. Histogram of results regarding values of sediment concentration estimated from continuous simulations using WEPP. 24

Figure 2.12. Hydraulic routing using (a) WEPP watershed (one hillslope) and impoundment; and (b) rock-fill check dam as the impoundment. 26

Figure 2.13. Inflow-outflow hydrograph for a simulated (a) 10-year event; and (b) 25-year event.....30

Figure 3.1. The (a) permeameter (clear acrylic tube) complete with eight pressure taps and manometer under hydrostatic pressure; and (b) with water flowing. 36

Figure 3.2. Experimental setup (not to scale) 39

Figure 3.3. Washing gravel through stainless steel mesh (No. 10 (4.75 mm) sieve size).....45

Figure 3.4. Concrete mixer (along with two heavy bricks) used to pulverize sediment from field site. 45

Figure 3.5. Macro-view of experimental setup.....46

Figure 3.6. SIGMA automated sampler and pressure transducer near outlet pipe 46

Figure 3.7. Wire basket used to retrieve pea gravel or woodchips from each layer.....47

Figure 3.8. One of the wire baskets buried in a layer of pea gravel 47

Figure 3.9. Method of retrieval: (a) plexiglass insert inside the headbox with hook, cable, and pulley to retrieve wire baskets; (b) pulling gravel into clear acrylic section. This photograph shows with "clean" pea gravel (without fine sediment deposited on it); (c) pulling with upward force, the natural heave of gravel locks it inside the clear acrylic section and allows it to be transferred into a collection bucket; (d) placing retrieved layer into bucket. When the clear acrylic section is lifted off, the gravel falls out into the collection bucket. 48

Figure 3.10. The sediment delivery mechanism. The orange parking cone serves as the sediment feeder, and the power drill with paint mixer attachment serves as the hopping mechanism. A bungee strap was used to support the shaft of the paint mixer. 49

Figure 3.11. Examples of pulling gravel layer into plexiglass insert after sediment test (a). A woodchip layer after sediment test (b). Top view of woodchip layer after sediment test (c).....50

Figure 4.1. Time-series of the hydraulic conductivity, K. (a) 100% pea gravel medium; (b) for 100% woodchip medium. (c) Layered combination of 50% pea gravel and 50% woodchips. (d) Layered combination of 75% pea gravel and 25% woodchips. (e) Mixed combination of 50% pea gravel and 50% woodchips. (f) Mixed combination of 75% pea gravel and 25% woodchips. 94

Figure 4.2. Time-series of measured and determined inflow and outflow rates. (a) Clear-water inflow rates (Test 1). (b) Clear-water inflow rates (Test 2). (c) Clear-water inflow rates (Test 3). (d) Clear-water outflow rates (Test 1). (e) Clear-water outflow rates (Test 2a). (f) Sediment-laden outflow rates (Test 2b). (g) Sediment-laden outflow rates (Test 3).....97

Figure 4.3. Graph of the Ergun equation. (a) With values computed for this study between black circles. (b) and (c) Magnified Ergun plot: values for clear-water (blue) and sediment runs (red). 100

Figure 4.4. Head box pressure (a) and an example of the estimated flow regime (b). ...102

Figure 4.5. Piezometer pressure, where the total head in the permeameter is H; piezometer P1 is at the top (15 cm below the surface) and is P8 at the bottom of the permeameter (120 cm below the surface). Piezometer pressure for Runs: (a) A1; (b) A2; (c) A3; (d) B1; and (e) B2. 103

Figure 4.6. Pressure difference between neighboring piezometers shown for Runs: (a) A1; (b) A2; (c) A3; (d) B1; and (e) B2....105

Figure 4.7. Time-series of hydraulic gradient for Runs: (a) A1; (b) A2; (c) A3; (d) A4; (e) B1; and (d) B2. 108

Figure 4.8. Time-series of hydraulic conductivity for Runs: (a) A1; (b) A2; (c) A3; (d) A4; (e) B1; and (f) B2. 111

Figure 4.9. Time-series of global hydraulic conductivity, K, showing consecutive runs....114

Figure 4.10. Stages of the relative hydraulic conductivity, K/K_0, for Run B2. 114

Figure 4.11. Example inflow-outflow hydrograph determined from Run B2. The blue line is the inflow rate, the red line is the outflow rate, the green line is the hydraulic conductivity, and the dashed, black line is the time at which the sediment inflow was cut-off. 115

Figure 4.12. Simulated clogging using bucket lids.....115

Figure 4.13. Potential pathways for wormholes illustrated by digitized slices of the top 25 mm of different types of media (Barton, 2004).....116

Figure 4.14. Filter cycle as proposed by Amirthararah and Ginn (1992). Attachment occurs at the same time as detachment. 116

Figure 4.15. Diffusion / dispersion. Simulated dispersion in a bead pack. Courtesy of The Victoria University of Wellington, 2011.....117

Figure 4.16. The three filtration mechanisms. Note the particle size dependence and difference in deposit morphology (McDowell-Boyer et al, 1986).....117

Figure 4.17. Mass of deposited sediment in the permeameter after all runs: 100% gravel shows most clogging occurring higher in the permeameter. Also the migration of a sediment front at two locations: from 0 to 30 cm and from 45 to 60 cm (a); 75% pea gravel / 25% woodchips shows a similar trend to the 100% gravel in (a) for the pea gravel section (b). 118

Figure 4.18. Visible intrusion of sediment from the surface at the end of Run A4. The maximum infiltration depth of fine sediments into a stable gravel bed has been reported to be between 10 and 30 cm (Beschta and Jackson, 1979; Diplas and Parker, 1984). 119

Figure 4.19. Observed bridging of sediment across grains of pea gravel in the permeameter.....120

Figure 4.20. Sediment deposited in the head box during an experiment. 120

Figure 4.21. Sediment being drawn into the top section of the permeameter due to a lack of hydrostatic pressure holding the sediment in place. Top: (a) seconds after the water has drained from the headbox; and bottom: (b) after several minutes, the rate of sediment intrusion slows to a sluggish pace. 121

Figure 4.22. Dried sediment at the surface of the permeameter. 122

Figure 4.23. Sediment "cloud" at interface between pea gravel and woodchips with different flow patterns in pea gravel and woodchips (a); and visibly higher amounts of sediment deposition in the woodchip layer (b). 122

Figure 4.24. Lifetime curve. On average, the ATI will last 75 events with high concentrations of suspended sediment in the runoff.....123

LIST OF SYMBOLS

A	Cross-sectional area of the intake
C	Suspended sediment concentration
C_0	Initial suspended sediment concentration
$\hat{C}$	Cropping-management factor normalized to a tilled area
D_{50}	Particle diameter for which 50% of bed material is finer
D_p	Particle diameter of suspended sediment
D_m	Particle diameter of porous medium
E	Erodibility
$\hat{E}$	Soil loss per unit area
f_k	Modified friction factor for flow through a porous medium
H	Total head
i	Hydraulic gradient
K	Hydraulic conductivity
K_0	Hydraulic conductivity of the clean porous medium
K/K_0	Relative hydraulic conductivity
K_{50}	Hydraulic conductivity of at 50% of run duration
K_{sat}	Saturated hydraulic conductivity of a porous medium
$\hat{K}$	Soil erodibility factor
L	Depth of the intake
L_i	Incremental depth of the intake
$\hat{L}$	Field length factor normalized to a specified plot length
$\dot{m}$	Sediment flux or mass rate
$\hat{P}$	conservation practice factor normalized to farming practice
Q	Volumetric discharge
$\hat{R}$	Rainfall erosivity factor
Re_*	Reynolds number modified for flow through a porous medium
S	Gradient of hillslope
$\hat{S}$	Field slope factor normalized to a specified gradient
v_s	Superficial velocity (macro velocity)

Greek symbols

ε	Porosity
γ	Specific weight of water
μ	Dynamic viscosity of water
ρ	Density of water
σ	Specific deposit
τ	Shear stress
τ_c	Critical shear stress

CHAPTER 1. INTRODUCTION

1.1 Motivation

It is estimated that nearly 90% of U.S. croplands are losing fertile soil, due to intensive land management practices, at a rate that is above the threshold for sustaining long-term productivity, and, as a result, Iowa has lost nearly one-half of its topsoil during the last 150 years of farming (e.g., Pimentel, 1995). Furthermore, this erosion depletes the organic-rich soil of valuable nutrients (e.g., Karlen et al. 2008). The nutrients are transported into rivers and streams by overland flow and through subsurface drainage systems. Once in the streams and rivers, the nutrients provide a food source for algae, which leads to eutrophication. To compensate for this loss, farmers must artificially pump "vitamins" back into the soils in the form of fertilizers, which has significant implications to water quality locally and at the national scale (e.g., Loperfido et al., 2010). This increased need for soil amendments has additional economic effects through increases in production costs, especially with the rising costs of inorganic fertilizers (Huang, 2009).

The study herein provides new insights into the design and performance of an improved method for limiting the removal of fertile topsoil and associated nutrients by runoff and erosion from the fields. This approach uses alternative tile intakes (ATIs), which consist of a vertical column of gravel augmented with a layer of woodchips. The gravel will help filter sediment and attached phosphorus from the runoff before passing to the drain tile, while an added benefit of the woodchip layer is to aid in denitrification of the applied inorganic fertilizers. Effective tile drainage is a practical means for controlling sediment and nutrient transport occurring with soil erosion. However, considerable investigation is required to determine the performance features of effective tile drainage systems, such as the ATI.

1.2 Objectives

The overall purpose of this study was to determine the effectiveness of ATIs in reducing sediment and nutrient loads produced by heavy rainfall in an intensively managed agricultural watershed. The primary innovative aspect of the present study concerns use of an added layer of wood chips placed in the gravel column of an ATI with desired action of improving the ability of the ATI to reduce dissolved nitrates loads by trapping sediment and relatedly acting to denitrify the sediment. There is precedent for the use of woodchips to denitrify water in applications concerning improvement of nutrient-laden water. ATIs are potentially an effective best-management practice for farm fields in this and other watersheds in the Midwest. This study involved as a test watershed the Clear Creek watershed in Iowa.

This study's specific objectives were threefold:

1. Obtain observations and quantitative data from a field study of a prototype ATI, located in the Clear Creek watershed.
2. Use numerical simulations, at the hillslope scale, to evaluate the influences of land management, soil type, topography, and climate on the flux of water and sediment generated by a hillslope of cropland.
3. Conduct laboratory experiments with a model ATI (1:1 scale by depth; 1:56 by cross-sectional area) to determine its drainage performance with both clear-water and sediment-laden flow; ascertain the main features of water flow and sediment transport through the ATI; and, evaluate the ATI's sediment trapping efficiency. The main research hypothesis associated with this objective is that the effectiveness of an ATI is controlled by sediment clogging of the ATI's porous structure.

Each of these objectives involved analytical assessment of ATI performance, as well as illustrations regarding aspects of ATI performance. The remaining section of this chapter

provides further background information about the magnitude of concerns about sediment and nutrient transport produced by erosion of cropland soil. Subsequently Chapter 2 describes the investigation methods this study used in addressing its three objectives. Chapter 3 explains the laboratory procedures used, and Chapter 4 presents and discusses their results. Chapter 5 reports the main conclusions drawn from this study, and outlines recommendations for further research.

The methodology of this work involved field work, numerical modeling, and experiments in the laboratory. A field campaign was conducted to determine the soil type, topography, land use, land management. Three prototype ATIs were installed at the field site, at the toe of three different hillslopes, within a sediment and flow detention basin situated between the hillslope and the berm of a terrace. Downslope of each of the installed prototype ATIs, are three conventional intakes, which are connected to the same tile pipe as their ATI counterparts. Drought over the two summers that the field work was conducted did not allow the effects of more than one rainfall event to be captured. As such, a numerical model was used to simulate rainfall events in order to compute the runoff depth and sediment yield from each event, which were used to determine (1) a ponded depth of water above the ATI by a hydraulic routing procedure; and (2) convert the sediment yield to a suspended sediment concentration. These two results from analytical computation of numerical results were then used as input to an experimental setup in the laboratory. The ponding depth was simulated in the head box and the suspended sediment concentration was simulated by applying sediment at a mass feed rate such that the sediment concentration could be achieved in a time-averaged sense.

1.3 Background

1.3.1 Soil Erosion and Nutrient Loss

Soil erosion starts as a soil particle detaches from its surrounding aggregate by rain drop impact. It is then entrained by runoff and delivered through sheet flow, or interrill erosion, into the rills. The runoff then transports the sediment and attached nutrients via the rills into water bodies like streams, rivers and lakes.

On agricultural hillslopes, land use and management practices have a profound influence on erosion rates (e.g., Abaci and Papanicolaou, 2009). For example, tillage breaks apart soil at the surface making it increasingly susceptible to runoff entrainment and soil erosion (Beare, 1994). The effects of tillage coupled with the removal of residue that exposures the surface soil particles to the rainfall and runoff energy enhances sediment erosion and nutrient loss (Dinnes, 2004). Additionally, soil compaction caused by tillage and wheel traffic increases runoff by increasing the bulk density and reducing the pore spaces of the soil to hold water. Alternatively, reduced or no-till soil management practices tend to decrease soil erosion by maintaining the soil structure and preserving the crop residue cover on the land surface, protecting it from rainfall impact, as well as allowing greater water infiltration.

The two major nutrients applied as fertilizer on farm fields are nitrogen and phosphorus. Although these amendments can help maintain soil quality, high concentrations in the streams and lakes below these fields can be considered as pollutants that degrade the water quality (MPCA, 2012). Excess amounts of nitrates and phosphates in the downstream waterbodies facilitate algal blooms that consume the dissolved oxygen and stresses (possibly fatally) the other aquatic life, such as macroinvertebrates and fish. Downstream effects of soil erosion and associated nutrient loss from agricultural fields are eutrophication and hypoxia (as seen most prominently near the mouth of the Mississippi River), as well as turbidity impairment of streams and rivers.

Figures 1.1 and 1.2 show the excess levels of phosphates and nitrates attributed to agricultural practices leaving sub-watersheds in the Mississippi River basin. Nutrients attached to sediments may account for up to 90% of the total amount transported in cropland runoff (Sharpley and Menzel, 1987; Fixen, 2001). However, dissolved nutrients, namely the nitrates, can lead to significant problems. Gulf hypoxia, eutrophication, harmful algal blooms, and the impairment of aquatic life are some of the water quality related problems caused by the runoff of dissolved nutrients. The most heavily tile-drained areas in the Midwest are large contributors of nitrate to Gulf of Mexico (Dinnes, 2004).

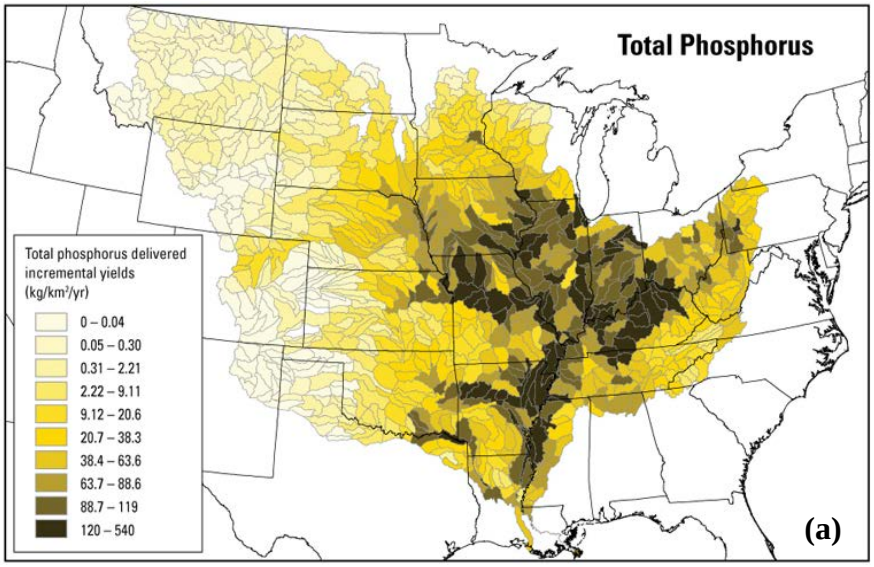

Figure 1.1. Total phosphorus transported in the Mississippi river basin. Courtesy of USGS (2009).

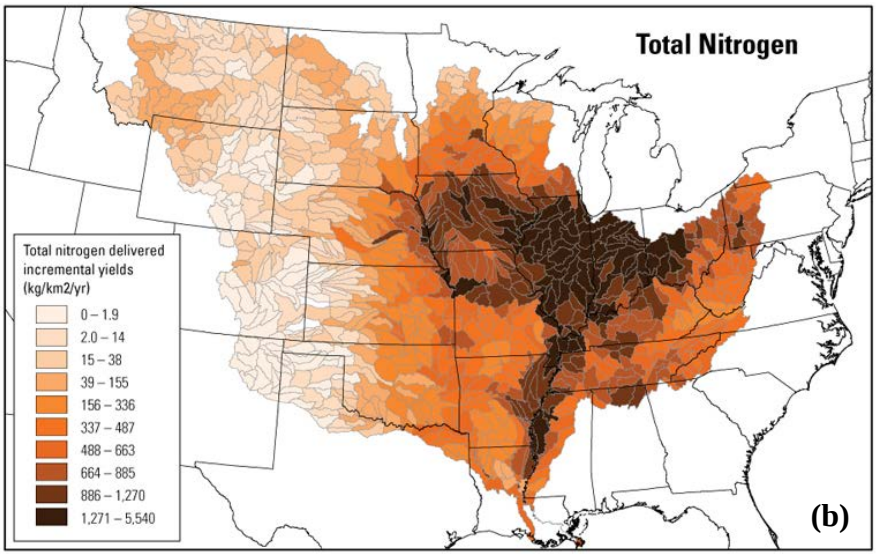

Figure 1.2. Total nitrogen transported in the Mississippi river basin. Courtesy of USGS (2009).

1.3.2 Tile Drainage

The Midwestern U.S. has implemented various forms of agricultural tile drainage for over 100 years. Agricultural tile drainage is indeed today an integral part of Iowa's landscape, with nearly 30% of Iowa's cropland being drained (Schilling & Helmers, 2008). Tile drainage allows for efficient crop production in Iowa's nutrient rich yet poorly drained soils by removing excess water from frequently inundated fields through subsurface pipe networks. However, the installation of these pipes into the subsurface has altered the hydrologic and ecological regime. For example, tile drainage is reported to increase the base-flow of streams and contribute high loads of suspended sediment associated with runoff from heavy rainfall. Recent research has focused on minimizing the impact that tile discharge has had on water quality in Iowa's streams and ultimately in the Mississippi River.

Surface tile intakes are widely used in the Midwestern U.S. to remove water quickly from surface depressions, and usually consist of orange slotted pipes (**Figure 1.3**)

extending up from the ground. These intakes are needed to pass water from the surface to the sub-surface, thereby allowing for the timely planting of crops or preventing excessive crop damage from drowning after heavy rainstorms. These slotted pipes facilitate the settling of sediment and attached nutrients before they flow down to the drain tile. Wilson et al. (1999) reported the range of effectiveness for this slotted intake as being up to 66% for sediment. Although somewhat efficient at keeping sediment on the field, these intakes have little ability to trap the finer sediment, which has the highest concentrations of sorbed nutrients and containments, or any dissolved nutrients.

Alternative intake designs are needed to reduce the discharge of fine eroded sediments and nutrients, as well as to mitigate downstream water quality issues, while maintaining profitable crop production. Alternative designs, such as gravel-fill intakes or ATIs, are possible solutions. The primary mechanism of sediment trapping in these intakes is by enhancing settling through ponding that develops around the intake. The secondary mechanism is the filtration of sediment by the porous media. Gravel intakes have a higher efficiency for trapping sediment and sediment-bound particulates and have been shown to efficiently trap between 80 – 98% of the sediment delivered to them (Wilson et al., 1999), as well as sediment-bound constituents, like phosphorus, which is an improvement over the 66% observed by Wilson et al. (1999) for just orange slotted pipes. Currently, there is very little information in the engineering literature on the flow and sediment dynamics within gravel intakes used in agricultural systems, with almost no information for the ATI design presented in this study.

1.4 ATI Performance Under Sediment Loading

Figure 1.2 is a common scene in farm fields where runoff and sediment (with attached nutrients) are ponded around a conventional tile drain. **Figure 1.3** shows an ATI draining water from the land surface under similar conditions as the conventional drain. Additional understanding is needed, however, regarding ATI performance, especially in

its capacity to pass sediment through, and the performance of the layer of woodchips, which is the focus of this study.

Figure 1.3. Ponding around a conventional tile intake, namely the orange slotted pipe at the Clear Creek, IA demonstration site.

Figure 1.4. Much reduced ponding at an installed ATI at the same site (The orange stand pipe indicates the ATI position).

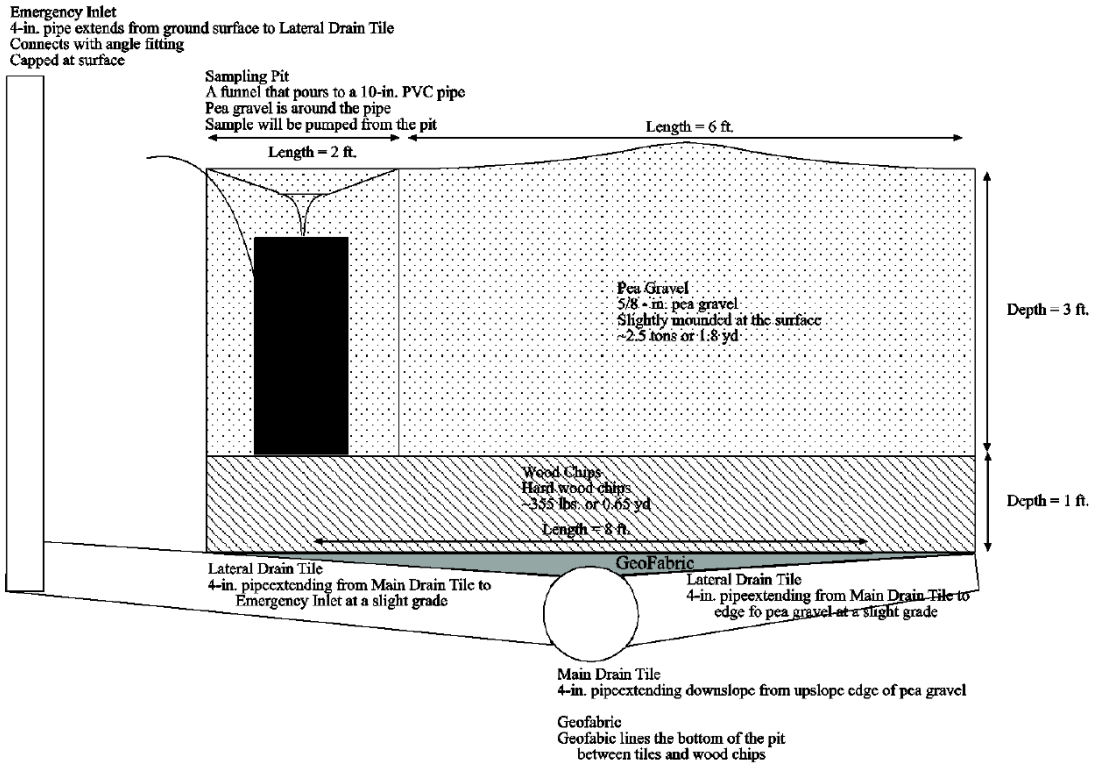

Figure 1.5. Vertical cross-section of an ATI.

Figure 1.3 shows the cross-section of an ATI with the gravel and the woodchips layered through the column. Over time, clogging of the ATI's media is inevitable. Clogging reduces the permeability of the ATI as particles deposit within the porous media. Major factors affecting clogging include the different phases of siltation and the ratio of sediment particle size to ATI media grain size, D_p/D_m. Schälchli (1995) reported three phases of siltation: (1) coarse particles clog big pores and crevices; (2) medium size sediment fills pores; (3) very fine particles form skin or seal near surface interface. Sedimentation, gravitation, and straining are important early on. With higher discharges, hydraulic conductivity increases to a maximum with general movement and full desiltation (Schälchli, 1995). The deposition of coarse and medium sized particles occurs by the process of bridging, where they are physically strained out of flow. Once sediment is delivered to and trapped by the porous media, it is always susceptible re-

suspension in the flow depending on the regime. With increasing siltation, particles deposit nearer to the surface layer due to wide size distributions of bed and particles Schälchli (1995).

The movement of fine sediment and its deposition in a gravel matrix relates also to the behavior of gravel-bed rivers, as they convey fine sediment as well as coarse, gravel-size particles.

According to Schälchli (1995), sediment in rivers is deposited in bed pore spaces during low-medium flows, but it is flushed during high flows as the armor layer breaks apart. These changes in siltation can be seen with changes in hydraulic conductivity, which decreases during siltation and increases during flushing. This process can be measured through changes in pressure along the bed (similar to sediment experiments in the laboratory). The goal in this study will be to identify the parameters governing the changes in conductivity during siltation within the ATI using the processes seen in gravel-bed rivers as an example.

Although flow through porous media is described by Darcy's Law, there are some situations where this is not entirely valid, especially when clogging of sediment occurs within a porous medium. Schälchli (1995) introduced an additional resistance term for the clogging of material, which is represented with five dimensionless terms: grain size distribution of the bed (d_{10}/d_m), water temperature (viscosity), Reynolds number, hydraulic gradient, and dimensionless shear stress. Riverbeds with a large value of d_{10}/d_m have a uniform distribution of porosity and infiltration velocities. Additionally, higher Re, higher temperature (lower viscosity), and hydraulic gradients lead to higher infiltration velocities. Higher infiltration velocities indicate that resistance is small, which yields more deposition of fines (and deeper) to fill in the dead storage. These considerations have to be taken into account when evaluating flow and sediment transport down through an ATI placed in the harsh environment of cropland subject to intense rainfall.

CHAPTER 2. FIELD MONITORING AND NUMERICAL SIMULATIONS

This study initially involved field monitoring conducted in the Clear Creek, IA watershed where 3 ATIs were installed and numerical modeling of runoff and sediment transport at this installation site. This information was used to develop laboratory experiments involving a physical model of an ATI, called a permeameter herein, to investigate the water and sediment flow through the gravel/woodchip matrix. The present chapter describes the field monitoring and numerical model simulations using the Water Erosion Protection Project (WEPP) model to develop the experimental conditions for the permeameter experiments. Due to the drought conditions that occurred during the study period (2012-2014), only limited field monitoring was completed, and thus increased dependence was placed on the WEPP simulations to simulate the field conditions at the Clear Creek site.

2.1 A Three-part Control Volume Approach

The runoff and sediment transport processes involved in how an ATI filters and passes water, sediment, and nutrients can be explained using a control volume approach shown in **Figure 2.1**. The ATI control volume can be divided into three segments through which the different constituents move. The first segment includes the processes occurring on the hillslope above the ATI and is the focus of this chapter. The second control volume consists of the ATI and the third segment is the drain pipe exiting the ATI. The permeameter and the involved laboratory work examines these segments.

The values from the hillslope (segment 1) include the overland flow or runoff, Q_{in}, which generates a ponding depth, H, above the ATI and was considered as the inflow to it. Additionally, the hillslope sediment yield, SY_e, was defined as the amount of eroded sediment transport out of the hillslope area, C_{in}. The values from the ATI (segment 2) are the subsurface flow, Q, and suspended sediment concentration (passing,

settling, filtering), C. The values from the Drain Tile (Segment 3), which controls the flow by throttling, are the outflow from the ATI into the pipe, Q_{out}, and the suspended sediment concentration, C_{out}.

The necessary data from the field monitoring and numerical simulation used as input to an experimental ATI setup in the laboratory were estimates of runoff depth and sediment yield associated with the different events, which were used to determine the following quantities:

1. The ponded depth of water above the ATI; and
2. The sediment yield in terms of a suspended sediment concentration.

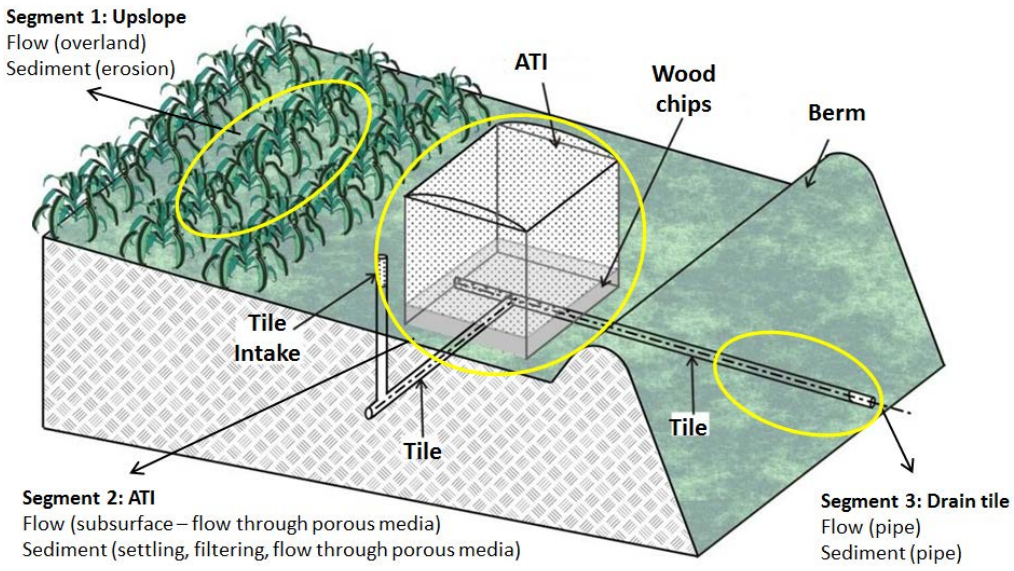

Figure 2.1. Three segment approach of analysis.

2.2 Field Work

Three prototype ATIs were installed, in conjunction with water and sediment control basins, along an actively farmed hillslope in the Clear Creek watershed (**Figure 2.2**). One of these ATIs was fitted with different monitoring instruments to quantify the

fluxes of water, sediment, and nutrients passing through it. Both a pressure transducer and water-sediment SIGMA autosampler were placed in the drain tile exiting the ATI to measure the flow and sediment concentrations of the ATI effluent. A control intake, which consisted of a traditional orange slotted pipe, was also monitored for comparison purposes. The delivery of material from the hillslopes above the ATI and the control were determined using the previously calibrated WEPP model for the location (Abaci and Papanicolaou, 2009; Dermisis et al., 2010).

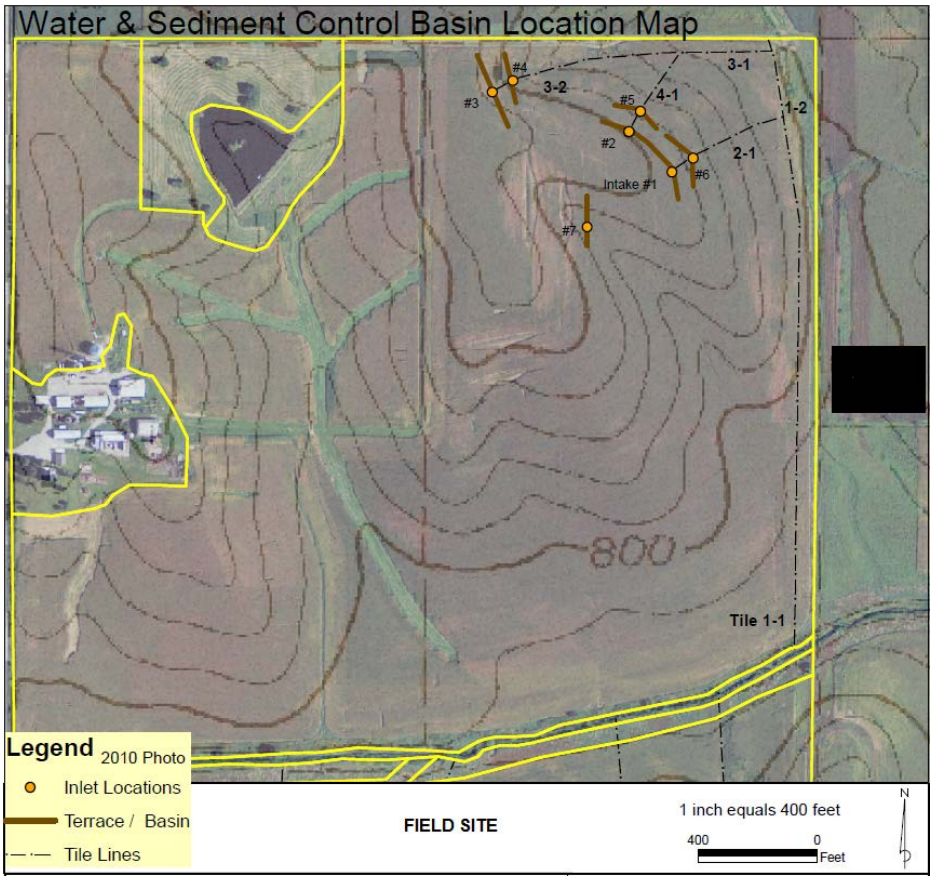

Figure 2.2. Locations of the three ATIs and associated control intakes downslope of the ATIs. All intakes are installed within water and sediment control basins. Source: NRCS (2010).

The field monitoring was to focus on rainfall events significant enough to generate ponded water above the intakes behind the sediment basins, this was initially assumed to be rain events greater than 1 inch. Due to the drought conditions that occurred during the study period (2012-2014), only one event was successfully measured.

Figure 2.3 shows the general configuration between the ATI and the control intake. The monitoring procedure at the field site (**Figure 2.4**) involved setting the SIGMA autosampler to either begin sampling immediately or after a delay based on the timing of the event. The sampler was also programmed to collect ~500 mL at 5-minute intervals. These values would provide the amount of sediment passed through the ATI. A SIGMA sampler was not used at the outlet of the control intake, because the sediment flux being measured here would have been the sum of both the outflow from the ATI and the control intake since the underlying tile was connected to both. As such, jar samples were planned at this location.

The pressure transducer was placed in the drain pipe outlet of the ATI and the inlet of the control. The pressure transducer was set to measure the water level of the flow moving through the pipe at 1-minute intervals. These measurements were used to determine the flow in the pipe using the Manning's equation.

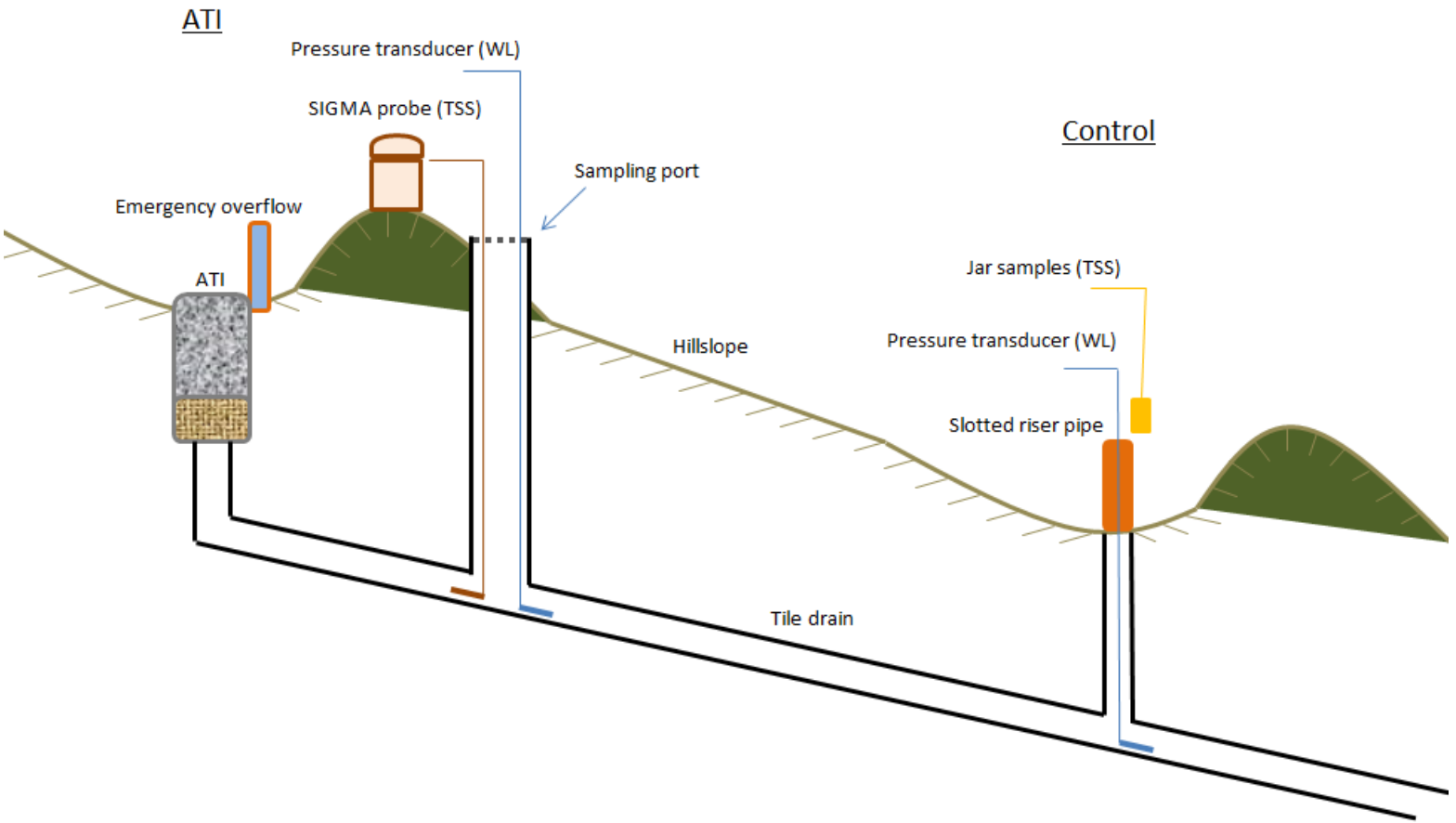

Figure 2.3. Side-view of the layout between the ATI and Control intakes (not to scale).

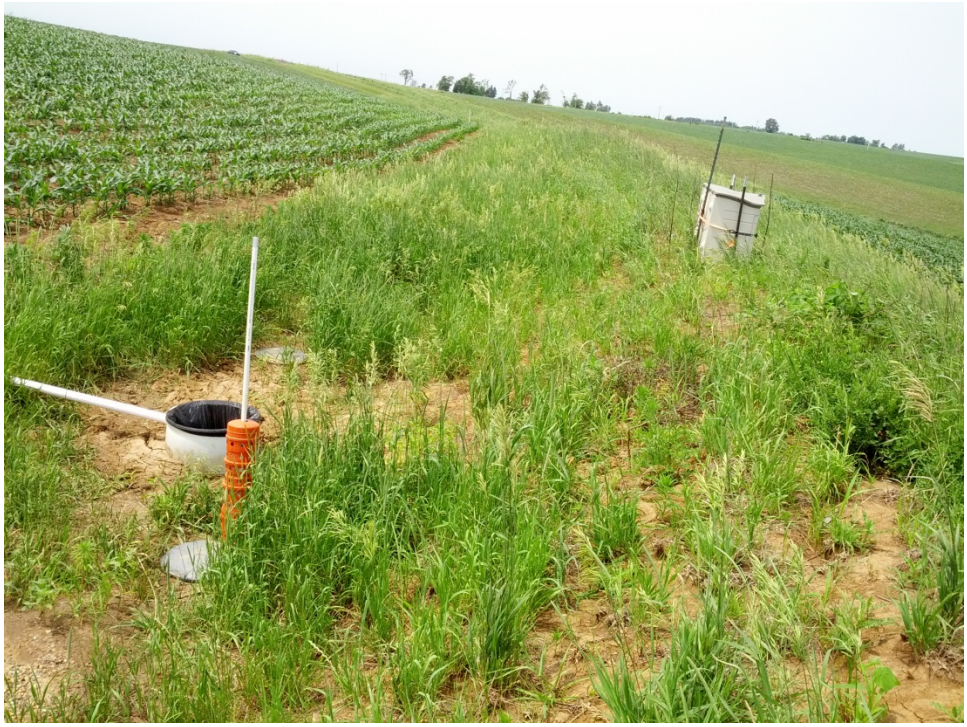

Figure 2.4. The monitored ATI in the Clear Creek watershed and its contributing hillslope. Downslope is the location of the control.

The sampled event for this study occurred on June 24, 2014, where nearly 2 inches of rain fell over a period of 15 hours (**Figure 2.5**). Observations of ponding were taken at the ATI, as well as measurements of depth of water (and thereby discharge) in outflow pipe (**Figure 2.6, Table 2-4**). The flow and sediment measurements are presented here as they were used to guide in the set-up of the experimental design.

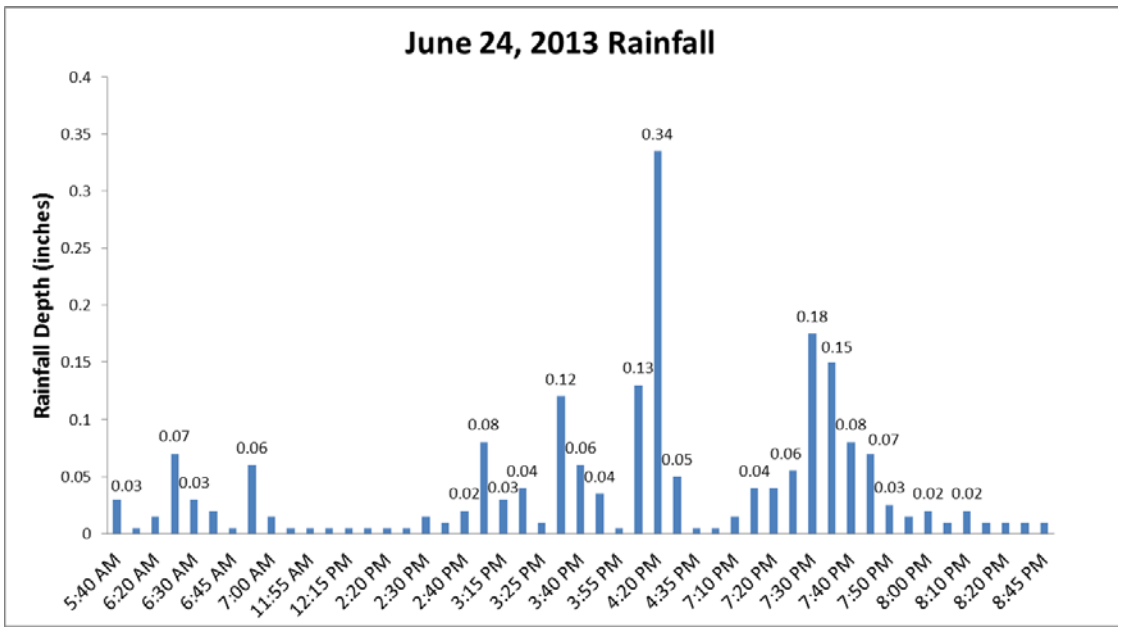

Figure 2.5. Rainfall amounts measured with the tipping bucket on June 24, 2013. A total of 2 inches of rain fell in 15 hours.

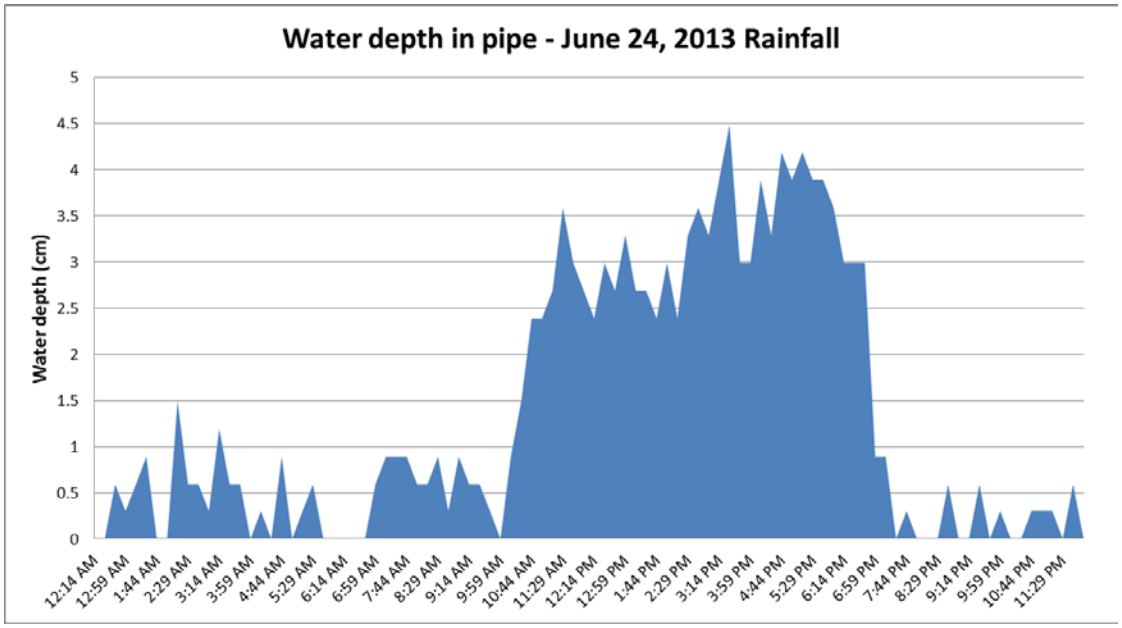

Figure 2.6. Water depth as measured by pressure transducer in the sampling port. Peaks correspond to rainfall in Figure 2.3. Max depth of 4.5 cm; pipe diameter is 12.7 cm; about 35.4% of the depth, so not pressurized flow, but indicative of clogging.

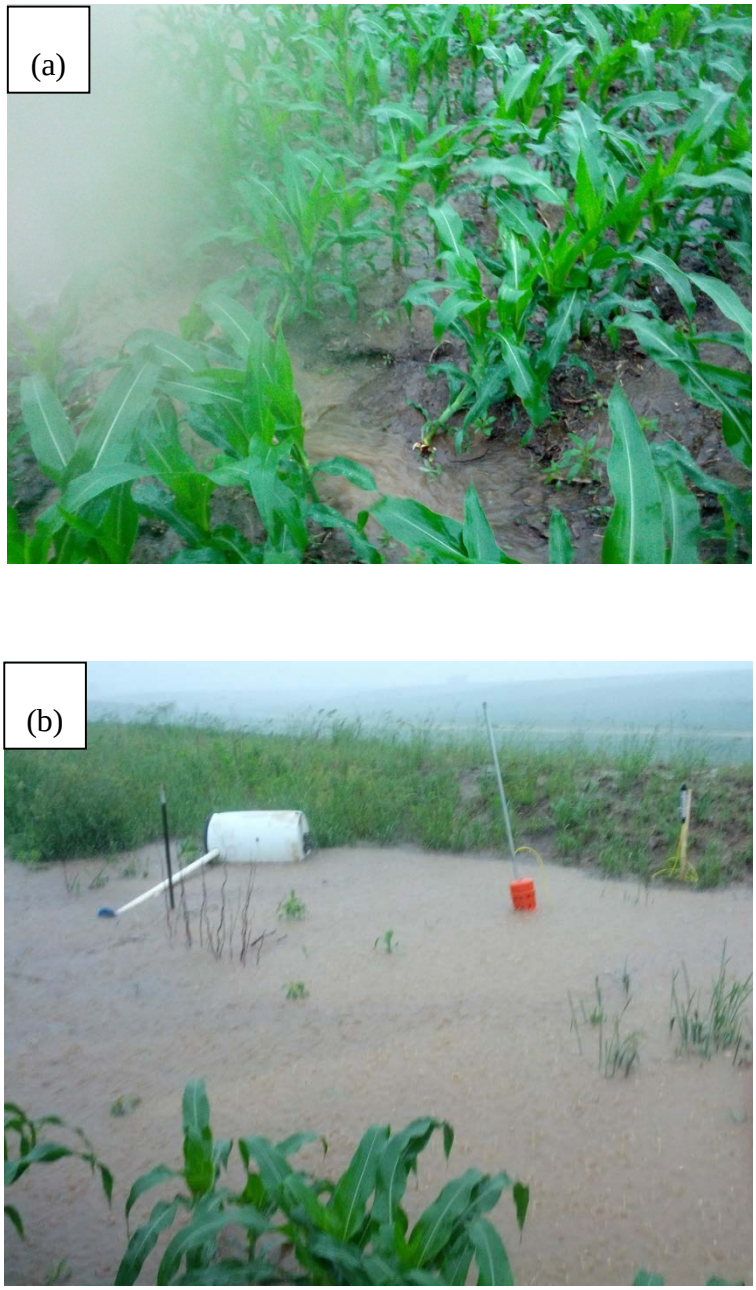

Figure 2.7. (a) Rill flow downslope; (b) ponding at a control intake.

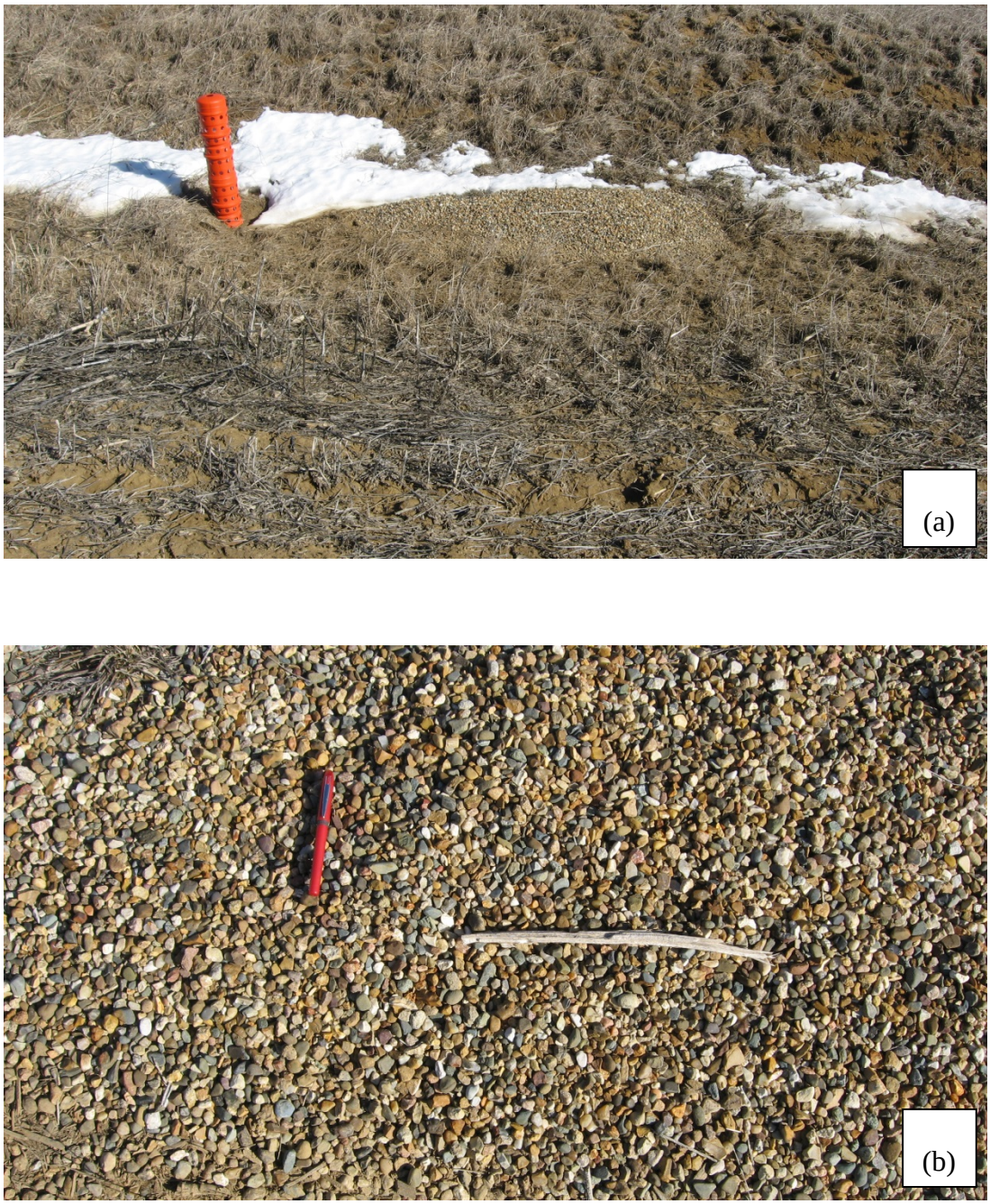

Figure 2.8. Recent photographs (February 2013) show one of the installed ATI prototypes has retained its structure and function; where (a) shows the entire ATI; and (b) shows the pea gravel surface un-affected by siltation.

Figure 2.9. (a) ATI surface (July 2013); (b) further silted and vegetated over ATI surface (October 2013).

2.3 Numerical Watershed Modeling with WEPP

WEPP simulations were used as an additional means to obtain "equivalent" field information for quantifying the site-specific ranges of flow and eroded sediment that could be delivered to the ATIs. Simulations were conduct for the peak rainfall season between April and August in Clear Creek to ensure obtaining maximum potential values of runoff discharges and sediment concentrations.

WEPP is a one-dimensional, process-based, hydrologic-erosion model capable of capturing the heterogeneous characteristics of the ATI hillslope (**Figure 2.10**) in terms of soil, land use, and topographic parameters by partitioning the hillslope into multiple sub-units (Flanagan and Livingston, 1995). Detailed descriptions of the calibration and validation of WEPP in Clear Creek can be found in Papanicolaou and Abaci (2008), Abaci and Papancilaou (2009), and Dermisis et al. (2010). Simulations with WEPP were conducted using the LiDAR-derived topography as well as other soil, land-use, and climate information collected as part of the National Science Foundation Intensively Managed Landscape-Critical Zone Observatory (IML-CZO).

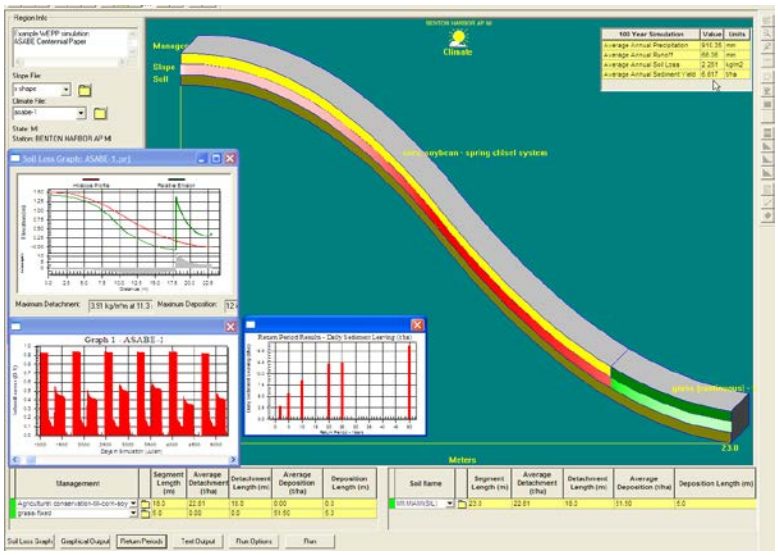

Figure 2.10. Screen capture of the WEPP interface. (Source: USDA, 2010)

Table 2-1. Input Parameters to WEPP.

Category	Parameter	Units	Minimum	Base	Maximum	Reference
Climate	Precipitation	(mm)	0	32	95	Abaci et al., 2009; Iowa Environmental Mesonet
Land Management	NTB-STC	(-)	(-)	(-)	(-)	Abaci et al., 2009
	FTC-NTB	(-)	(-)	(-)	(-)	Abaci et al., 2009
	NTC-FTB	(-)	(-)	(-)	(-)	Abaci et al., 2009
Soil	Effective Hydraulic Conductivity	(mm/h)	0.15	0.78	1.13	Papanicolaou et al., 2008; Abaci et al., 2009
	Bulk Density	(g/cm^3)	1	1.2	1.5	Abaci et al., 2009
	Initial Saturation	(%)	30	70	90	Deer-Ascough LA. 1995
	Interrill Erodibility	($kg\ s/m^4$)	100,000	4,400,100	10,000,000	Nearing, 1990; Abaci et al., 2009
	Rill Erodibility	(s/m)	0.002	0.005	0.0076	Nearing, 1990; Abaci et al., 2009
	Critical Hydraulic Shear Stress	(Pa)	1.0	3.5	8	Nearing, 1990; Abaci et al., 2009
Slope	ATI 1	(%)	0.33	5.6	11.71	Field Measurements
	ATI 2	(%)	2.08	9.8	15.53	
	ATI 3	(%)	0	7.1	13.37	

Over 200 single-storm simulations were conducted with different combinations of rainfall events and initial (field) conditions. These initial conditions included crop cover (based on time in the growing season) in conjunction with a land management practice (same for all hillslopes), and soil moisture (see **Table 2-1**).

A total of six different rainfall events were simulated to estimate the runoff depth and sediment yield for each event. Four of these were events involved measured rainfall data obtained with tipping bucket rain gauges in Clear Creek (Dermisis et al., 2010). Two of the six events were Natural Resources Conservation Service TR-55 design events (10- and 25-year return period) and both of which yielded sufficient runoff depths that would cause ponding conditions as replicated in the laboratory experiment (discussed further in Chapter 4).

A total of five different initial (field) conditions were used that represented most of the growing season (i.e. June – September) at the field site. The initial conditions for June rainfall events produced the largest soil loss, often 10 times greater than the average, with about the same amount of runoff generated. This mimics what is observed usually in the fields of Clear Creek (e.g., Abaci and Papanicolaou, 2009; Wilson et al., 2012; Sutarto et al., 2014)

WEPP was also run using continuous simulations with generated long-term daily climatic data from a stochastic climate generator, known as CLIGEN (Nicks et al., 1995). A 100-year continuous simulation of the ATI site, which entailed 1,360 rainfall event simulations, was conducted and a histogram of the resulting sediment yield, converted into values of suspended sediment concentration, revealed that the distribution was log-normal, as shown in **Figure 2.11**. The continuous simulations of WEPP were used as a virtual simulation of steady state conditions at the ATI site.

Table 2-2. Sediment concentration statistics estimated from the 100-year continuous simulation using WEPP.

	arithmetic mean	harmonic mean	Standard deviation	median	mode
Sediment Concentration (g/L)	6.8	4.0	4.6	5.4	3.1
Runoff Depth (mm)	12.3	6.4	11.9	8.7	8.6

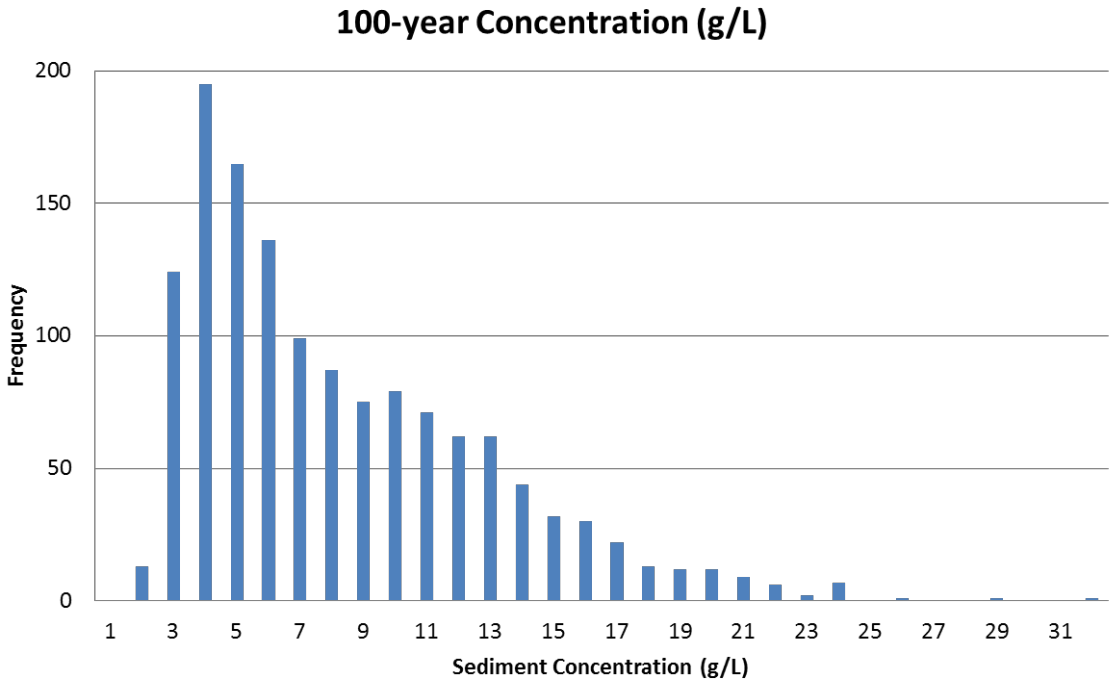

Figure 2.11. Histogram of results regarding values of sediment concentration estimated from continuous simulations using WEPP.

Overall, both the single event and continuous simulations yielded similar values for runoff flow volumes (**Table 2-1**). Both sets of simulations produced meaningful

average sediment concentration values; i.e. 11.5 g/L for single events; 6.8 g/L for continuous events. However, BMP design in Iowa uses single storms with a 10-year return event and continuous simulations with WEPP mask extreme events, because CLIGEN under-predicts extreme events (Papanicolaou, 2012). Hence the single-event simulation runoff and resulting ponding depths, as well as the concentrations were used in the ATI laboratory experiments (see below). Furthermore, the single event simulations accounted for a wide range of initial field conditions over the growing season. Additionally, it was decided to test the worst-case scenario for the ATI and therefore the concentrations determined using the initial conditions that produced the greatest sediment yield were used, which increased the average value of sediment concentration by about 50 percent to 17 g/L.

2.4 Depth of Ponding at the ATI

To determine the depth of ponding at the ATI, stage-discharge relationships were simulated with the WEPP watershed module using the impoundment component and a rock-fill check dam below hillslope to mimic the sediment basin in the field using four of the six events mentioned above. A hydraulic routing procedure was used to relate the runoff depth from single event simulations to the corresponding ponding depth of water above the ATI (**Figure 2.12**).

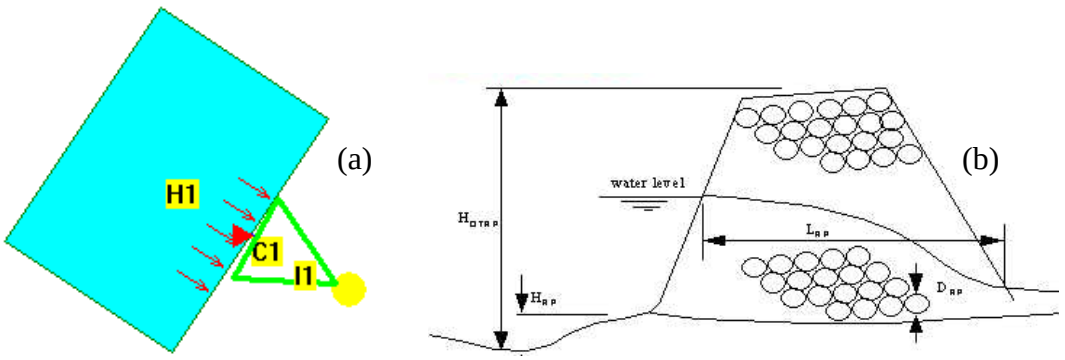

Figure 2.12. Hydraulic routing using (a) WEPP watershed (one hillslope) and impoundment; and (b) rock-fill check dam as the impoundment.

The landscape of the hillslope above the check dam was modeled as a four component problem. The upland component had a gradient S1; the flatter section just upslope of the ATI had a gradient S2; and the ATI just downstream of the flatter section has a similar gradient S3 as the flatter section but was more permeable relative to the soil due to the presence of gravel; the fourth section was the impoundment (sediment basin terrace). WEPP was used to calculate the flow depths over S1, S2, and S3.

Several different scenarios were simulated in order to achieve the most accurate results from the rock-fill impoundment. The D_{50} of the pea gravel was used in the ATI but woodchips were unable to be accounted for in the hydraulic routing procedure. The following assumptions were also considered: (1) the cross-sectional width of the impoundment was the same as that of the ATI; and (2) the length of the impoundment, *L*, which is the flow distance from the upstream to the downstream side of the check dam impoundment, was set to be 1.2 m, 2 m, and infinity. Scenarios 1 and 3 (**Table 2-2**) had L = 1.2 m; scenario 2 had L = 2 m; and Scenario 4 with a permeable ATI using an approximate hydraulic conductivity of 5 cm/s, assuming that the rock-fill check dam has

L = infinity and therefore there are no losses through the check-dam. In this case, most of the losses occur through the ATI.

Table 2-2 shows the results for those scenarios. Scenario 4 was the most believable as it showed that there is no ponding for Events 6br and 4r and "corrects" the flow depth for the 10-year and 25-year return periods because L = infinity, meaning that there was no loss of flow through the check dam. Additionally, scenarios 1-3 do not account for the hydraulic conductivity through the ATI, as they were considered more to test the sensitivity of WEPP using the check dam. Since there is gravel and woodchips, the porosity is high with small losses, yielding no significant ponding. From this analysis, it was determined that the hydraulic conductivity plays a more important role in the generation of ponding than the rock-fill check-dam impoundment.

To iterate closer to a more realistic computation of ponding depth, the number of scenarios was expanded to include three new scenarios (5, 6, and 7). These scenarios accounted for the ATI conductivity as well as that of the check dam, which is reflective of the field site configuration of the ATI and the berm/terrace. The difference between these three scenarios is the rock diameter. For Scenario 5 the D_{50} was specified as 0.1 m; for Scenario 6 the D_{50} was specified as 0.01m; and for Scenario 7 the D_{50} was specified as 0.006 m. Unlike Scenario 4, where the length of the dam was set to infinity, the length of the dam in Scenarios 5, 6, and 7 was set to 1.2 m.

As noted above, the estimated depths in Scenarios 6 and 7 were close to the depths estimated in Scenario 4. Based on photographs of the berm/terrace, Scenario 7 with the smallest D_{50} (0.006 m) appears to be the most likely scenario that mimics the conditions in the field. Hence, Scenario 7 (highlighted in the **Table 2-2**) was selected for the experimental design in the laboratory. It was assessed to be the closest to what actually happens at an ATI subject to ponding, which occurred only for the 10-year and 25-year return period storms.

Table 2-3. WEPP Watershed Model with Impoundment.

	Max Depth (m)			
	Event 6br	**Event 4r**	**10 yr**	**25 yr**
Scenario 1 (Rock-fill Dam) L = 1.2m, D_{50}=0.01m, XS Width = 1.83 m, Overtopping stage = 1m	0.146	0.186	0.263	0.302
Scenario 2 (Rock-fill Dam) L = 2m, D_{50}=0.01m, XS Width = 1.83 m, Overtopping stage = 1m	0.147	0.186	0.266	0.305
Scenario 3 (Rock-fill Dam) L = 1.2m, D_{50}=0.006m, XS Width = 1.83 m, Overtopping stage = 1m	0.149	0.191	0.269	0.308
Scenario 4 (ATI+Rock-fill Dam) ATI discharge ~ 0.022m^3/s Rock-fill Dam: L = infinity	No ponding	No ponding	0.154	0.215
Scenario 5 (ATI+Rock-fill Dam) ATI discharge ~ 0.022m^3/s Rock-fill Dam: L = 1.2m, D_{50}=0.1m, XS Width = 1.83 m, Overtopping stage = 1m	No ponding	No ponding	0.116	0.153
Scenario 6 (ATI+Rock-fill Dam) ATI discharge ~ 0.022m^3/s Rock-fill Dam: L = 1.2m, D_{50}=0.01m, XS Width = 1.83 m, Overtopping stage = 1m	No ponding	No ponding	0.144	0.201
Scenario 7 (ATI+Rock-fill Dam) ATI discharge ~ 0.022m^3/s Rock-fill Dam: L = 1.2m, D_{50}=0.006m, XS Width = 1.83 m, Overtopping stage = 1m	No ponding	No ponding	0.148	0.207

The delivery of water to the ATI is only one component to quantifying the ponding depth. The outflow from the ATI through the drain tile also controls the ponding depth as the outflow pipe is a constriction, which can cause the flow to back-up at the soil surface. The large cross-sectional area and well-sorted pea gravel medium of the ATI allow for a large conveyance of flow relative to the subsurface 5 inch corrugated plastic

pipe. Consequently, high flow rates through the ATI, exceeding the capacity of the drainage pipe, cause the pipe to control the outflow from ATI. The occurrence of the intense rainfall events would characterize these types of flows, where the maximum drainage rate would be quickly realized. The inflow-outflow hydrographs for the 10-year and 25-year design events (**Figure 2.13**) reflect the restricting affect of the subsurface drain pipe on the flow through the ATI. The ponding depths were generated by the difference in flow volume between the inflow and outflow hydrographs. Furthermore, this ponding would aid in the settlement of particles entrained in the runoff. The potential of sediment settling-out in the subsurface outflow pipe would enhance the backing-up of flow (and the level of ponding).

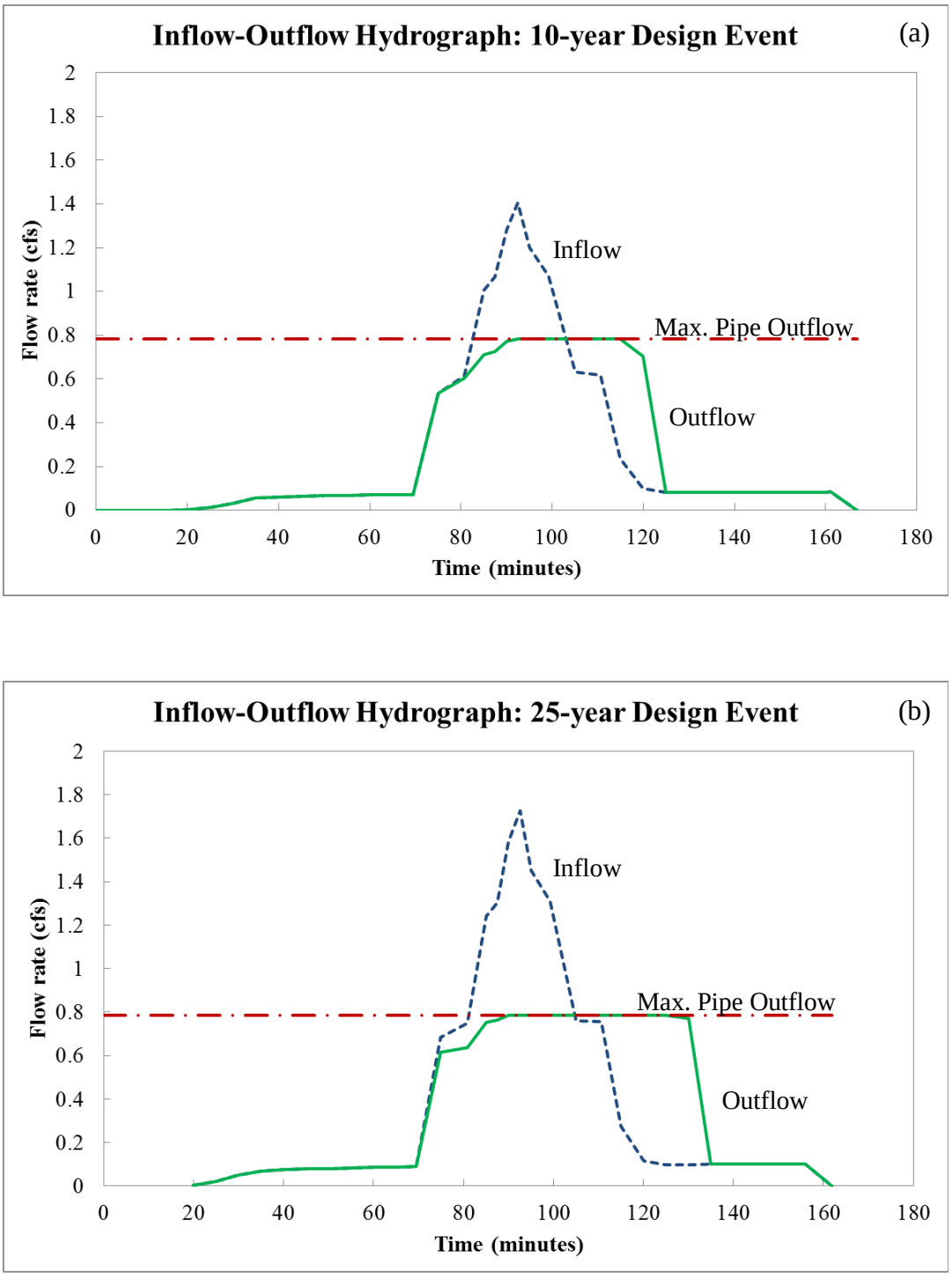

Figure 2.13. Inflow-outflow hydrograph for a simulated (a) 10-year event; and (b) 25-year event.

The computed runoff depth by WEPP was verified by computations with the Rational Method, which provided a close approximation (+ 2.64 mm). The Rational Method is based on the simple equation

$$Q = CiA \tag{2-1}$$

where Q = runoff depth; I = rainfall intensity; A = area of watershed; and C = a runoff coefficient. This method is approximate, but gives a useful sense of magnitude associated with runoff from the monitoring site.

2.5 Suspended Sediment Concentration and Mass Loading Rate

The single-event rainfall simulations were also used to compute the sediment flux, $\dot{m}$, in grams/second, calculated by the sediment yield mass divided by the duration of the rainfall event. The corresponding value of suspended sediment concentration, C, was then calculated using the sediment yield mass divided by the runoff volume of the rainfall event.From the different simulations with combinations of rainfall events and initial field conditions, it was found that the variation in sediment concentration was sensitive only to changes in the initial field conditions, while event magnitude and intensity had a relatively little effect. For example, when the sediment concentration was compared between 10-year and 25-year events, it varied only slightly between them despite differences in flow volumes. Even though the 25-year event produced higher loads of suspended sediment, it also produced larger amounts of runoff, which diluted the concentration of sediment. The 10-year event produced less eroded sediment and runoff, so the proportion of the two was approximately equal to that of the 25-year event.

A family of $\dot{m}$ vs. Q curves was developed using the range of rainfall events simulated with the same initial conditions. Regression analysis was then used to determine the range of $\dot{m}$ corresponding to flow rates that achievable in the laboratory due to experimental limitations.

The range of ṁ determined using the regression analysis was able to be verified by back-calculating ṁ with the following equation:

$$\dot{m} = E((\tau/\tau_c) - 1) \quad (2\text{-}2)$$

where the ranges of erodibility, *E*, and critical shear stress, τ_c, were determined from an experimental plot in the Clear Creek watershed with similar soils to the ATI site (Dermisis, Papanicolaou, 2012), and the initial condition-specific applied shear stress, , was determined using the equation

$$\tau = \gamma HS \quad (2\text{-}3)$$

where γ is the specific weight of water, H is the average runoff depth for each simulated event and S is the average slope of the ATI hillslope.

The sediment yield computed by WEPP was verified using measurements from theabove mentioned Experimental Plot and the USLE equation,

$$\hat{E} = \hat{R}\hat{K}\hat{L}\hat{S}\hat{C}\hat{P} \quad (2\text{-}4)$$

where $\hat{E}$ is the soil loss per unit area (tons per acre); $\hat{R}$ is the rainfall erosivity factor, where a Type II rainfall distribution for this region was used; $\hat{K}$ is the soil-erodibility factor (tons per acre); $\hat{L}$ is the field-length factor normalized to a plot length of 72.6 feet; $\hat{S}$ is the field-slope factor normalized to a field slope of 9%; $\hat{C}$ is the cropping-management factor normalized to a tilled area with continuous fallow; and $\hat{P}$ is the conservation-practice factor normalized to straight-row farming up and down the slope.

The experimental plot in Clear Creek yielded sediment concentration values ranging from 1.6 – 18.1 g/L (**Table 2-3**). The calculation of the USLE equation yielded a sediment concentration of 36.6 g/L. The USLE equation works well with the extreme events in a small drainage area where Sediment Delivery Ratio (SDR) is close to 1. However, USLE overestimates small events because the “piston” approach does not work in small events. Instead, the watershed behaves like a “spring” with different modes of elasticity (or better resistivity). These modes introduce lag times which their limit is equal to zero only if the events approach the historic extreme events.

Table 2-4. Ranges of sediment concentration for verification of computations using WEPP results.

Approach	Method		Hydrologic forcing	Number of simulated events	Runoff depth (cm)	Ponding depth (cm)	Sediment Concentration (g/L)
Numerical	WEPP	Single event	Gauged-rainfall	140	1.9	0	0.3 – 50.8 (11.5)
		Single event	Design events (10, 25-yr)	40	5.8	14.8, 20.7	**4.1 – 50.5 (17.0)**
		Continuous	CLIGEN	1360	4.7	N/A	0.9 – 30.6 (6.8)
Experimental	Field measurements		Rainfall Simulators	15	1.0	N/A	1.6 – 18.1 (7.2)
Analytical	USLE		Type II Rainfall Distribution	1	6.7	N/A	36.6

The minimum, mean, and peak suspended sediment concentrations over peak growing season (June, August, and September) were selected for the experiments. The resulting values of $\dot{m}$ and C for the different calculation methods were close due to the range of Q (~1.0 – 1.4 L/s) in the experimental setup, where $C = \dot{m}/Q$. All values in table are time-averaged over the test duration. **Tables 2-3** and **2-4** provide a basis of inputs for laboratory experiments. In other words, the output of the numerical modeling will be the input for the physical modeling.

2.6 Input to Laboratory Experiments.

In order for the results from the numerical modeling to be transferred and utilized in the laboratory experiments, as described in **Chapter 3,** it was necessary to satisfy three axioms or conditions:

1. Maintain C determined for the field site, calculated by the relation C = ṁ/Q; where ṁ and Q are dependent through H (water depth in head box).
2. Physical constraints on the watershed determined through WEPP.
3. Experimental constraints dictated mostly by the head and flow rate that can be achieved in the laboratory.

Once these axioms were considered satisfied, then the following results from the numerical watershed modeling were used as input to design the experiments in the laboratory:

1. Ponding depth, H, corresponding to the SCS 25-year design event, which was 20 cm (**Table 2-5**).
2. Hillslope sediment flux (mass rate, ṁ) and suspended sediment concentration, C, corresponding to the minimum, average, and peak months of September, August, and June respectively, which were 18 g/s and 17 g/L respectively (**Table 2-5**). This relates to field/crop conditions over growing season.

Table 2-5. Experiments to test single and dual media combinations with sediment loading and runoff specific to the initial field site conditions simulated with WEPP. All values reflect amounts used in the physical model.

Event	Single Medium (100% gravel)	Dual Media (75% gravel - 25% woodchips)	Mean Clear Water Inflow Rate, **Q** (L/s)	Mean Pond Depth (Head Box), **H** (cm) *	Clean Media Hydraulic Conductivity, **K** (cm/s)	Sediment Flux, **ṁ** (g/s)	Mean Sediment Concentration, **C** (g/L) *	Sediment : Media Ratio, $\mathbf{D_p/D_m}$ (%)
25-yr	X	X	1.09 (17.3 gpm)	20	4.2 – 5.7	18	17	0.17
Scale (Model : Prototype)	1 : 1	1 : 1	1 : 56	1 : 1	1 : 1	1 : 56	1 : 1	1 : 1

CHAPTER 3. EXPERIMENTAL SETUP

3.1 Facilities and Instrumentation

The experiments were conducted at IIHR – Hydroscience & Engineering of The University of Iowa. They involved a physical model-permeameter to enable detailed observations and measurement of flow and sediment movement through the column of gravel and a layer of wood chips that mimicked the ATI placed in at the field site in Clear Creek. This chapter describes the experiment setup used for the experiments, the functioning of the setup, and summarizes the procedure followed in acquiring data and observations from the experiments.

3.1.1 Overview of Physical Model

The experimental setup involved numerous components for measurement and visualization purposes. Its main components consisted of a head box, the permeameter, 1.5 horsepower pump, two inflow-regulating valves, intake PVC pipe, excess flow outlet PVC pipe, main outlet PVC pipe with flow meter and CR800 data-logger, and outlet valve. The setup was equipped with a cable and pulley, wire baskets, and a hooking tool to retrieve the wire baskets (**Figure 3.9**) after tests are concluded. A stairway was erected in front of the permeameter in order to conduct procedures in and above the head box.

The principal component of the experiment set-up was the permeameter, which had a length of 121.92 cm and a circular cross-sectional area of 197.93 cm^2. **Figure 3.1** shows the permeameter with the head box (15.88 cm ID) attached to the clear acrylic column. This column had eight pressure taps installed at 15 cm intervals, and connected with Tygon® tube piezometers to a manometer board. During testing, the column portion of the permeameter was filled with a porous medium of pea gravel and woodchips.

At the upstream end of the permeameter, a 1.5-horsepower, self-priming centrifugal pump delivered a flow of water from a 3.7 m^3 sump above the head box, and then into the column filled with gravel and/or woodchips. Two 2-inch (nominal) diameter Powell gate valves were used to regulate the flow into the head box via the centrifugal pump. Flow recirculates during clear water flow.

When sediment was entrained in the flow, flow at the downstream end was diverted to a 1.78 m^3 sump with an open drain at the bottom (**Figure 3.2**) to prevent contamination of the clear water intake sump.

Figure 3.1. The (a) permeameter (clear acrylic tube) complete with eight pressure taps and manometer under hydrostatic pressure; and (b) with water flowing.

3.2 Functioning of Experiment Setup

The experiment setup was designed for conducting two types of experiments, each requiring a consistent series of procedural steps:

1. constant head tests; and
2. sediment flux and trapping tests.

The constant head tests were conducted first followed by the sediment tests. Other tests were run, but were used as checks to understand the physics of the system and to isolate variables for the main experiments. For each experiment a different procedure was followed. The purpose of the constant head tests was to determine the time-series of the saturated hydraulic conductivity, K_{sat}, for a particular combination (percentage of each type of gravel and wood chips) and arrangement (layered or mixed) of pea gravel and wood chips. The purpose of the sediment flux and trapping tests ("sediment tests" for short), was to determine the decrease in the hydraulic conductivity, K, due to clogging of pore spaces by sediment. The degree of clogging of the pore spaces depended on the influx of sediment delivered to the system, and the flow rate into the system which governed the head of water in the head box.

The following functional procedure was used to achieve flow rate of 16 to 20 gallons per minute (gpm) with a sediment feeder designed to delivery suspended sediments to column of various combinations of pea gravel and wood chips. The head of water to be tested was determined from a design storm with a 25-year recurrence interval. Dry, pulverized sediment was delivered via the sediment feeder, comprising of an inverted parking cone, corded power drill and paint mixing attachment, each with specialized mountings. The desired concentration of the suspended sediment was based upon test results obtained from the WEPP model simulations described in the previous chapters, where runoff volume and eroded sediment were computed for a given hillslope, land management practice, soil type, and weather conditions, such as prevailed at the

selected field test site in Iowa. The suspended sediment concentration for a 10-year rainfall event was determined using results from the WEPP model.

A small irrigation pump was used to generate flow of water from the intake reservoir at a constant rate. Water was backfilled through the outlet pipe and into the permeameter filled with the porous media. This step was taken to saturate the media and prevent air bubbles from forming when there is an inflow of water from the pump through the inlet pipe. Once the permeameter was completely backfilled with water, and filled up to a depth roughly 5 cm below the desired head in the tank, residual air was taken from the piezometers with the use of a shop vacuum modified for water intake. Once air from the piezometers has been removed, all piezometers will have the same pressure and stand at the same height. The fact that the piezometers have the same pressure revealed that all pore spaces experience the same hydrostatic pressure developed by the pressure head of water in and above the porous medium.

After the permeameter was purged of air, the centrifugal pump was switched on to introduce an inflow delivered from a sump to the head tank above the permeameter. Once the inflow begins, a valve at the outlet of the system was fully opened, thereby allowing a constant flow of water through the system. Get valves in the inlet pipe were adjusted in order to achieve a constant head of water in the head tank. Once a constant head of water was achieved in the tank, the inflow equaled the outflow, such that steady state flow occurred through the permeameter. This was the requisite initial condition before the start of the sediment experiments.

The system used for the sediment tests was identical to that of the constant head tests, but with the addition of the sediment feeding device, its mount, and two video cameras (for head box and piezometers), as shown in **Figures 3.2 and 3.5**. The waterfall due to water flowing overtop the head box provided a mechanism to mix the sediment into the static water level in the head box, maintaining a relatively well-mixed solution.

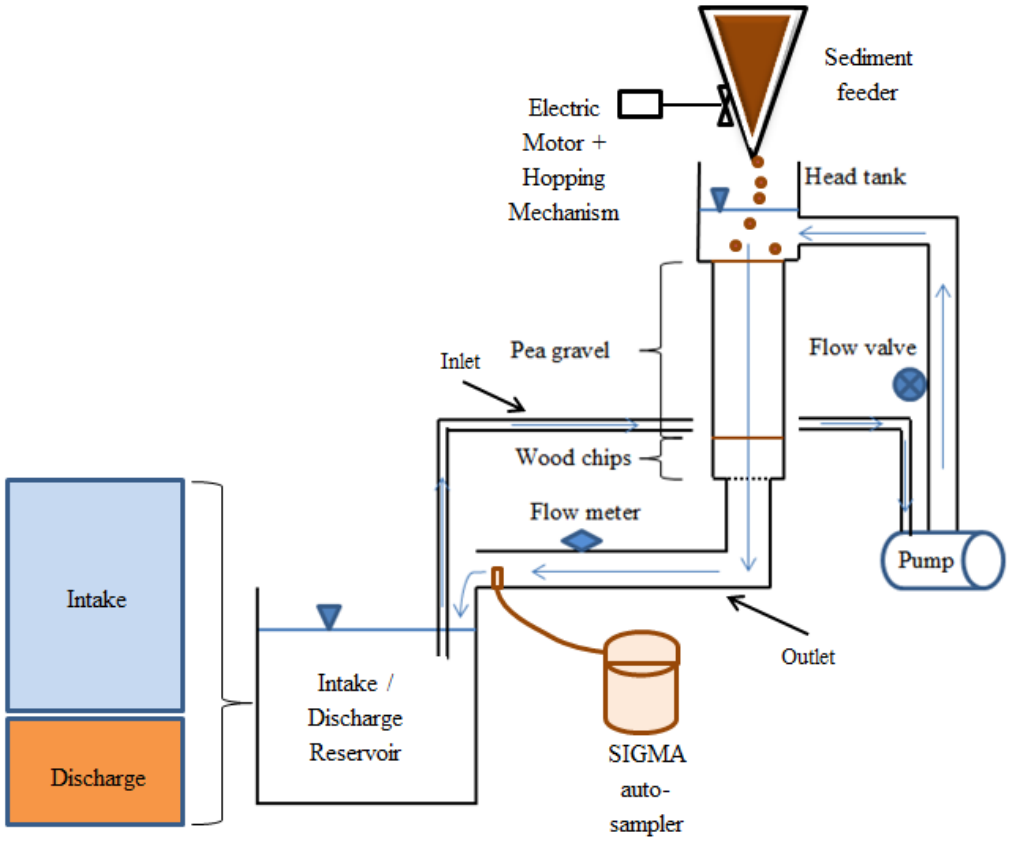

Figure 3.2. Experimental setup (not to scale)

3.3 Data and Observation Acquisition

The experiments entailed a fairly complex procedure for obtaining data and observations of water and sediment movement through the permeameter. A description of this procedure ensues.

A camera was mounted at the rear of the filter column, and was focused on the headbox. Another camera was mounted in front of the manometer to record the time variation of pressure (piezometer level) in each piezometer. Video recordings from each camera were converted to an image sequence corresponding to each experiment. These image sequences, comprised of thousands of images, were imported into image processing software called ImageJ, which was used to track changes in their height. In

the constant head experiments, the flow meter on the outlet/discharge pipe was used to measure instantaneous flow rate of the outflow. However, it was not possible to use the software with the highly turbid water of the sediment experiments. To measure the amount of sediment leaving the permeameter, a SIGMA automated sampler (**Figure 3.6**) was to be used to take discrete samples of total suspended solids (TSS) from the pipe, as well as bucket samples taken from the outlet for confirmation of the SIGMA samples. However, it was found that the automated sampler was too cumbersome for the purposes of this study, and therefore it was not used.

3.3.1 Experiment Procedure for the Constant Head Experiments

The constant head experiments involved the following procedure for setting up an experiment and then acquiring observations and data:

1. The pea gravel for the permeameter was carefully washed to remove fines by placing a 4' x 2.5' stainless steel mesh (No. 10 (4.75 mm) sieve size) over two 55-gallon drums (**Figure 3.3**). Two 5-gallon bucket loads of pea gravel were poured onto the steel mesh and washed using a garden hose, as well as periodically churning the pea gravel to ensure all fine sediment had been washed away.
2. A 5-gallon bucket of woodchips was poured into another 55-gallon drum, one quarter-full of water, so as to soak overnight.
3. The system was initially flushed of any potential debris by switching the irrigator pump on (leaving the main outlet valve open) and letting this run for 5 minutes.
4. The pump was then shut off, and all excess water in the system was purged by gravity.
5. The metal grate at the bottom of the headbox was removed in order to fill the permeameter with pea gravel and/or woodchips – depending on the combination of media to be tested.

6. From the top of the headbox, the ATI media was lightly dropped at a steady rate to ensure sufficient packing is achieved (woodchips require use of a rod to pack at intervals). A small diameter PVC pipe was used to compact the woodchips inside the permeameter by tamping the material after the material had been dropped in layers of several inches at a time. The mass of fill media was recorded to determine packing density while compacting the media to the density similar to the prototype ATI in situ.
7. The bottom layer (layer 8) of woodchips was loaded into the permeameter without a wire basket. The next woodchip layer (layer 7) placed in a wire basket (first of 7) and lowered into the permeameter, setting it on top of the bottom layer, just above piezometer port number P7. It was important, when lowering and placing the wire basket in the column, that it was weighed-down with either woodchips or pea gravel. Once it was lowered and placed, more woodchips or pea gravel were loaded on top of it until the column has been filled up to the next port.
8. The loaded material then was switched to pea gravel, so that the next layer (layer 6) was placed onto layer 7, with the wire basket sitting just above piezometer port number P6 (**Figure 3.8**). Loading then continued with pea gravel layers 5, 4, 3, 2, and 1 respectively in the manner described in step 1, above. Once pea gravel had been filled to the surface, a slight mound of pea gravel was formed above surface so as to mimic the prototype topography typical of the field site;
9. Once the appropriate volume and packing of the ATI media was achieved, the metal grate was replaced at the annulus of the permeameter at floor of head tank.
10. The main outlet valve above the intake sump was closed and a hose was connected to the spigot attached to the outlet pipe. Tests were performed at room temperature (22 ± 1°C) with water temperature between 12°C and 5°C.
11. The hose was turned on, slowly turning it to release water into the main outlet pipe. This action backfilled the ATI media and entire system with water to

eliminate as many air bubbles as possible and produced hydrostatic pressure. It was important to backfill water into the main discharge pipe at very low flow rate so as to not disturb the packing of media and create more air bubbles.

12. When the water rose to the desired head of water in the headbox, the backfilling of water was terminated by closing the spigot in the outlet pipe. Bubbles were removed from the piezometers by means of a wet vacuum with a brass fitting to fit inside the 7mm (¼-inch) diameter piezometer tube;
13. The centrifugal pump was turned on to prime the intake pipe and generate the inflow of water for the test. As the pump was priming, the 1.5" diameter outlet valve was set at approximately 70% closed, and that the 1.5" diameter intake valve was approximately 50% open. This step was a good starting point, and finer adjustments were made once water was flowing - the amount of fine tuning depended on the media in the permeameter. Also, the irrigator pump took approximately 1 minute to prime and send water through the T-joint, which regulated how much water entered the headbox by diverting a portion of the flow to the intake sump. Gate valves in either direction controlled the amount of flow going to the intake sump and headbox.
14. When water began flowing into the headbox, it was allowed to reach the overflow level at 15 cm height. Then, the outlet valve above the intake sump was opened to ensure that the head tank did not overflow. Water first exited the 35mm (1.5 in.) diameter outlet approximately 10 seconds before entering the 100mm (4 in.) diameter inlet pipe to the headbox.
15. Once the outlet valve was fully open, the water head in the head tank was checked should there be any valve adjustment needed. The flow meter was then plugged-in. Also, for any given overflow, it was important to keep a constant water level at the mouth of the overflow pipe, which helped stabilize the constant level of water;

16. Once a relatively constant water level was achieved, flow measurements began at the determined time interval. The water elevation in the headbox was monitored to ensure a constant head of water prevailed at the determined height. The readings of flow rate from the insertion flow meter and the head (water level in the headbox) were used in determining the saturated hydraulic conductivity by means of Darcy's Law.

3.3.2 Experiment Procedure for the Sediment Trapping Experiments

The experimental procedure for the sediment experiments began with the same initial steps as for the constant head experiments. The additional experiment steps then were as follow:

1. Soil from field site was pulverized by placing it, along with two heavy bricks, in a concrete mixer (**Figure 3.4**). Once the soil has been pulverized down to a fine, flour-like powder, it was then sifted through a screen to remove dry chunks of sediment.
2. Enough soil was sieved to achieve the desired weight of sediment to be delivered during experiments (e.g., the required mass rate equaled 18 grams/second for duration of 15 minutes).
3. The sediment feeder (**Figures 3.10 (a) and (b)**) was plugged before being filled with pulverized, sieved sediment. Additional, 20 liter (5-gallon) buckets of sediment were lined up for refilling the sediment feeder.
4. Once the constant head of water was established in the head box by adjusting two gate valves downstream of the pump (upstream of the head box). The piezometer video camera and head box video camera were then turned on.
5. The actual experiment was begun by switching on sediment feeder, and thereby applying a continuous supply of sediment into the top of the permeameter.

6. Sediment concentration in the outflow from the permeamter was measured with the SIGMA instrument (**Figure 3.6**), and by taking discrete samples in a bucket;
7. When the water level in the head box approached 35 cm, sediment feeder was switched off. As the water level approached 40 cm, the escape valve from the pump was opened to divert water back towards the intake sump. Then,
    a. for a subsequent run/test, the water level in the headbox was returned to its height by repeating procedure from step 7, and
    b. to terminate the series of runs/tests, the centrifugal pump and allow water was switched off so as to drain from the system. Step 12 then continued.
8. After a waiting period of 24 hours the pea gravel and woodchips were removed for analysis. This waiting period enabled the deposited sediment and water to firm-up and better adhere to the porous media for removal, thus enhancing the subsequent measurement steps;
9. Each load layer of pea gravel and woodchips was unloaded from the permeameter using the hook, cable, and pulley system to lift the wire baskets out of the permeameter. **Figure 3.11** shows the removal procedure and an example layer with accumulated sediment;
10. Each unloaded layer of sediment was placed in a sealable plastic bag labeled in accordance with the layer's position in the permeameter;
11. The permeameter was then flushed with clear water, getting it ready for the next experiment.

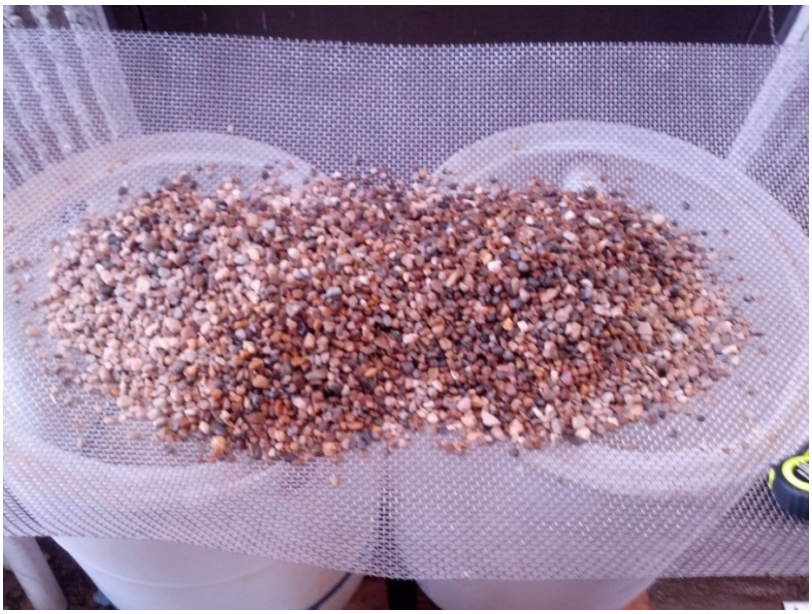

Figure 3.3. Washing gravel through stainless steel mesh (No. 10 (4.75 mm) sieve size)

Figure 3.4. Concrete mixer (along with two heavy bricks) used to pulverize sediment from field site.

Figure 3.5. Macro-view of experimental setup

Figure 3.6. SIGMA automated sampler and pressure transducer near outlet pipe

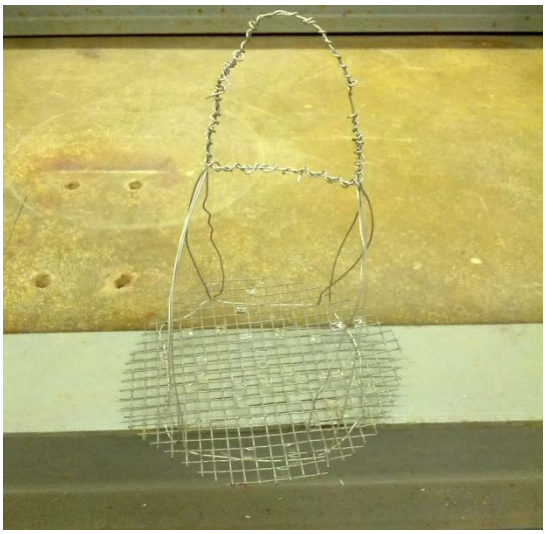

Figure 3.7. Wire basket used to retrieve pea gravel or woodchips from each layer

Figure 3.8. One of the wire baskets buried in a layer of pea gravel

Figure 3.9. Method of retrieval: (a) plexiglass insert inside the headbox with hook, cable, and pulley to retrieve wire baskets; (b) pulling gravel into clear acrylic section. This photograph shows with "clean" pea gravel (without fine sediment deposited on it); (c) pulling with upward force, the natural heave of gravel locks it inside the clear acrylic section and allows it to be transferred into a collection bucket; (d) placing retrieved layer into bucket. When the clear acrylic section is lifted off, the gravel falls out into the collection bucket.

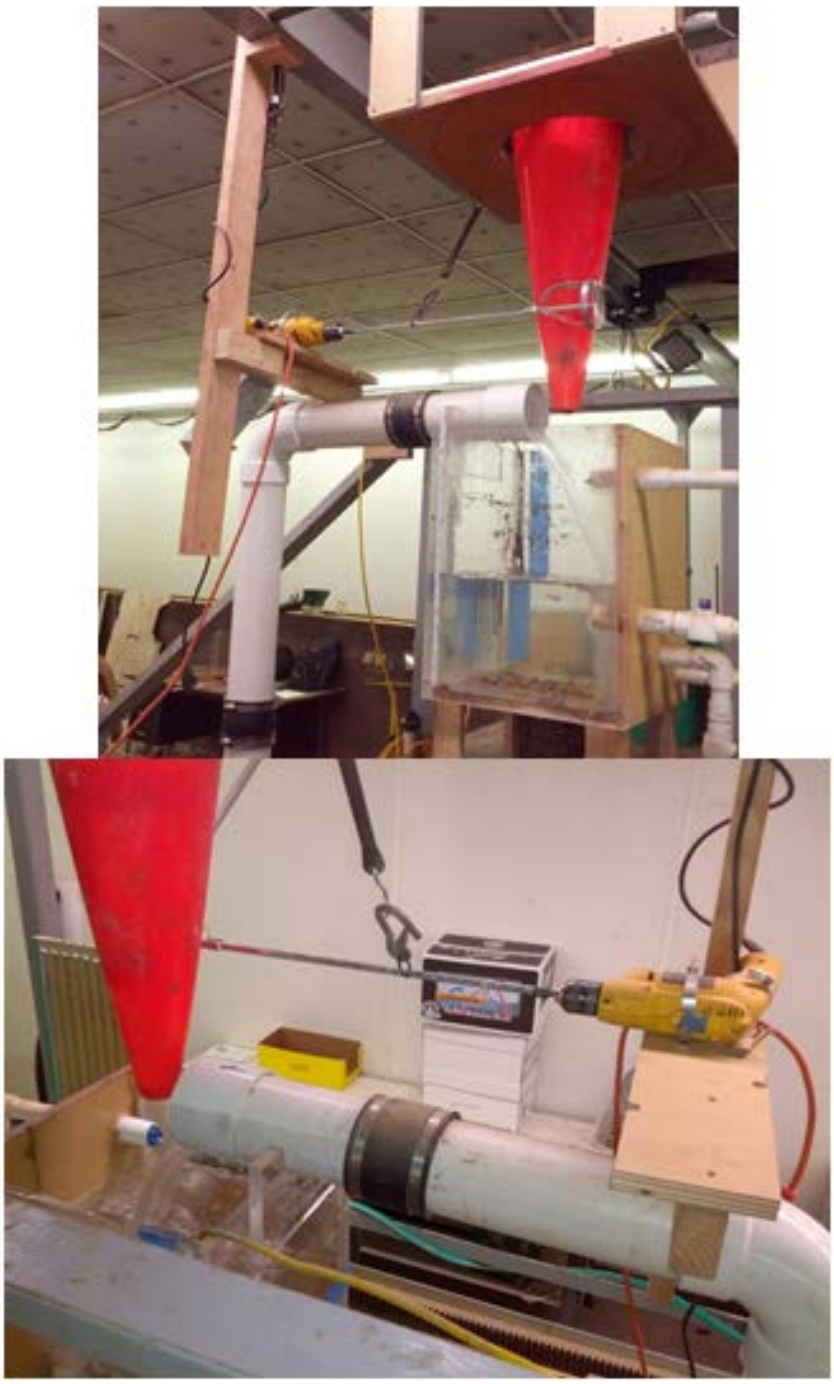

Figure 3.10. The sediment delivery mechanism. The orange parking cone serves as the sediment feeder, and the power drill with paint mixer attachment serves as the hopping mechanism. A bungee strap was used to support the shaft of the paint mixer.

Figure 3.11. Examples of pulling gravel layer into plexiglass insert after sediment test (a). A woodchip layer after sediment test (b). Top view of woodchip layer after sediment test (c).

CHAPTER 4. LABORATORY RESULTS

4.1 Introduction

This chapter presents the results of experiments conducted using the experimental set-up described in chapter 3. The results address the thesis' main hypothesis that the effectiveness of the ATI is controlled by the clogging of the ATI's porous structure and thus the need for laboratory experiments to determine changes in pressure (and corresponding flow frictional characteristics) within the different ATI medium combinations.

The results are organized as follow. Presented first are calculations of the clear-water, saturated hydraulic conductivity for different combinations of porous media, namely pea gravel and wood chips, which are encapsulated in the clear acrylic permeameter (ATI model). Presented next are the findings of the flow rate tests to assess flow dynamics for different combinations of porous media and also verify the readings obtained from a flow meter inserted in the outflow pipe from the permeameter; these findings were also used to determine a method by which to calculate the outflow rate from the permeameter when the flow meter readings become invalid with high concentrations of sediment in the flow from the permeameter. The calculations of Reynolds number, corrected for flow in a porous medium, are given subsequently, along with calculations of a modified friction factor for flow through a porous medium. The results from these clear-water experiments were used as baseline or reference conditions regarding the results obtained from conducting flow tests with suspended sediment.

The results from the sediment experiments consist of twelve sets of information presented in the chapter's eight sections:

1. The time-series of total head (pressure) increase in the head box due to partial clogging of the media;

2. The time-series of head increase in the piezometers, connected via ports over the depth of the permeameter, due to the partial clogging of the media;
3. The time series of the decrease in hydraulic conductivity, during each sediment experiment, over the entire permeameter (global) and at each piezometer (local);
4. The time-series of hydraulic gradient, i, for the whole system (global) and at each piezometer (local);
5. The time-series of the hydraulic conductivity, K, "globally" and "locally". Globally is again defined throughout the permeameter; locally denotes at the porous scale or port loci.
6. Continuous series of K with time;
7. Relative conductivity, K/K_0, where K_0 is the hydraulic conductivity of the clean media, and K is the reduced hydraulic conductivity with time once sediment is introduced to the flow;
8. Targeted tests to simulate clogging effects and a discussion on the mechanisms of clogging
9. Modified friction factor, Reynolds number, and head loss due to sediment-laden flow;
10. Inflow-outflow hydrographs and associated hydraulic conductivity for the experimental runs;
11. Mass of deposited sediment in the permeameter; and,
12. An analytical approximation of the lifetime of the ATI.

These parts provide substantial insights into ATI performance that could enable improved design of ATI's and an estimation of ATI working life.

4.2 Clear-water Flow Experiments

The findings from two main sets of experiments regarding clear-water flow are considered here:

1. Constant head tests; and,
2. Flow rate tests.

4.2.1 Constant Head Tests

From the outset of the constant head tests, two key observations were made regarding values of conductivity, K_{sat}. First, for the permeameter medium consisting of 100% pea gravel, the value of K remained constant during the entire experiment as expected. Second, the K_{sat} values of the woodchips decreased toward an asymptote, or a constant, time-averaged value. This further trend indicates a swelling of wood chips, and the shrinking of the pore spaces, as the duration of flow increased.

For the full set of constant head tests conducted, all the combinations of porous media (pea gravel and wood chips) yielded an average value of K_{sat} equaling 4.61 cm/s ± 0.39 cm/s. The experiments were consistent in their replication of clear-water flow through the permeameter, an outcome that reflects the reliability of the permeameter and the results described subsequently.

Figures 4.1 (a) – (f) show the results from the constant head tests. They are time-series of the saturated hydraulic conductivity, K_{sat}, for different mixtures of pea gravel and woodchips placed in the permeameter. A constant head in the head box above the permeameter was maintained, whereby the inflow approximately equaled the outflow rate. Considerable effort was taken to ensure the experiment setup produced a constant inflow rate from the centrifugal pump. The coarse and fine control valves in the exit pipe from the pump were adjusted until the inflow rate to the permeameter equaled the outflow rate (with less than 6% deviation). The water level in the head box was

measured using a submerged pressure transducer, and it was visually verified with a tape ruler attached to the front side of the head box.

The values of K_{sat} were determined using the Darcy-type equation expressing flow conductivity, K, as

$$Q = KiA \tag{4-1}$$

where Q is the flow rate through the permeameter, the hydraulic gradient, i is the hydraulic gradient, where $i = \Delta H/L = (H+L)/L$, H is the head of water in the head box, and L is the depth of the porous media beneath the head tank. **Eq. (4-1)** was found to be of reliable use for the clear-water experiments.

As mentioned above, for experiments with 100% pea gravel, the value of K remained constant during the entire experiment although deviations of ± 0.5 cm/s occurred between identical runs. In some of the 100% pea gravel runs the K_{sat} value increased until eventually the time-averaged K_{sat} became constant. If the pea gravel was not pre-washed of fine sediments (these were in the fine sand to clay size range) before being loaded into the permeameter, the K would increase with time before reaching an asymptote or steady value; this process increased pore openings and therefore permeability. This trend indicates clear-water flushing of existing sediment fine deposits trapped in the gravel matrix during the placement of the pea gravel medium in the permeameter as well as effects from the potential readjustment of the flow. It could also be due to minute changes in the inflow rate from the valve readjustment yielding variability in K_{sat}.

In general, however, the pea gravel was washed before the tests in order to reduce the amount of time needed to reach a steady-state value of K, and to reduce uncertainty in the values of K for the subsequent sediment tests. For the cleaned pea gravel, the values of K remained fairly constant during the experiments, since there was no change in pore spacing (e.g. due to swelling of grains or slight clogging by fine sediment).

In the case of the woodchips, the initial decrease in K values resulted, in part, from the absorption of water by the woodchips, causing them to swell. This swelling decreased the surrounding pore spacing and the reduced flow area, which reduced flow velocity through the wood chips. Presoaking the woodchips reduced this swelling effect.

Other factors may have reduced wood-chip conductivity. In overall terms, it was found that the woodchips were slightly less conductive of water (about 89% of the conductivity obtained with pea gravel). This can be attributed to the irregular shape, sorting, roughness and overall greater surface area of the woodchips. Also, it is likely there was too high a concentration of finer fractions of woodchips for some of the experiments (woodchips were not of the same size but provided in different fractions). Additionally, for some experiments, the woodchips had been soaked several days longer than other tests. All these considerations may explain some of the variability found in the results obtained for the woodchip conductivity.

The heterogeneous nature of layers of pea gravel and woodchips reduced the hydraulic conductivity compared that for to 100% pea gravel.

The values of $K_{z(eq)}$ for layered media were determined using the equivalent hydraulic conductivity concept as:

$$K_{z(eq)} = \frac{H_o}{\frac{z_1}{K_{z1}} + \frac{z_2}{K_{z2}} + \cdots + \frac{z_n}{K_{zn}}} \qquad (4\text{-}2)$$

Here, $K_{z(eq)}$ is the equivalent hydraulic conductivity in the vertical (z) direction and K_{z1} to K_{zn} are the vertical hydraulic conductivities of the first to the nth layer, H_o is the total thickness of the soil mass. Because conductivity depends on the permeability of the entire configuration of a permeable medium, non-uniform media will have variable hydraulic conductivity along their length. This tendency was observed for the

experiments with the mixed gravel and wood chips, and complicated estimation of a representative average value of conductivity.

As noted earlier, minor fluctuations in hydraulic conductivity were observed around a mean value during each run. They were due to pulsations of the flow as it moved through the irregular flow paths around the gravel and wood chips, as could be seen through the sides of the permeameter. Some paths developed increases or decreases in conductivity with time, and thereby caused momentary fluctuations in values of K. These fluctuations were especially noticeable as fine sediment washed through the gravel.

The steady state value for saturated hydraulic conductivity, K_{sat}, for all tests with combined use of pea gravel and wood chips was 4.61 ± 0.39 cm/s; the fluctuation here represents a standard deviation of the measurements. **Table 4-1** summarizes the values of obtained saturated hydraulic conductivity for variable combinations of porous media placed in the permeameter.

Table 4-1. Clear-water values of hydraulic conductivity, K, and the equivalent hydraulic conductivity in the vertical (z) direction, which accounts different strata.

Material	**Hydraulic Conductivity, K**
100% pea gravel	5.34 cm/s ± 0.18 cm/s.
100% woodchips	4.76 cm/s ± 0.20 cm/s
50% pea gravel / 50% woodchips (layered)	4.29 cm/s ± 0.22 cm/s $K_{z(eq)}$ = 5.04 cm/s
75% pea gravel / 25% woodchips (layered)	4.59 cm/s ± 0.36 cm/s $K_{z(eq)}$ = 5.18 cm/s
50% pea gravel / 50% woodchips (mixed)	4.09 cm/s ± 0.29 cm/s
75% pea gravel / 25% woodchips (mixed)	4.59 cm/s ± 0.61 cm/s

The values of K summarized in **Table 4-1** for pea gravel generally agree with values reported in the extensive literature on the permeability of gravel. For example, Wilson et al. (1999) fount the average hydraulic conductivity to be about 6.31 cm/s with a range of 5.0 – 7.9 cm/s. Another study (Oveson, 2001) found the average hydraulic conductivity to be about 5.69 cm/s with a range of 4.85 – 7.10 cm/s for three types of gravel.

The values of K_{sat} summarized in **Table 4-1** for wood chips generally agree with values reported in the literature on the permeability of wood chips For woodchip media, Christianson (2010) found the average K_{sat} of a type of woodchips to be 9.50 cm/s, with values ranging between 7.33 and 11.11 cm/s. In another study, Chun et al. (2009) documented hydraulic conductivities of 2.7 to 4.9 cm/s in a laboratory-scale woodchip bioreactor.

For a mixture of pea gravel and wood chips, it was difficult to make a direct comparison with the literature. For example, Christianson (2010) used pea gravel and woodchips in bioreactors for denitrification and found that pea gravel added to wood chips significantly increased the hydraulic conductivity of woodchips used alone, which is in accord with the finding of the present study. However, the values of saturated hydraulic conductivity, K_{sat}, determined by Christianson were much higher than those determined for these experiments. The study provided a good measure of the initial hydraulic conductivity of woodchip media used in denitrification bioreactors, for which it is thought that over several years of bioreactor operation any carbonaceous material will break down altering the hydraulic conductivity of woodchips (Christianson, 2010).

Clearly, the above findings reveal the effects that layering or mixing the pea gravel and woodchips have on hydraulic conductivity. Evidence of this can be observed in piezometer pressure (**Figure 4.5**). The hydraulic conductivity properties of the woodchips had a significant effect not only flow of water but also the “migration” of sediment through the permeameter. As velocity relates proportionally to pressure and

velocity to the square of friction, the significantly reduced pressure in the layer of woodchips indicates a reduced flow velocity, potentially causing sediment particles to accumulate in this layer. A 30% difference in K can have significant effects on sediment accumulation.

Because K_{sat} depends heavily upon the condition of the flow pore structure (i.e. width, continuity, shape, and overall tortuosity) within a medium, it is difficult to relate porosity and permeability or permeability solely to grain size distribution especially in the case of a non-uniform medium (Hillel, 1998). Also, because K_{sat} depends on the permeability of the medium, non-uniform media will have variable hydraulic conductivity, as seen with **Figure 4.1 (a) – (f)**.

For the stated above reasons the average or steady state value of K was used as a baseline condition for the subsequent sediment experiments. The steady-state values of K were used as the initial or clear-water hydraulic conductivity, K_0.

4.2.2 Flow-Rate Tests

These tests had two purposes:

1. Confirm the flow rate readings from the flow meter; and compare them against two other methods; and
2. Find an alternative method to determine the flow rate, because the flow meter was found not to work with the highly turbid water discharged into the permeameter.

Figures 4.2 (a) – (g) show the time series of inflow and outflow rates from the permeameter recorded during the clear water experiments. The outflow rates were determined by three different methods: (1) collecting the flow exiting the permeameter in a bucket during a period timed with a stopwatch; (2) readings from the insertion flow meter; and (3) calculated using the clear water inflow rate and subtracting from it the rate of change of water volume in the head box.

The three different flow rates were determined at the same time step for comparison purposes. The flow rates are in close range of each other, with the calculate flow rate and the flow rate readings from the insertion meter being found to fluctuate less than those determined using the bucket method. All bucket and flow-meter measurements yielded very similar values for tests with clear-water flow, but the runs with sediment revealed a great difference in bucket measurements compared with flow meter readings, shown in **Figure 4.2 (g)**. The high sediment concentration used in this study, created highly turbid water in the outflow from the permeameter and caused the flow meter readings to quickly rise above what was observed during either constant head runs or flow runs.

With the flow meter not able to function correctly during the sediment tests (due to the highly turbid water in the outflow), the manually determined flow rate via the bucket measurements served as a check for the analytically determined flow rate that utilizes the change in water depth in the head box. Accordingly, it was decided that the calculated flow rate could be used for the main sediment experiments and, thereby, resolve the issue of not being able to measure the flow rate.

It was not possible to maintain an absolute constant water depth in any of the runs. Due to unsteady aspects of flow dynamics within the permeameter, the water level in the head box would slowly rise or fall. As prescribed in the Chapter 2, a steady state flow was decided when the rate of increase or decrease of the water level was slow enough to be virtually unnoticeable (less than 0.5 cm to 1 cm) after about 10 minutes. In this manner, it was possible to obtain essentially a steady average value of steady flow rate within the 10 minute time window. **Table 4-2** summarizes the flow rates obtained. It gives the average value and standard deviation of flow rates in **Figures 4.2 (f) and (g)** (Runs 2b and 3) from the bucket measurements only, because the flow meter readings deviated too much from the expected value, and were considered unreliable.

Table 4-2. Summary of flow rates measured using the bucket method.

Experiment #	Flow Rate Measured (gpm)
Inflow 1	18.0
Inflow 2	17.1
Inflow 3	16.2
Outflow 1	17.3
Outflow 2a	17.1
Sediment Outflow Test 2b	17.9
Sediment Outflow Test 3	22.4

These flow rates are comparable to those reported by prior similar studies of flow through a permeameter comprising a gravel medium. For example, Wilson et al. (1999) reported a flow rate of 17 gallons/minute through the rock media of similar size (D_{50} = 13.6 mm) to this study.

The results from this set of runs verify the readings from the flow meter inserted in the outflow pipe by measuring the outflow with a bucket and timer. Bucket and timer measurements provided useful measurements of the inflow rate delivered from the pump, and enabled comparison of the inflow and outflow rates, so as to check that the continuity equation was satisfied for flow through the permeameter. Further, these runs provided a means for determining the outflow rate when the flow meter readings during runs with sediment were determined to be invalid. The main overall findings of these experiments are that an analytically determined flow rate could be used for the main sediment tests. Moreover, the experiments showed that conductivity depends on the permeability of the medium, and that non-uniform media have variable hydraulic conductivity, and thus produce a variable flow rate through each medium.

4.2.3 Reynolds Number and Friction Factor

This section discusses the following parameters and relationships of relevance to clear-water flow through the permeameter and therefore to an ATI:

1. The modified Reynolds Number, Re_*;
2. The Ergun equation (see Chapter 2: Methodology) and modified friction factor, f_k; and,
3. The Ergun graph, indicating the location of Re_* and f_k with regard to the experimental ATI.

Here the particle Reynolds number, Re_*, is defined as

$$\mathrm{Re}_* = \frac{\rho v_s D_{50}}{\mu(1-\varepsilon)} \tag{4-3}$$

where ρ and μ denote the density and dynamic viscosity of water, respectively; ε is the spatially-averaged porosity of the medium, D_{50} is the median particle diameter of the porous medium; and v_s the superficial velocity (equal to Q/A) of flow through the porous medium (v_s is the input velocity as described in the preceding sections).

The following equation from Bird (1960) is a non-dimensionalized form of the pressure drop in fluid flow across a length of porous medium. The friction factor, f_k, is modified for flows through a porous medium, and is defined as

$$f_k = 75\frac{(1-\varepsilon)^2}{\varepsilon^3}\frac{\mu}{\rho \upsilon_s D_p} + \frac{7}{8}\frac{(1-\varepsilon)}{\varepsilon^3} \tag{4-4}$$

where all variables in (4-4) are defined in eq/ (4-3) as well as in Chapter 2.

All the head-loss data points calculated from measurements for the clear water flow and the sediment-laden flow fall within the transitional region of the Ergun plot, nearest to the turbulent regime, as **Figure 4.3 (a)** shows. This result is not surprising, considering that the flow "adjusts" with time as it moves through the permeable bed, disperses or advects sediment depending on the depositional patterns of sediment within

the porous structure of the media. It is reasonable here to assume that the flow initially entering the pea gravel column behaves as if laminar, but as time progresses, flow moves through the gravel, and intrusion of sediment occurs, there is a progression toward the turbulent regime. **Figure 4.3 (a)** shows that the Ergun equation reflects both flow regimes and serves as a good approximation to obtain estimates of friction for the present experiments.

The flows of sediment-laden water can be treated as flows of a fluid more viscous than clear water at the same temperature. The Ergun equation is shown to be a good approximation for flow resistance encountered with the experiments on sediment-laden flow. **Table 4-3** indicates the regime of flow to be transitional, where laminar $Re_* < 10$, transitional $10 \leq Re_* \leq 2000$, turbulent $2000 < Re_*$.

Table 4-3. Calculated superficial velocity, v_s, modified friction factor, f_k, and modified Reynolds number, Re_*.

	$\mathbf{v_s}$ (cm/s)	$\mathbf{f_k}$ (-)	$\mathbf{Re_*}$ (-)
Range	3.0 - 5.9	1.93 - 2.11	422 - 824
Average	4.7	1.98	658
SD	0.13	0.007	17.4

In order to use the Ergun model, for the present experiments, the permeameter's porous column was considered to be a bundle of tubes, such that the friction factor for flow through the column is a function of the effective diameter and length of each tube, the pressure drop (a function of Re_*) down the column, and the so-called superficial flow velocity (a function of the void fraction of the gravel in the column). Since values of pressure drop are a function of Re_*, they were determined over the laminar, transitional, and turbulent flow regimes.

The shear stress for flow through a packed bed was estimated as

$$\tau = \frac{f}{8}\rho V^2 \tag{4-5}$$

where ρ is the fluid density, and V is the velocity of the fluid. In accordance with Bird (1960), the Darcy-Weisbach friction factor for laminar flow can be estimated as

$$f = \frac{(1-\varepsilon)^2}{\varepsilon^3}\frac{75}{(D_p G_0 / \mu)} \tag{4-6}$$

For transitional flow it is

$$f = 75\frac{(1-\varepsilon)^2}{\varepsilon^3}\frac{\mu}{\rho \upsilon_s D_p} + \frac{7}{8}\frac{(1-\varepsilon)}{\varepsilon^3} \tag{4-7}$$

and for turbulent flow it is

$$f = \frac{7}{8}\left(\frac{1-\varepsilon}{\varepsilon^3}\right) \tag{4-8}$$

These relationships, **Eqs. (4-5)** through **(4-8)**, become less accurate and useful as fine sediment gradually accumulates in the gravel-woodchip media, because the characteristics of the assumed equivalent bundle of tubes change. Ranaivoson (2004), for example, suggests that as particle deposition in the filter bed increases, a different relationship should be derived based on standard concepts of filter parameter derivation; head loss across the filter bed is expressed as a function of deposition. Methods of finding functions relating filter coefficient and head loss to deposition can be developed (Ranaivoson, 2004), but this task is beyond the scope of the present study.

Figures 4.3 (b) and **(c)** show the range of f_k versus Re_* values specific to this study, and relates them to the curve developed by Ergun (1952). Values for the clear-water flow runs and sediment runs are represented. The latter set of values shows that values of Re_* are smaller for sediment-laden flow than with clear water flow. Viewed in terms of small-scale flow processes, the sediment-laden water entered the permeameter flowing in the turbulent regime, but sediment deposition gradually contracted the flow paths and, following continuity considerations, acted to increase flow velocity locally.

Viewed in terms of macroscopic flow behavior and increased head loss, however, depositing sediment can be seen to dampen flow turbulence during steady inflow of sediment-laden water. Consequently, values of the superficial velocity, v_s, would decrease with sediment flow compared with the values with clear water only. Since v_s is the macro-scale indicator of velocity through the permeameter, and a function of the overall pressure head (per the Ergun equation), it can be reasoned that local values of flow velocity (the Darcy velocity) are, at some locations where the flow concentrates, actually higher than the macro velocity. During the present experiments, it was not possible to measure such local velocities within the permeameter, although variations were visible through the permeameter's clear Plexiglass column.

From the measured head loss data, it can be inferred that all three flow regimes occurred within the permeameter. This finding certainly is supported by the range of Re_* values in **Table 4-3**. Additionally, all three may have occurred at the same time, but at different locations within the permeameter, as flow likely phased in and out of each regime as variations in sediment fluxes and the local disposition media grains affected local values of Re_*.

While the turbulent flow regime is common for natural flows of water percolating through gravel (Joy, 2010), in the permeameter the estimated values of Re_* indicate a transitional – turbulent regime. For reliable design performance, a permeameter (or ATI) should preferably pass flow in the turbulent flow regime, though not have such high velocities as to cause erosion or scour near and within the permeameter. Transitional flows are notoriously unstable in their characteristics, and therefore are usually not desired for design purposes.

4.3 Sediment-laden Flow Experiments

Considered here are the results of the experiments with the same clear-water flows as described in **Section 4.2**, but now with a constant mass rate of suspended

sediment load added to the volume of water in the head box (fixed input concentration, see Methodology). These experiments examine the effect of suspended sediment on the flow properties, notably hydraulic conductivity, of the permeameter media. Of focal interest is the development of sediment clogging and its effect on hydraulic conductivity over time. For all the experiments, only partial clogging developed. The sediment loads, which correspond to the field conditions of sediment transport, were insufficient to cause full clogging of the permeameter; the magnitudes of the sediment loads correspond to measurements at the field site, and are supported with anecdotal evidence from the landowner of the field site.

4.3.1 Head Box Water Level During Partial Clogging

As sediment accumulated and partially clogged the permeameter, the water level in the permeameter's head box increased so as to offset the increased resistance to flow through the permeameter. This thesis section presents data and observations regarding the following aspects of head box performance when sediment-laden flow was discharged into the permeameter:

1. Time-series of head (water level) increase in the head box as sediment clogging developed in the permeameter;
2. The total pressure difference in the head box for each run;
3. The average rate of head increase for each run; and,
4. The estimated flow regime (laminar, transitional, turbulent) at different stages within each experiment run.

Figures 4.4 (a) and **(b)** present the data obtained with these runs. **Figure 4.4 (a)** shows the time series of the pressure head (water level) in the head box during the six experiments with sediment-laden flow. **Figure 4.4 (b)** shows the calculated flow regime the correspond to the change in flow characteristics observed over these experiments.

Table 4-4 lists the conditions associated with these experiments, which consisted of 2 sets of runs, where a given inflow rate of sediment and water entered the permeameter, and the rate of permeameter clogging was determined. The first set of experimental runs, represented by the blue lines, consisted of four runs. The second set, represented by the green lines, consisted of two additional runs. Although each run began by establishing a constant flow-through rate with clear water, this portion of the test is not included in **Figure 4.4 (a)**. Accordingly, time = 0 corresponds to the beginning of sediment delivery to the permeameter head box. The delivery of sediment was terminated when the permeameter became sufficiently clogged with sediment to cause the water in the head box to back up to the point of almost overflowing. The blue dot represents when the sediment was stopped. The top of the head box is at 48 cm, as shown in **Figure 3.3**.

Table 4-4. Variables for the experimental runs. Note: at the beginning of each run, $Q_{in} = Q_{out}$.

Run	Stop Sediment Feed, $\dot{m}$	Head Box Depth, H	Stop inflow, Q_{in}	Head Box Depth, H	Inflow, Q_{in}	Final Outflow, Q_{out}
#	min	cm	min	cm	gal/min	gal/min
A1	4.52	43.5	4.75	45	17.5	15.9
A2	12.45	38	15.95	45	15.9	15.4
A3	12.67	30.5	35.83	45	15.4	15.3
A4	13.60	23	13.60	23	15.3	15.2
B1	8.70	45.5	8.70	45.5	17.5	16.4
B2	11.28	34.7	21.17	48	16.4	16.2

Each sediment run included three phases. An initial phase was used to establish a constant clear-water inflow rate. A constant flow rate was determined by visually assessing the depth of water in the head box. If the depth was constant relative to the tape measure on the side of the head box for at least a period of 20 minutes, then the flow

was considered constant. The second phase, which immediately followed included the delivery of sediment at a fixed rate to the head box. Sediment was added to the head box at a rate of 17 g/s (determined via generic simulations from WEPP). During this phase, some of the sediment infiltrated fully through the column, while some of it deposited within the permeameter and began clogging it. The depth of water in the head box began to rise as clogging increased. Once the depth of water practically reached the top of the head box, the sediment delivery was terminated and the water-flow rate reduced by adjusting the control valves on the pump. This action began phase three, where clear water at a reduced rate was added to column until the depth returned to the original level, before the next test was begun. The clear water flow flushed deposited sediment from the permeameter.

Video images of the changes of water level (head) in the head box and the pressures in the piezometers were collected while the sediment was added to the head box. These images were analyzed and converted into image sequences using Adobe Premiere Pro software. Each image sequence was then analyzed using ImageJ to obtain the change in water depth in the head box and pressure head of the piezometers along the depth of the permeameter. **Table 4-5** lists the average rate of water level rise in the head box as determined for each run.

Table 4-5. The average rate of head increase in the head box. The sediment concentration used was approximately 17 g/L.

Run A1	**Run A2**	**Run A3**	**Run A4**	**Run B1**	**Run B2**
(cm/min)	(cm/min)	(cm/min)	(cm/min)	(cm/min)	(cm/min)
4.3	**1.52**	**0.72**	**0.11**	**2.93**	**1.27**

Throughout each sediment test, the pressure in the head box increased over time as function of the amount of sediment delivered. **Figure 4.4 (a)** shows the increasing depth of water in the head box for each run following a concave shape until the sediment delivery was cut off, which is represented by the blue dot followed, in some cases, by a change in the curvature of a line to a more convex shape. The convex segment of the curve indicates blockage at the surface, as well as within the column, but with no further addition of sediment. Therefore, the curve makes the characteristic change from concave (fast increase) to convex (slower increase) as the permeameter adjusts itself to the inflow of clear water only. The hydraulic conductivity, K, began to rebound after the sediment delivery was cut-off and clear water flow flushes some of the deposited sediment out of the column. This adjustment process involved flow paths opening up within the regions of sediment accumulation within the permeameter.

The two families of curves show a similar and interesting pattern through the progression of runs. There is an increase in the time that it takes for the flow to backup for each subsequent run. This is seen in the graph with a decreasing slope between the lines in each run sequence. For example, the slope of A2 is less than the slope of the preceding run A1. The reason for this result is that a smaller flow rate is needed to maintain the constant head after a previous run because the porosity of the matrix has been reduced and cannot convey as much fine sediment. The explanation of this common trend can be interpreted from the piezometer readings along the permeameter, and indicates a re-distribution of sediment through the permeameter. The re-distribution of sediment through the permeameter was caused by (1) the flow establishing more efficient flow paths for passing the sediment with each subsequent run; and (2) previously deposited sediment was worked down the permeameter and spread or dispersed throughout, thereby reducing the initial blockage.

Observations of sediment disposition in the permeameter, and the variation in head box water level, infer that Run A1 was in the turbulent flow regime, and that Run

A4 was in a pseudo-laminar regime, where Darcy's law is assumed applicable. Pseudo-laminar implies that a flow regime with a range of Re_* greater than, but near $Re_* = 10$. The initial laminar flow conditions for clear water flow are described using Darcy's law. Further, this law also pertains to the rapid constriction of flow paths by sediment deposition, which causes flow to occur in the transitional-turbulent regime. These trends are shown in **Figure 4.4 (b)**, which plots water level (and thus pressure head) in the head box versus time. This figure is representative of the trends observed for all the runs.

Run A1 backed up the quickest due to the initial shock of sediment clogging the surface of the permeameter. The subsequent runs (i.e., Run A2 – A4) took increasingly longer to back up, because the blockage of the upper-section of the permeameter by sediment began to disperse within the porous matrix. Observations through the Plexiglass column of the permeameter revealed that accumulated sediment tended to gradually descend through the gravel medium. This dispersal was facilitated in part by the period of clear-water flow between the runs, although such dispersal also was observed over time with the sediment-laden flows.

Run B1 is equivalent to Run A1 in terms of the stage of clogging of the porous matrix, as both tests began with a clean matrix. Hence an ATI with a clean matrix (Run A1 and B1) was quicker to clog as the initial shock of highly concentrated sediment "rushing" into the porous surface caused a temporary seal that backed up the inflow. Once the sediment delivery in an individual run was terminated as the flow depth approached the top of the head box, clean water was allowed to run until the flow depth reached a maximum, and the inflow valves were adjusted to re-stabilize the water level at its original depth. The clear water potentially dispersed any sediment plugs that developed from the previous run. The decreased rate of flow backup and rise of water level, V_{rise}, corresponds with the decrease in flow rate, Q, through the permeameter. The decrease in Q reflected the decrease in pore space, ε, in the permeameter. Therefore,

decreasing V_{rise} indicates decreasing ε. The representative example in **Figure 4.4 (b)** depicts the measured trend found for Run B2.

Diffusion of deposited sediment through the permeameter occurred, for the most part, during the clear-water flow period between runs. It is representative of the portion of a storm event (typically near the end of a storm) where sediment is no longer being transported nearly as much as the beginning of an event, which relates to the induction period, when there is a peak in suspended sediment concentration.

As the porous matrix became partially clogged with each subsequent run, its diminished hydraulic conductivity reduced the rate of outflow with each subsequent run. As the outflow rate decreased with each subsequent run, while the mass rate in of sediment remained constant, the outflow conveyed an increased concentration of sediment. This concentration can be determined as

$$C = \dot{m}/Q \tag{4-9}$$

where C is the suspended sediment concentration (g/L), $\dot{m}$ is the mass rate in of sediment (g/s), and Q is the steady state flow rate (inflow = outflow).

The present observations of sediment transport and deposition in a gravel medium showed many of the same features described by Sakthivadivel and Einstein (1970) in their groundbreaking study. For example, they concluded that only certain sediment sizes totally clogged the matrix, while others were deposited only to a small extent without increasing the flow resistance. Observations through the Plexiglass column of the permeameter revealed that this selectivity of particle transport also occurred in the present runs, and that examples of bridging occurred after sediment particles had been retained in a pore by straining, which led to more particles in congesting the pore space. Straining accumulation reduced the effective pore size, and caused subsequent particles arriving at that pore to form a bridge with the particles already retained in the pore space.

The random sediment movement through a vertical porous column suggests that the sediment deposition process in a matrix can be described by probability concepts, as proposed by Sakthivadivel and Einstein (1970). The critical parameter which controls the clogging of the matrix by sediment is the ratio of the typical pore size of the matrix to the sediment size. Sediments with diameter equal to or greater than half the critical pore diameter of the matrix will deposit and in time totally clog the matrix. Sediment with diameter less than half the critical pore diameter will deposit only in the "dead space" of the matrix by the straining mechanism. The initial probability of bridging the pores by sediment depends on the ratio of the pore size to the sediment size (d_m/d_f) and the fluid flow velocity and is independent of the sediment supply rate. The hydraulic resistance of a clogging matrix is represented by an equation similar to the Kozeny-Carman equation for head loss in flow through porous media and is verified experimentally (Sakthivadivel and Einstein, 1970).

For this study, the ratio of the D_{50} of the infiltrating sediment to the D_{50} of the pea gravel was used as a metric of clogging, which was calculated as D_p/D_m = 0.017 mm / 10.33 mm = 0.17% for this study. This relates to the d_m/d_f by Einstein (1970), where sediment with diameter less than half the critical pore diameter will deposit only in the "dead space" of the matrix by the straining mechanism. Schälchli (1995) reported d_{10}/d_m, which is representative of the grain size distribution. If there are relatively smaller pores, and consequently lower infiltration velocities, the fine particles deposit predominantly in the upper part of the subsurface layer – thus a less-deep clogging layer and higher K_{min} results. Both high temperatures and high gradients increase the infiltration velocity, so that the particles intrude deeper into the riverbed, and more fines in total are deposited in the subsurface layer. This results in a lower value for K_{min}.

Sediment concentration was variable throughout the experiment, but it was well within the physical range determined for the field site (i.e. 3 – 50 g/L) (Dermisis, 2007; Wilson, 1999; Ranaivoson, 2004).

The present study's findings also concur with observations reported by Oveson (2001), who found that there was little change in the permeability of the permeameter's gravel medium (in her case, roughly the same diameter of pea gravel) when sediment concentrations were in the range of 13 g/L to 64 g/L; this range coincides with values used in the present runs. The D_{50} of the gravel was 13.6 mm compared with 10.3 mm in this study. However, Oveson found that plugging occurred instantaneously when sediment concentrations exceeded about 200 g/L, although generally both sediment particle size and rock (pore) size have a significant effect on the total sediment mass that can be passed through a gravel core. The loading rate did not greatly influence the mass of sediment that could be loaded into a gravel core before plugging occurred (Oveson, 2001). After 110 kg (245 lb) was loaded into the core the permeability was only 70% of the clear water value and the run was stopped. The trend suggested that it would take a large amount of inflow sediment mass to plug the core. The results of her study, supported by those from the present study, indicated that the sediment size is more important in the reduction of the gravel media permeability than the rate at which the sediment is loaded into the rock media. For example, she found that a reduction in permeability did not happen in cores of pea gravel loaded with sand. The present laboratory results generally support Oveson's findings.

The head-box data were used to determine the rate that the ATI model began to clog, and flow to back up, consequent sediment accumulation. The variation in this rate, and time-to-clogging, helps in determining which clogging mechanisms occurred during the runs. Each curve generated from the head-box, water level data was placed into a family of curves that represents how well the model ATI worked during a simulate runoff event and over a series of such events.

An increase in time-to-clogging corresponds to a decrease in the inflow of the model ATI (permeameter) as the ATI's outflow rate dropped because of partial clogging by sediment. A secondary mechanism causing an increase in time-to-clogging relates to

the diffusion of a sediment congestion or partially formed seal down the permeameter. This sediment seal forms in the column by two means:

1. The initial shock wave of sediment that enters the surface of the permeameter and smothers the surface of an upper stratum in the porous matrix, then eventually migrates into the permeameter; and,
2. A cover of sediment that forms once the flow rate through the permeameter is stopped, allowing water in the head box to drain. The drainage of this water eliminates the hydrostatic pressure holding the sediment deposited in the head box in place, thereby drawing substantial amounts sediment from the surface (the largest deposit of sediment in the entire permeameter) into the top section (i.e. 15 – 30 cm) of the porous matrix,), as shown in **Figure 4.21**.

The cycle of wet and dry periods that usually occur between runoff events (including the simulated storm events used in this study) were carefully considered in the analysis and interpretation of the data produced from the runs. **Figure 4.4 (b)** shows the initial stage of a run with a transitional-turbulent regime flow. As a migratory front of sediment infiltrates the media, the flow quickly transitions into a laminar-transitional regime. The intermediate turbulent region is when there are wormhole-like zones or pathways being created by water flow as it forces its way down through the column of gravel and woodchips (illustrated in **Figures 4.13** and **4.14**). These pathways often corresponded to localized zones of high velocity, as indeed could be seen through the side of the permeameter. The flow enters a transitional region when the sediment delivery is discontinued, but with the clear water flow continuing. The hydraulic conductivity then rebounded, and the sediment in the flow diffused down throughout the column and homogeneously distributed across the column. It is reasonable to assume that the dispersed sediment located throughout the column acted to dampen or reduce flow turbulence, therefore returning the flow to a pseudo-laminar regime. This

discontinued sediment flux may be representative of an actual rainfall event, when there is an induction period and first flush of sediment near the beginning of the event, followed by a period of subsiding sediment concentration towards the end of the event. In real terms, the induction period relates to the early erosion of exposed and more erodible soil, while the latter period relates to the increased resistance to erosion of soil in the vicinity of the ATI (Wilson et al., 2009).

4.3.2 Partial Clogging Effects Observed with the Piezometers

Presented herein are the following results regarding piezometer measurements recorded during partial clogging of the permeameter by sediment:

1. Time-series of head increase in the piezometers;
2. The total pressure difference in each piezometer for each run;
3. The average rate of head increase in each piezometer for each run; and
4. The pressure drop between neighboring piezometers during each run.

Figures 4.5 (a) – (e) show the time-series of pressure in each piezometer over the course of the experiment runs involving sediment-laden flow. In these figures, the y-axis gives the pressure in centimeters, as read from each piezometer over a time step of 0.1 seconds. Each data line represents the pressure profile at an individual piezometer; with pressure tap, P1, at the top, down to P8 at the bottom. The magnitude of pressure corresponds to their physical location over the depth of the permeameter. The black line represents the global pressure, which is calculated from adding the pressure in **Figure 4.4 (a)** to the total depth of porous media in the permeameter.

These data were derived from series of images taken from video recordings of the piezometers during each run. The image analysis software, ImageJ, was used to analyze the series of images, especially measuring the change in height of each piezometer. It is

necessary to note that the duration of Run A3 would have extended beyond the displayed timeline on the plot, but the piezometer measurements for this run were interrupted by camera battery failure.

The pressure increased as function of sediment delivery rate over time. The positive slope increased with height in the permeameter (ATI) column, with piezometers closer to the top of the permeameter indicated faster increases in pressure. Conversely, the further from the top, the slower the increase in pressure observed. Furthermore, between consecutive runs, the global (and local) pressure gradient decreases with each successive run. This result, already mentioned in Section 3.2, occurred because the rate of increase in pressure head in the head box increased at a slower rate with each successive run. Further, the slower rates of pressure head increase enabled each successive test (in each set A and B) to continue for a longer duration; until the water level in the head box reached its maximum limit.

Because little change was observed in the bottom piezometer, P8, during each run, the video camera confirmed that the pressure profile with time was virtually a flat line for all the runs. From **Figure 4.5 (a) – (e)**, it can be seen that the rate of pressure increase in all piezometers (except P8) reduced with each subsequent run. Some piezometers experience greater reductions than did other piezometers, because of sediment redistribution in the permeameter. For example, in Run B2 (**Figure 4.5 (e)**), at times the pressure in piezometer P4 dropped to nearly that at P5. Within the layer of woodchips, piezometers P7 and P8 experience the smallest change in pressure, yet they accumulate greater amounts of fine sediments than the upper piezometers.

The total pressure difference recorded for each piezometer from beginning to end of each run is shown in Table 4-6. The total pressure difference in each piezometer for each run. For each run, the pressure always increased from a starting value recorded for clear-water flow to an eventual maximum value as the sediment inflow caused a backup of flow within the permeameter, increasing the water depth in the head box so as to

produce this maximum value. The pressure difference was calculated by subtracting the starting value from the maximum or final value recorded at each piezometer. The average rate of pressure increase for each piezometer is shown in Error! Reference source not found.. These values were calculated by dividing the total pressure difference for each piezometer by the period of the readings during each run. The % error of a pressure difference measurement was calculated as the pressure difference divided by the total height of water in a piezometer tube. These data advance the work of Wilson et al. (1999), who used a manometer to track the change in permeability of a column of gravel medium, but could not show the detail of results obtained in the present study that used a set of piezometers positioned up the permeameter column.

Table 4-6. The total pressure difference in each piezometer for each run.

Run #	**P1** (cm)	**P2** (cm)	**P3** (cm)	**P4** (cm)	**P5** (cm)	**P6** (cm)	**P7** (cm)	**P8** (cm)
A1	24.11	23.78	23.23	22.06	22.04	19.26	3.60	<< 3.60
A2	28.49	27.45	26.80	25.10	25.06	23.42	5.80	<< 5.80
A3	25.42	23.44	21.62	19.79	19.66	18.05	7.20	<< 7.20
A4				no data				
B1	27.40	24.78	25.07	24.78	23.91	23.33	7.70	<< 7.70
B2	29.50	27.00	25.00	23.90	22.80	20.40	8.55	<< 8.55

Table 4-7. The average rate of pressure increase (cm of water per minute) determined for each piezometer during the runs.

Run #	P1 (cm/min)	P2 (cm/min)	P3 (cm/min)	P4 (cm/min)	P5 (cm/min)	P6 (cm/min)	P7 (cm/min)	P8 (cm/min)
A1	5.14	5.07	4.95	4.70	4.70	4.11	0.77	<< 0.77
A2	1.39	1.28	1.18	1.13	1.08	0.96	0.40	<< 0.40
A3	0.70	0.65	0.60	0.55	0.54	0.50	0.20	<< 0.20
A4	no data							
B1	3.15	2.85	2.88	2.85	2.75	2.68	0.88	<< 0.88
B2	1.39	1.28	1.18	1.13	1.08	0.96	0.40	<< 0.40

The piezometer data was used to locate where clogging was affecting flow within the permeameter column and pinpointing locations of altered conductivity during and between runs. Of particular importance was identifying, over time, the location of the main body of sediment accumulated within the column. The topmost piezometer, P1, was found to be most responsive to clogging development and related changes in head box water level. The piezometers decreased in responsiveness with depth into the pea gravel medium, particularly in the woodchip layer. This trend was visually observed during the laboratory experiments and verified with the collected video data and ImageJ analysis. It occurred for several reasons:

1. The friction loss in the permeameter was least between the head box and P1;
2. The accumulation of sediment began in the upper region near P1 and was greatest there; and.
3. The change of medium from pea gravel to wood chips in the vicinity of P7 and P8 always generated a relatively (compared to other regions of the permeameter) large head loss due to friction, because of the forced changes in flow paths between the two media. This effect, together with their distance below the

locations of sediment accumulation, substantially reduced the responsiveness of these two piezometers.

Not all piezometer locations experienced pressure changes reflecting all phases of the cycle of flow regimes (laminar—turbulent—pseudo-laminar) described in **Section 4.3.1**, or responded similarly as water level change in the head box. When the influx of sediment began, the initial change to the porous matrix was first experienced by the top one or two piezometers, P1 and P2, with delayed effects experienced by P3 and into P4; although these latter two piezometers certainly experienced the change, it was slightly diminished in magnitude, as **Tables 4-6** and **4-7** indicate. This finding lends support to the notion that a slug of accumulating sediment gradually descended through the permeameter. Additionally, the somewhat diminished effect on the lower piezometers, suggests that the slug of sediment disintegrated over the course of a run, and was inclined to disperse homogenously within the permeameter. This notion is corroborated by examining pressure variations across all piezometers.

The pressures in the piezometers relative to their neighboring piezometers were quantified, as **Table 4-8** summarizes, and used to determine the evolution in pressure along the entire permeameter column. **Figures 4.6 (a) – (e)** and **Table 4-8** show that the pressure gradient across piezometers P1 to P8 decreased with each subsequent run, meaning that the difference in pressure between neighboring piezometers decreased with each subsequent run. This information strongly indicates that the permeameter experienced an increasingly homogenized infilling of fine sediment along its length. **Figures 4.6 (a) – (e)** presents the time-series of pressure differentials between neighboring piezometers. At each time interval the pressure in each piezometer was subtracted from the pressure in the piezometer above. These figures reveal that the pressure difference between neighboring piezometers decreased with each consecutive run. In other words, the global pressure gradient along the entire permeameter decreased

with each subsequent run, thereby reflecting the dispersal of sediment down the permeameter.

Table 4-8. Average values of pressure difference between neighboring piezometers.

Run #	**P1-P2** (cm)	**P2-P3** (cm)	**P3-P4** (cm)	**P4-P5** (cm)	**P5-P6** (cm)	**P6-P7** (cm)	**P7-P8** (cm)
A1	12.12	10.44	10.48	9.93	14.06	57.68	33.41
A2	9.93	8.93	8.62	7.81	13.09	64.96	31.36
A3	9.31	7.09	5.16	4.91	10.02	77.45	34.24
A4				no data			
B1	9.69	10.88	9.38	10.35	11.63	48.42	37.65
B2	9.54	7.23	6.63	4.37	10.51	79.58	34.33

4.3.3 Hydraulic Gradient

Presented herein are the time-series of global and local values of hydraulic gradient along the permeameter, i, which directly relates to the depth of water in the head box at the top of the permeameter. As would be expected, variations in the values of i demonstrate that water depth in the head box influences the pressure at each of the piezometers. The values of i can also be interpreted to determine the effects of sediment movement and accumulation within the permeameter. Here, *global* refers to the entire permeameter; in this case, the pressure gradient across the entire permeameter; and *local* refers to a specific location along the depth of the permeameter, particularly at the pressure tap of a piezometer. Also, the initial global hydraulic gradient is designated as i_0 and the final global hydraulic gradient after the sediment run as i.

The local hydraulic gradient at each piezometer compared with the global gradient from the head box can be expressed approximately as:

$$i = \frac{\Delta H}{L} = \frac{H + L_i}{L_i} \tag{4-10}$$

where H is the depth of water in the head box; and L_i is both the height of the permeameter above the port, and the vertical distance of flow to the port. This approximation works around the need to use the pressure in the piezometers in order to calculate the local hydraulic gradient at each port. It also assumes that hydrostatic pressure prevails in the permeameter, and that the minor head loss at the flow entrance to the permeameter is negligible. The low values of superficial velocity of flow, Q/A, (**Table 4-3**) support these assumptions. A more exact value of i results if L_i in the numerator of **Eq. (4-11)** is substituted by the pressure head at each piezometer.

The presence of water (and head, H) in the head box causes the hydraulic gradient, i, to increase with elevation toward the top of the permeameter. Relatedly, as the gradient is highest at piezometer P1, this piezometer was the most sensitive to changes in H. Piezometer P1 consistently responded more quickly to changes in head box water depth.

The initial global hydraulic gradient is i_0 and the final global hydraulic gradient after the sediment test is i. They are defined by **Eq. 4-10**.

This means that, for the piezometers, the sensitivity of each is influenced by proximity to atmospheric pressure (how close it is to the surface).

$$h_L = f \frac{L}{D} \frac{V^2}{2g} \tag{4-11}$$

4.3.4 Hydraulic Conductivity

The values of hydraulic gradient were used in the Darcy equation to determine global and local values of hydraulic conductivity, $K = Q/iA$. The initial value of $K = K_0 = Q_0/i_0A_0$, where i_0 is the initial value of i at the start of a run; Q is the volumetric flow rate (cm_3/s), i is the hydraulic gradient (cm/cm), and A is the cross-sectional area (cm^2) of the permeameter encapsulating the porous media. This section presents the following information related to values of K and K_0:

1. Time-series of global and local values of K are presented for each run;
2. The time-series of global K for consecutive runs, so as to show the overall decrease in K over time, and the rebounds in K with subsequent clear-water flow; and,
3. The variation of K/K_0 during each run.

Figures 4.8 (a) – (f) show the time-series of K over the duration of each experimental run. The results of two sets of runs are shown: Runs A1 – A4 (**Figures 4.8 (a) – (d))** and Runs B1 –B2 (**Figures 4.8 (e) and (f))** at time $t = 0$, $K = K_0$. Also, because i_0 was least for the deepest piezometer location (P8), the value of K0 was highest for this location.

In **Figure 4.8 (a)**, if time plotted on a logarithmic scale, it would reveal practically an instantaneous drop in K from the clean media, K_0, and eventually leveling toward a value associated with sediment movement through the permeameter. This initial drop in hydraulic conductivity at the beginning of the run is due to the wave of sediment that initially smothered the surface of the permeameter when the sediment flow began.

The shape of the curve for each piezometer is similar for all piezometers, but the gradient itself changes significantly. This plot shows that, at the beginning of the test, the top two piezometers (i.e. P1 and P2) experience the largest negative slope. At the deepest piezometer, P8, there is a steeper decrease in hydraulic conductivity, but the percentage

decrease (15% for Run A1), is less than for the upper piezometers (e.g., for P1 it is 35%). This is due to the initial wave of sediment that temporarily forms a partial seal near the surface of the intake. Throughout the test, the slope levels off until the bottom layers accumulate more sediment, which is delayed by the long and tortuous travel path that the sediment and flow must travel down the permeameter. Nearing the end of the test, the slope becomes steeper for piezometers near the bottom (e.g. P7 and P8).

The spacing between the curves for each piezometer is governed by an exponential relation attributable to the effect of the head loss through the permeameter and the rise in head box water depth, H, felt over the length of the permeameter, as expressed in **Eq. (4-11)** and the Darcy equation. This relationship reflects the clogging mechanisms that develop earliest higher in a deep column of gravel medium and, therefore, are felt greatest as reduced hydraulic conductivity in the highest layers of the medium. In other words, the higher pressure differential at or near the surface means there is a higher range in K values at these upper piezometers. Again, it is worth noting that the duration of Run A3 would extend beyond the displayed timeline on the plot, but the data was cut off due to camera battery failure.

Table 4-9 displays the K_0 and K values for each run. The values indicate that the rate of decrease in K reduces across a series of runs. The initial reduced pore space in the upper permeameter drastically decreases K, reducing Q for the next run, which in turn slows the rate of clogging, and increases the settlement of sediment at the surface in lieu of infiltrating deeper into the permeameter (or ATI in the field). It is as if a positive feedback loop is generating increasingly favorable conditions for settlement at the surface than through the permeameter. All the while, the rate of clogging decreased to a steady state value as Q decreased, thereby transporting less sediment. The values of K did not drop to as little as 10% of its clear-water value, which would render the permeameter practically useless, as defined by prior studies (e.g., Wilson et al., 1999).

It is useful to show the permeameter performance for a series of cycles of sediment-laden flow followed by clear-water flow, as may occur in the field. **Figure 4.9** shows a plot of K determined for consecutive experimental runs of sediment-laden and clear-water flows. Here the global trend over the full series shows K decreasing gradually with each cycle, albeit at an increasingly slower rate. It is evident that the K was far from reaching the minimum value, $K_{min} = 0.10K_0$.

Observations through the permeameter's clear Plexiglass sides revealed steady-flowing amounts of fine sediment moving down toward the bottom of the permeameter as the set of runs progressed. Relatedly, highly concentrated amounts of fine sediment could be seen creeping along the bottom of the clear Plexiglass outflow pipe, downstream of the permeameter, as the run progressed. In the outflow pipe, the bed load of sediment moved in the form of dunes, made up of coarser sediments that passed through the porous column.

Each subsequent run clogs at a slower rate. This finding means that, at lower flow rates, the permeameter is slower to clog; or at higher flow rates, the permeameter is quicker to clog. The higher flow rate of sediment-laden water contributes significantly to the shock accumulation of sediment forming at the top of the permeameter, choking and backing up the flow. Since the inflow water is always clear, this aided in flushing-out the gravel and prolongs the permeability.

Figure 4.10 shows a plot of K/K_0 plotted versus depth down the permeameter column for an example run, Run B2. The piezometer locations correspond to elevations at 15 cm intervals (e.g. P1 = 15 cm, P2 = 30 cm, …, P8 = 120 cm). This figure also displays curves of K/K_0 at several stages of the run's duration, using the 0, 25, 50, and 100 percentile values of K/K_0 over the course of each run:

- at the initial stage; $K = K_0$;
- 25% into the duration, $K = K_{25}$;
- 50% into the duration, $K = K_{50}$;

- 75% of the duration, $K = K_{75}$; and,
- at the end of the run, $K = K_{100}$.

Values of K/K_0 were computed at each piezometer depth over the course of each run. The overall trends were the same for all the runs. This **figure** shows that the largest decrease in conductivity occurred at the surface of the permeameter, and the lowest at the bottom of the permeameter. The K/K_0 trend exhibits an exponential decrease conductivity with elevation in the permeameter. This corresponds with **Figure 4.18** where the second largest mass of sediment in the permeameter was found near the surface (with the largest accumulated in the woodchips).

It is useful to compare the findings from the present study from the perspective findings from prior studies on sediment movement through gravel or crushed rock media. Such comparison indicates that the present findings are supported by prior studies. For example, according to Mays and Hunt (2003), clogging depends on fluid velocity. Given a set specific deposit, σ (volume of deposited particles per total volume of porous media), constant-flow experiments conducted at higher fluid velocity clog much less (Mays and Hunt, 2003). Wu and Huang (2000) refer to σ as the specific deposit. The "high" velocities reported by Mays and Hunt (2003) are on the order of 0.1 – 0.6 cm/s. The velocities in the present study (i.e., 3.8 – 4.7 cm/s) qualify as high velocities. As the flow rate is decreased with each subsequent run, the rate of clogging occurs at an increasingly slower rate. It is assumed by Mays and Hunt that σ is exponential with depth with high velocity flows, which is supported by **Figure 4.10**. With constant head boundary conditions, the fluid velocity drops as clogging proceeds (as in **Figure 4.3**). Mays and Hunt (2003) concluded that (1) hydrodynamics are important during clogging; (2) deposit morphology is the key factor, while depth of particle penetration is secondary; and (3) their model can be extended to clogging with constant head boundary conditions.

As K varied with depth along the permeameter, it was possible to develop a qualitative relationship using the spacing between piezometers. The relationship also

links to void ratio or porosity in terms of useful pore spaces, which ties into the suggestion made by Schälchli (1995). Also, to be considered are the influences on K exerted by increase in friction, and the occurrence of non-Darcian flow in the permeameter; the calculations of Re_* based on Ergun (1952) indicate non-Darcian flow occurred. Further evidence for non-Darcian flow in the media stems from the relatively large flow velocities calculated for the runs. In these cases, the hydraulic gradient would then no longer be $\Delta H/L$, which is better described as a measure of permeability. The horizontal axis in **Figure 4.10** is then simply a relative measure of flow rates (Wilson et al., 1999). Permeability was estimated from a Darcy-type equation: $K = Q / (A(H/L))$.

4.3.5 Inflow-Outflow Hydrographs from Experimental Runs

The results from each experimental run have been summarized in **Table 4-9** and with an example inflow-outflow hydrograph in **Figure 4.11**. The inflow is represented in blue and the hydrograph is rectangular due to the inflow rate being constant. The outflow hydrograph is represented in red and there is a decrease to a certain point before a slight increase. This is an error related to the method in which the outflow rate was calculated.

The outflow curve decreases (as it should), but then begins to increase. This is because the time-series of Q_{out} is calculated by $Q_{in} - \Delta Q = Q_{out}$, where Q_{in} is the inflow rate, ΔQ is the rate of change of Q_{out} calculated by the change in volume (by the head) over each time step. The reason why we can get Q_{out} to decrease (concave curve) consistently is because the ΔQ keeps increasing. However, when ΔQ begins to decrease, Q_{out} begins to increase, since Q_{in} is fixed.

Table 4-9. Summary of results.

Run	Stop Sediment Feed, $\dot{m}$	Depth, H	Stop Inflow, Q_{in}	Depth, H	Inflow, Q_{in}	Final Outflow, Q_{out}	i_0
#	min	cm	min	cm	gal/min	gal/min	-
A1	4.52	43.5	4.75	45	17.5	15.9	1.20
A2	12.45	38	15.95	45	15.9	15.4	1.13
A3	12.67	30.5	35.83	45	15.4	15.3	1.16
A4	13.60	23	13.60	23	15.3	15.2	1.17
B1	8.70	45.53	8.70	45.53	17.5	16.4	1.14
B2	11.28	34.7	21.17	48	16.4	16.2	1.17
Run	**i**	**K_0**	**K_n**	**K/K_0**	**C_0**	**C_n**	**C_0/C**
#	-	cm/s	cm/s	-	g/L	g/L	-
A1	1.37	4.64	3.7	0.80	15.4	16.9	0.91
A2	1.36	4.35	3.6	0.78	16.9	17.5	0.97
A3	1.36	4.27	3.58	0.77	17.5	17.6	0.99
A4	1.19	4.17	4.05	0.87	17.6	17.7	0.99
B1	1.35	4.85	3.88	0.80	15.4	16.4	0.94
B2	1.39	4.46	3.72	0.77	16.4	16.6	0.99

4.3.6 Mechanisms of Clogging

Two sets of experiments were performed in order to simulate the effects of clogging on the porous media:

1. Volume displacement in the head box (sediment bag) experiments; and
2. Surface blockage (bucket lid) experiments

The sediment bag experiments were conducted to determine the effects of deposited sediment presence on water volume displacement in the head box and, therefore, on the rates of water inflow to the permeameter and eventually the outflow from it. Sediment presence in the head box potentially affected the inflow of water and sediment to the permeameter. These experiments involved placing in the head box a sequence of sealed plastic bags filled with the same sediment used in the experiments.

The bags were 1 liter in volume, and weighed 1.7 kg each. Three of these bags approximately represent the amount of sediment deposited in the head box during a run, the actual amount ranged about 4 to 6 kg, with 4.3 kg being the average from series eight experimental runs, which are described further in **Section 4.3.7**.

Four experiments were run with up to ten 1-liter bags of sediment placed in the head box. It was found that the addition of each 1 liter bag of sediment caused approximately a total rise of 1 cm in the head box for the first four to five bags, with no noticeable rise in water level after the addition of the 6^{th} bag. This means the head increased about 4-5 cm from the initial level with the addition of all 10 bags – more than three times the amount of sediment that would settle out in the head box. This is outside the determined range of error of 2-3 cm due to Q_{in} approximately equal to Q_{out}, as mentioned in **Section 4.2.2 (flow-rate runs)**. What was interesting was that, with the bags of sediment left in the head box, the water level would rebound (reduce) back to ~1 cm above the original depth. This means a self-correction in water level occurred and the flow had reached a "new" equilibrium (coinciding with the original depth). As a supplementary experiment, two-gallon buckets of water were added to the head box in order to observe the effects on the water level. Again, highly similar results were obtained when the water level in the head box self-corrected back to its original depth.

Next, a series of surface blockage experiments using bucket lids were conducted, where three bucket lids, each with a different orifice size cut through the center with a hole-saw, were placed over the entrance to the column of porous media, known as the annulus. These experiments sought to mimic sediment presence to equivalent flow openings through the permeameter column; the bucket lids conveniently fitted within the head box. Once a bucket lid was placed over the annulus, the water level in the head box was recorded at set time intervals to determine the rate of increase for comparison to the sediment tests. **Figure 4.12** shows three groups of curves, each generated by placing a lid with a different sized orifice over the entrance to the permeameter.

A significant difference was found between the shapes of the curves from these experiments with those from the sediment experiments. The data from the bucket lid experiments yielded convex curves (**Figure 4.12**), indicating a slower rate of increase in water level in the head box; whereas the data from the sediment experiments yielded concave curves (**Figure 4.4 (a) and (b)**), indicating a faster increase in water level in the head box. However, once the sediment delivery to the head box was cut-off, the shape of the curve tended to become convex, indicating some difference. These bucket lid tests allowed a decomposition of the different mechanisms of clogging (e.g. **Figure 4.16**) that occur with rates of intruding sediment to the surface and subsurface of porous media.

The results from the volume displacement experiments, using bags of sediment, led to the hypothesis that volume displacement in the head box has very little effect on the rate of water level increase in the head box, as determined by (i) placing bags of sediment with known volume and (ii) pouring water of known volume. Both head box and piezometers were checked. The results of the surface blockage experiments by the bucket lids, showed that the blockage from the surface of the ATI model had great effect on the ability of the porous structure to convey the flow of water.

The same image analysis procedure that was used to analyze the videos of the experiment runs with sediment was used for the experiment runs with the bucket lids, but due to time constraints, only one was performed in order to verify the shape of the curves shown in **Figure 4.12**. The average rate of increase of the water level in the head box from the runs with the bucket lids (**Table 4-10**) can be compared with the runs from the sediment experiments (**Table 4-5**); for example, the rate of water level increase for the 1-inch orifice can be compared with Run A1, the 1.25-inch orifice can be compared with Run A3, and the 1.50-inch orifice can be compared with Run A4.

Table 4-10. Average rate of water level increase for each type of bucket lid orifice.

Run	1.50 inch orifice	1.25 inch orifice	1.00 inch orifice
#	Average rate of increase (cm/min)		
1	0.19	0.45	3.94
2	0.17	0.55	4.12

The simulated clogging at the surface was done to isolate the mechanisms of clogging (e.g. **Figure 4.16**) at work during each sediment experiment. It was designed that a orifice cover (bucket lid) will match a rate of head increase from a particular sediment run with a different orifice cover that matches the rate of head increase from another (e.g. subsequent) sediment run.

As the bucket lid runs were performed with clear water, the flow meter was able to be used. As such, the outflow rates from these runs were also used to verify the calculated outflow rate from the runs with sediment. The bucket lids are most likely an over-estimation of what we see with sediment infiltration, but they yielded estimates of equivalent flow openings during the runs. It can be said that for Run A4, the integrated diameter of all tubes in the bundle is equivalent to the 1.5-inch orifice bucket lid. Run A1 is approximately equivalent to the 1-inch diameter bucket lid, or about 20% (1.00-inch opening divided by the original 6.25-inch opening of the annulus) of clean media conveyance.

4.3.7 Sediment Deposits by Layer

The experiments enabled the mass of sediment to be determined for each layer of medium in the permeameter. This section presents the following data:

1. The mass of accumulated sediment accumulated in the permeameter and its layers; and
2. The trapping efficiency (%) of the permeameter and its layers.

Table 4-11 lists the overall values of sediment mass entering and accumulated in the permeameter as well as the trapping efficiency of the permeameter. This latter value is calculated from the mass measurements. The characteristic of the trapped sediment and sediment passed through the permeameter could be determined with diagnonsis of sediment trapped in the permeameter or passing through it. It was observed that the sediment passing the permeameter did not necessarily appear finer in particle size than that entering it. Such diagnostics were done for the present study, and are recommended as a further topic of investigation regarding ATI performance.

Table 4-11. The mass of sediment accumulated in the permeameter (kg) and the filter efficiency (%).

estimated sediment delivery (kg)	167.7
deposited sediment (kg)	7.5
total sediment passed (kg)	160.2
trapping efficiency (%)	4.5

The values in **Table 4-11** are the result of sediment accumulation after a series of 8 consecutive experimental runs conducted on the same batch of pea gravel and woodchips. The purpose of this was to determine the effects of consecutive simulated storm events encountered in the field on the model ATI (permeameter). It was not

possible to retrieve the collected/accumulated sediment after each individual run because this would remove the very media (pea gravel and woodchips) being put to the test under a constant loading of highly concentrated flow with sediment. As such, the values represented in **Table 4-11** do not reflect the measurements from Runs A1 – A4 or B1 and B2, which is the central focus of this study. For these runs, however, it is safe to assume that the trapping efficiency listed in **Table 4-11** is representative as the global conditions in the permeameter are identical. It is hard to match identical porous structure at the microscale in the permeameter although the differences are not expected to be significant.

The trapping capacity, or the total amount of sediment that can be collected by the model ATI (permeameter), was not able to be determined. This can be considered fortunate for the objectives of this study, where the ATI itself must function as a hydraulic intake (albeit, increasing the capability of flow attenuation compared to the conventional intake) above its function at trapping sediment. This by and large can be attributed to the ratio of D_{50} of the infiltrating sediment to the D_{50} of the porous media, D_p/D_m. The pea gravel is poorly graded (or well-sorted in geological terms) and has a relatively large D_{50} compared with most gradations of sand, which is considered to be more of a *filter* medium, which classes the pea gravel as more of a *drainage* medium.

Photographs and observations from the experiments are used here to provide substantial support for the measurements in **Table 4-11** and the many of the statements throughout this chapter. For example, **Figure 4.18** shows the visible intrusion of sediment from the surface at the end of Run A4. This was caused by the seal that forms once the flow rate through the permeameter is stopped, allowing water in the head box to drain. The drainage of this water eliminates the hydrostatic pressure holding the sediment deposited in the head box in place, thereby drawing substantial amounts sediment from the surface (the largest deposit of sediment in the entire permeameter, as shown in **Figures 4.20 and 4.21**) into the top section (i.e. 15 – 30 cm) of the porous matrix.

This relates to the relative hydraulic conductivity, K/K_0, in **Figure 4.10**, where the value of K/K_0 was determined at each piezometer.

There was no direct way of determining the hydraulic retention time for the different configurations of the wood chips but this could be explored in future research using the hydraulic conductivity.

A matter of practical importance is the likely design life of an ATI. The laboratory results described in this chapter enable an approximate estimate to be made, at least in terms of years or rainfall events of given intensity and probability of exceedance (or return period). Such an estimate requires an assumption about the ATI condition at the end of an ATI's working life. A simple assumption made here is that an ATI would cease to be functional when it becomes totally clogged with sediment, and when the pressure gradient along the ATI equals 0 (i.e., i = 0). In other words, for the present permeameter setup, all piezometers down the permeameter would reflect about the same pressure at each depth along the permeameter and the entire porous structure will be silted-up. **Figure 4.24** suggests, based on trends extrapolated from the present experiments, and using simulations with WEPP, that the model ATI would last 75 event simulations with concentrations of suspended sediment comparable to that used in the main set of experiments of this study. It is acknowledged that this estimate is approximate and uses a fairly frequent storm of moderate-high intensity (10-year event). A source of uncertainty in this estimation concerns the sediment variables that influence clogging; i.e., the concentration of sediment in a flow (relates to ground/crop cover and soil erodibility), and the particle size distribution of sediment entering the ATI (this relates to D_p/D_m as a factor of clogging). These variables differ with installation site. Low concentrations of sediment could lead to the design life of the ATI being on the order of hundreds of years, which is unrealistic. Then again, small storm events could generate flows with high concentrations of suspended sediment, as described in Chapter 2 (Methodology). The concentration of suspended sediment depends heavily on the ground

cover, and so another consideration is the occurrence of a storm and the relative stage of a growing season. A refined estimate requires more accurate assumptions regarding the number of storms each year that would generate suspended sediment concentrations near 17 g/L or higher, such as used in the present experiments. It is noteworthy for working life estimation of an ATI, that a 100-year continuous simulation with WEPP yielded a mean sediment concentration of 6.8 g/L (harmonic mean = 4.1 g/L because it is a log-normal distribution), minimum of 0.7 g/L, and a maximum of 30.6 g/L. Out of all events, 6.32% yielded a concentration large enough to challenge the sediment capacity of an ATI model.

The present estimate of approximate duration of working life, however, does indicate the feasibility of ATIs as a means for managing sediment erosion on farmland.

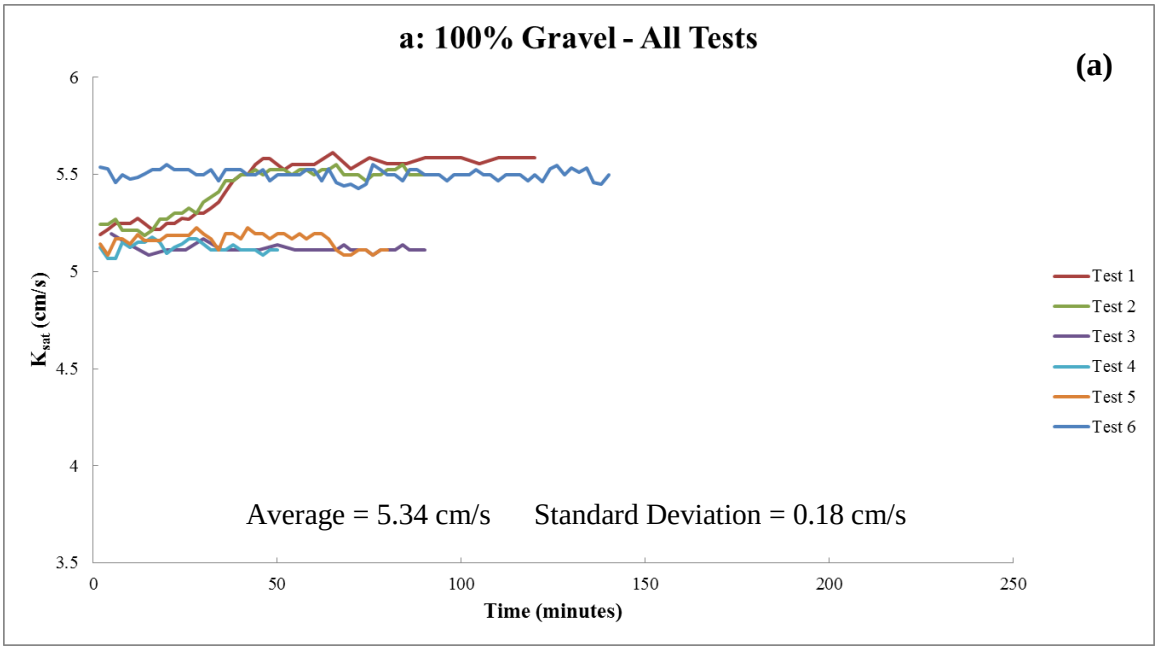

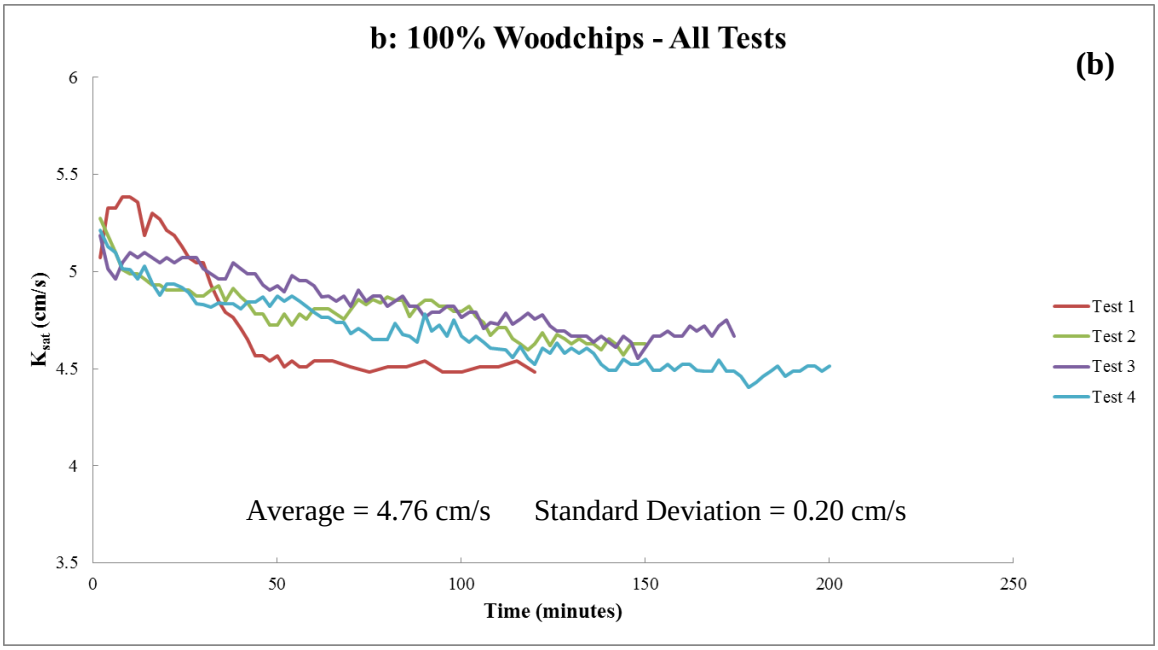

Figure 4.1. Time-series of the hydraulic conductivity, K. (a) 100% pea gravel medium; (b) for 100% woodchip medium. (c) Layered combination of 50% pea gravel and 50% woodchips. (d) Layered combination of 75% pea gravel and 25% woodchips. (e) Mixed combination of 50% pea gravel and 50% woodchips. (f) Mixed combination of 75% pea gravel and 25% woodchips.

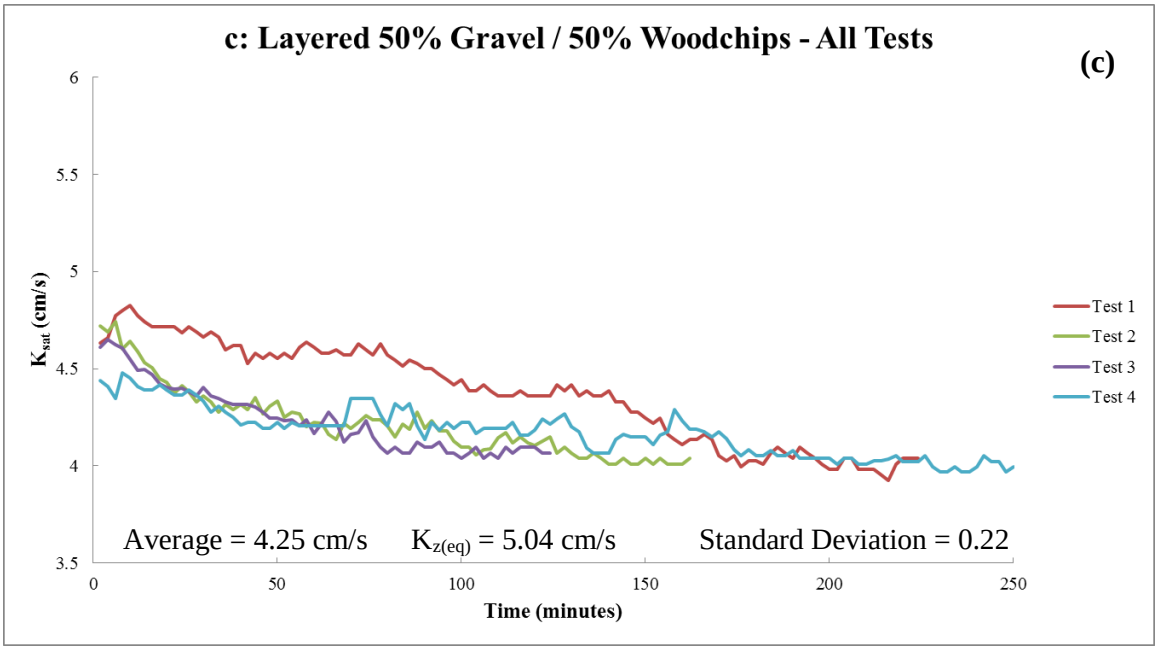

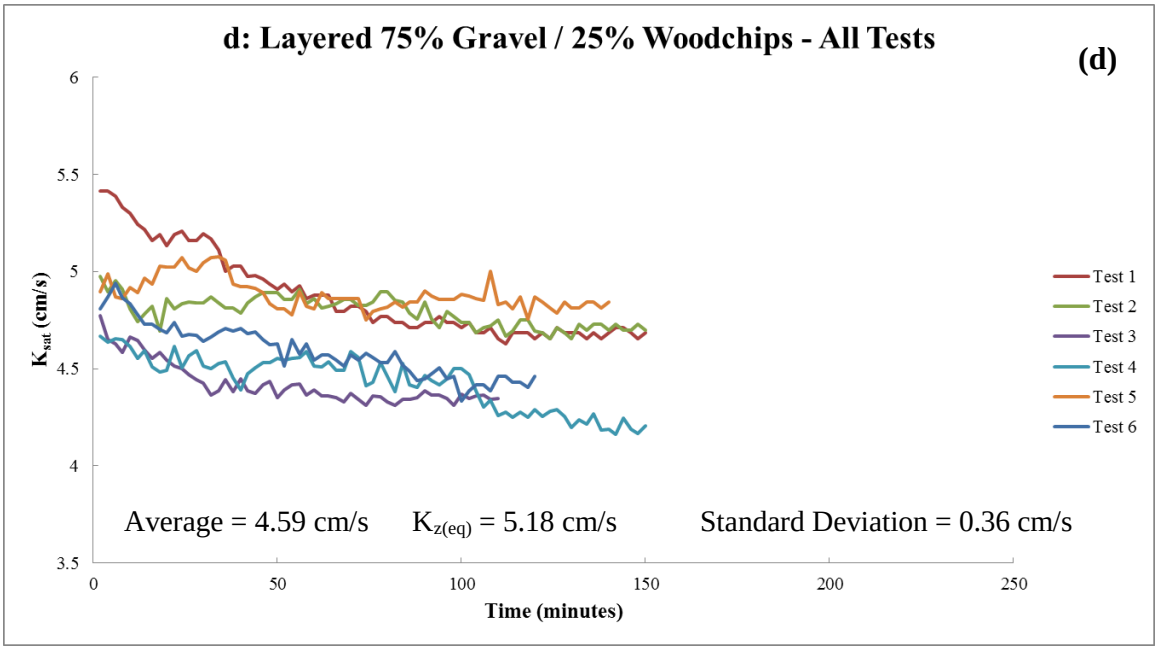

Figure 4.1. Continued.

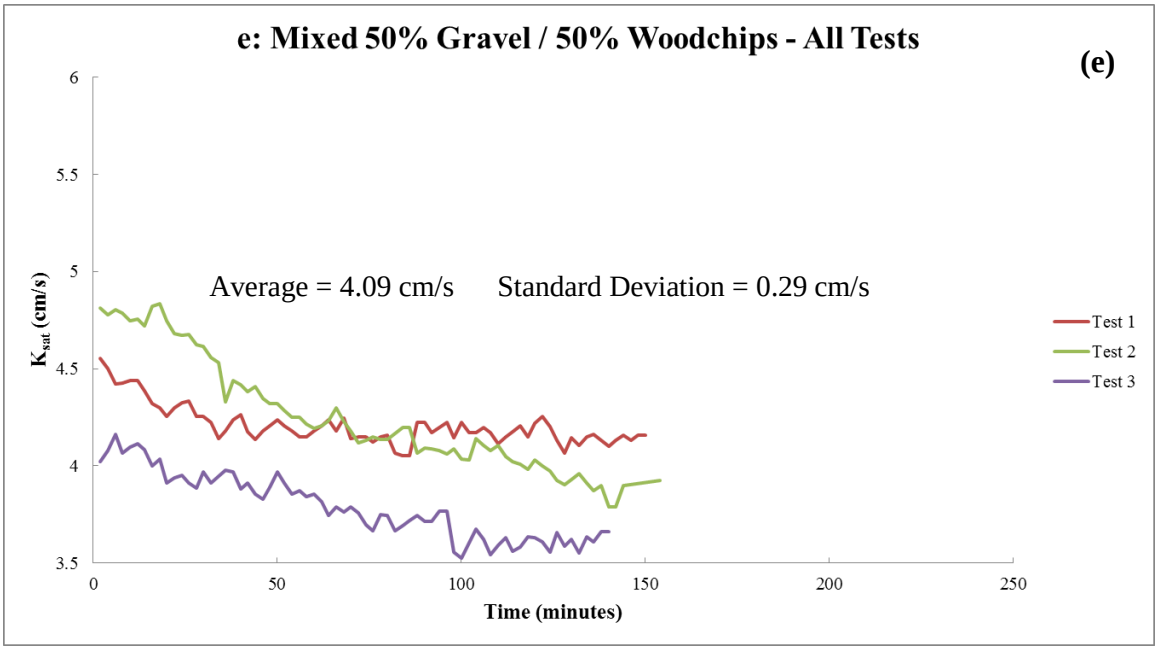

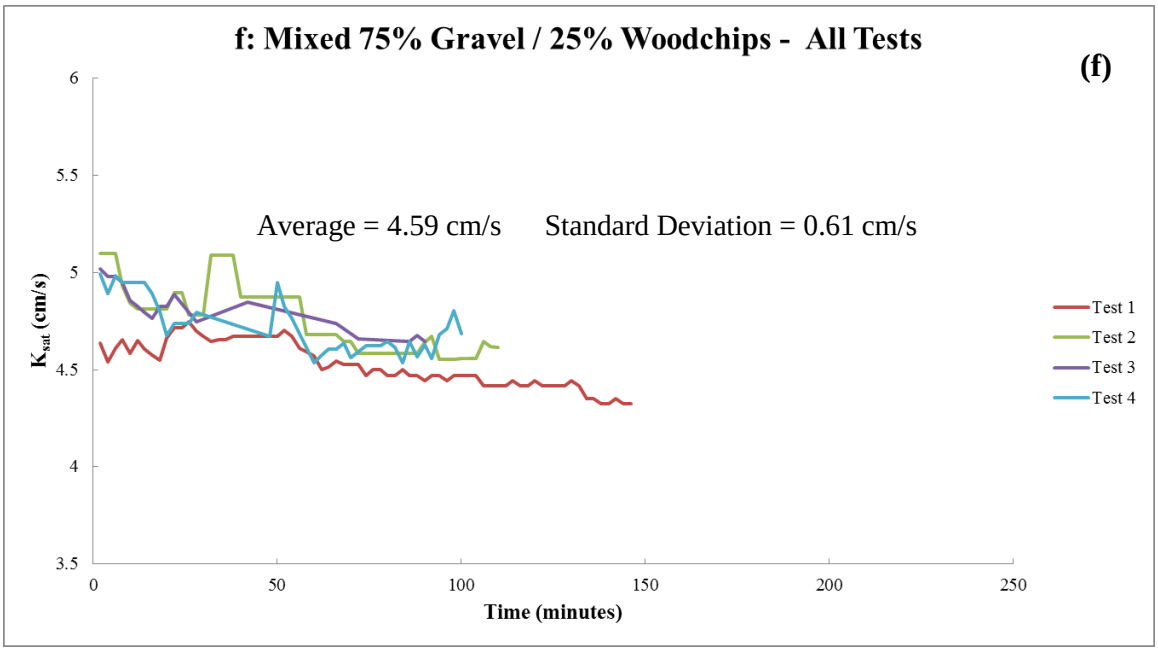

Figure 4.1. Continued.

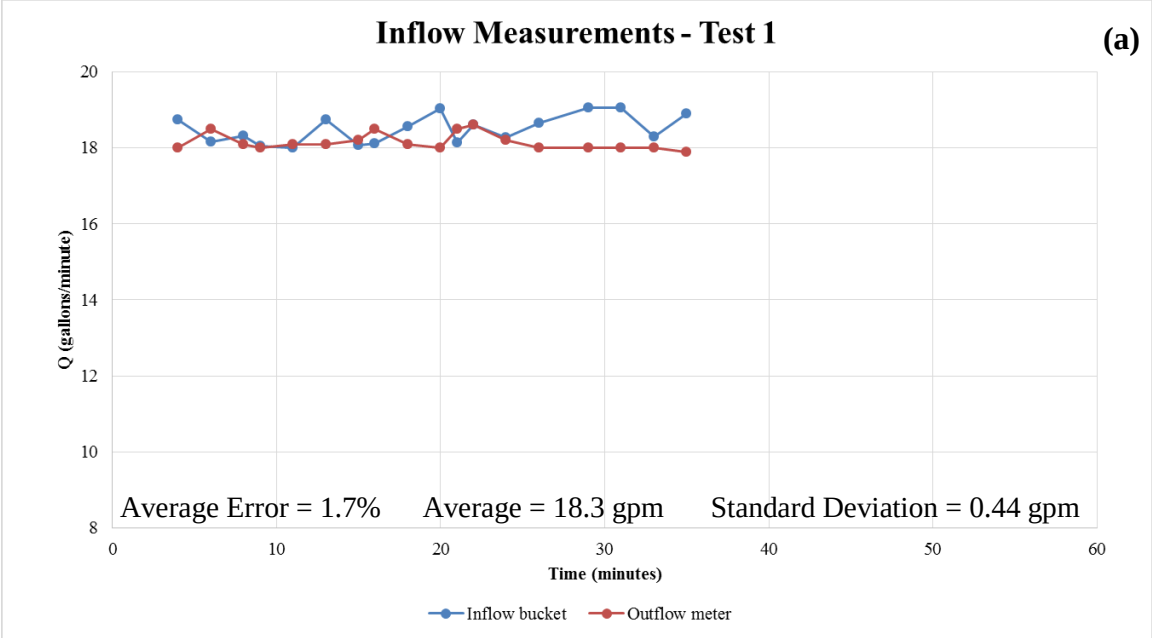

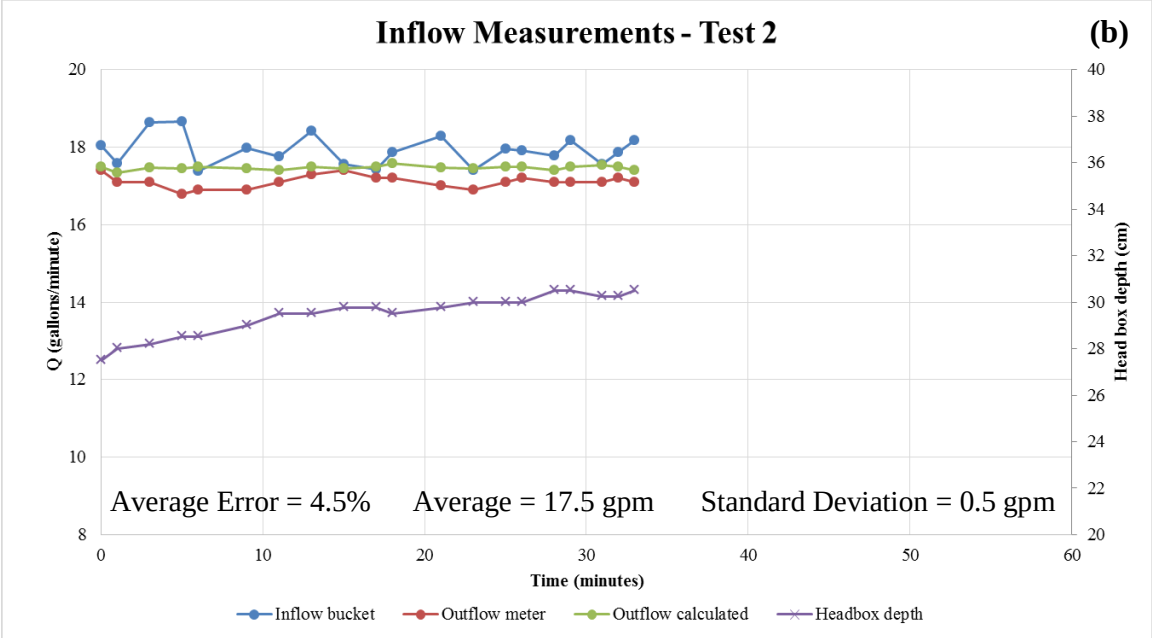

Figure 4.2. Time-series of measured and determined inflow and outflow rates. (a) Clear-water inflow rates (Test 1). (b) Clear-water inflow rates (Test 2). (c) Clear-water inflow rates (Test 3). (d) Clear-water outflow rates (Test 1). (e) Clear-water outflow rates (Test 2a). (f) Sediment-laden outflow rates (Test 2b). (g) Sediment-laden outflow rates (Test 3).

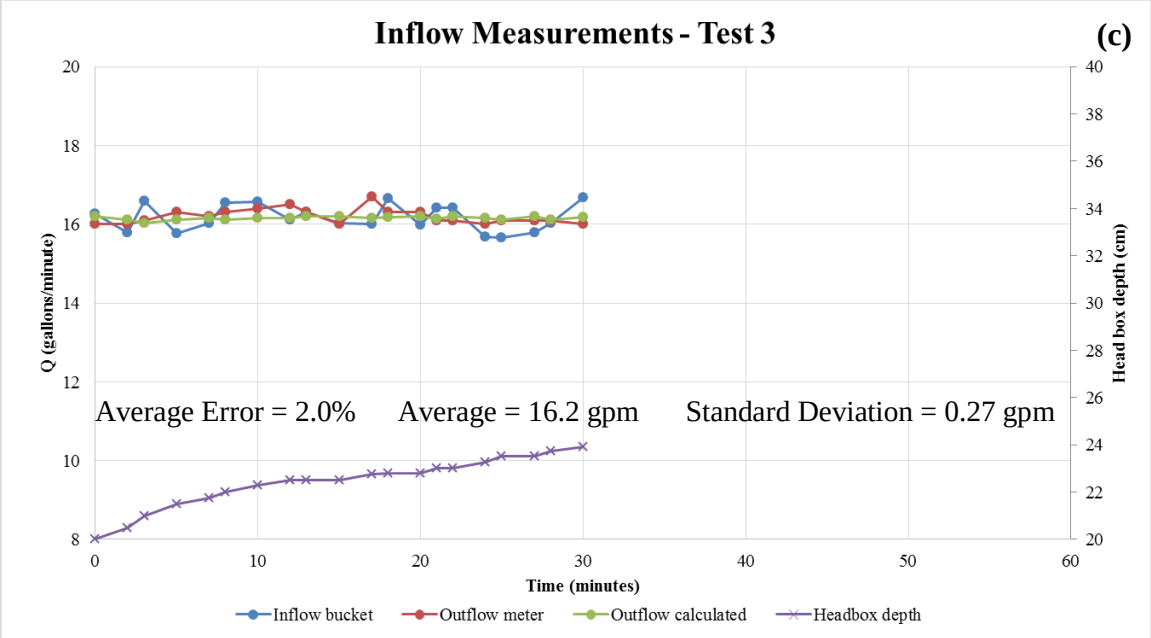

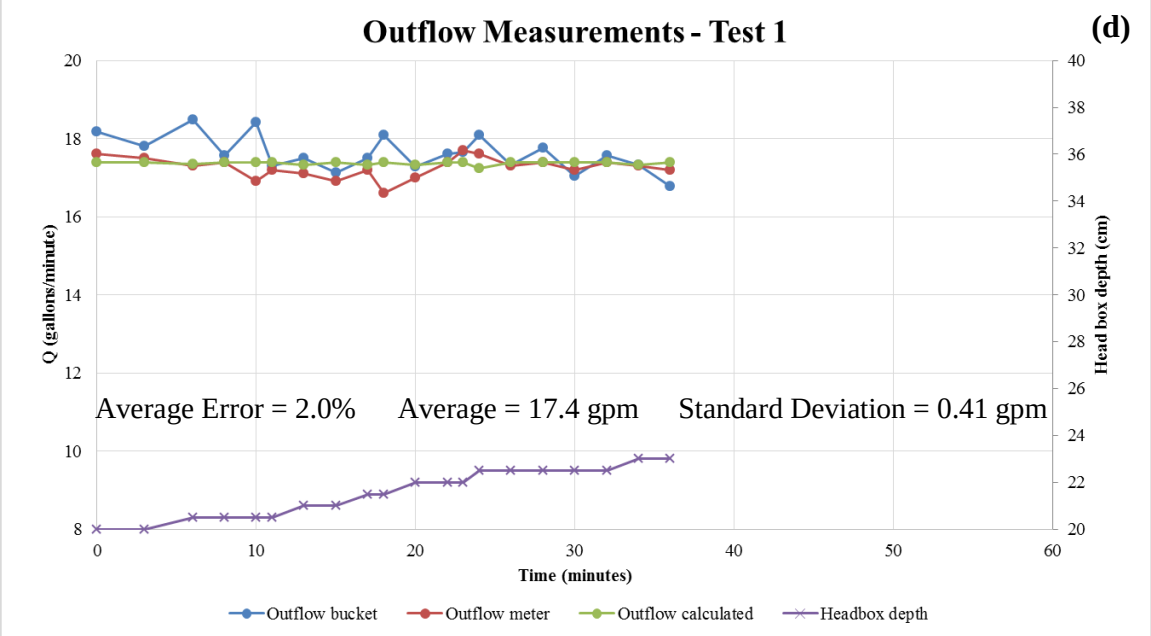

Figure 4.2. Continued.

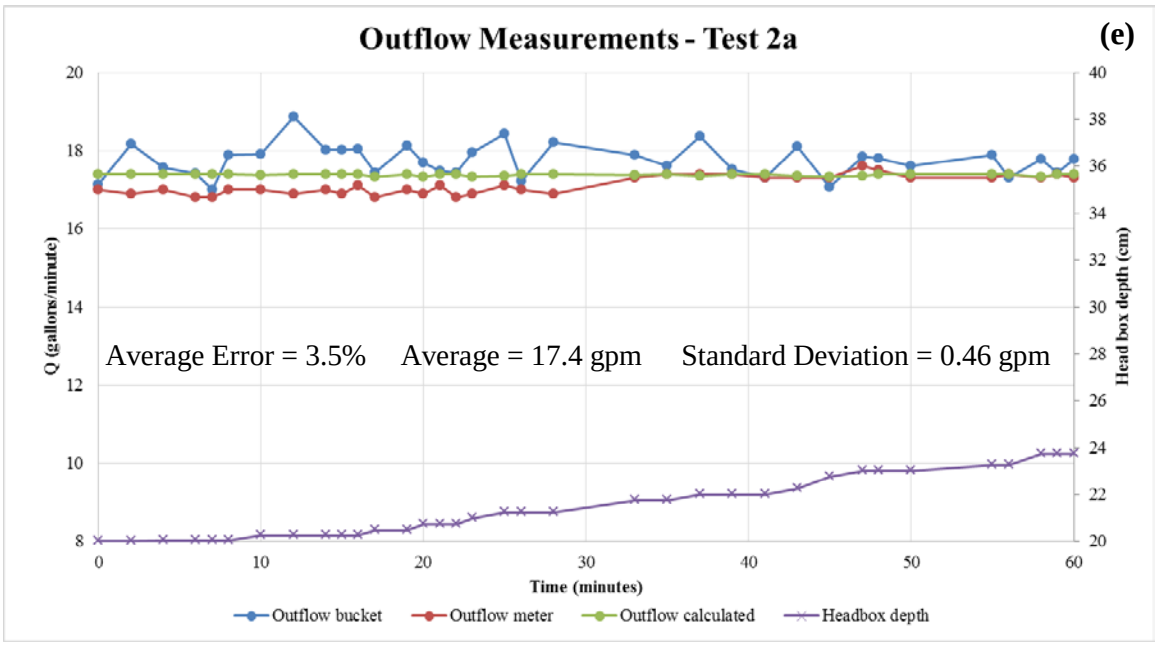

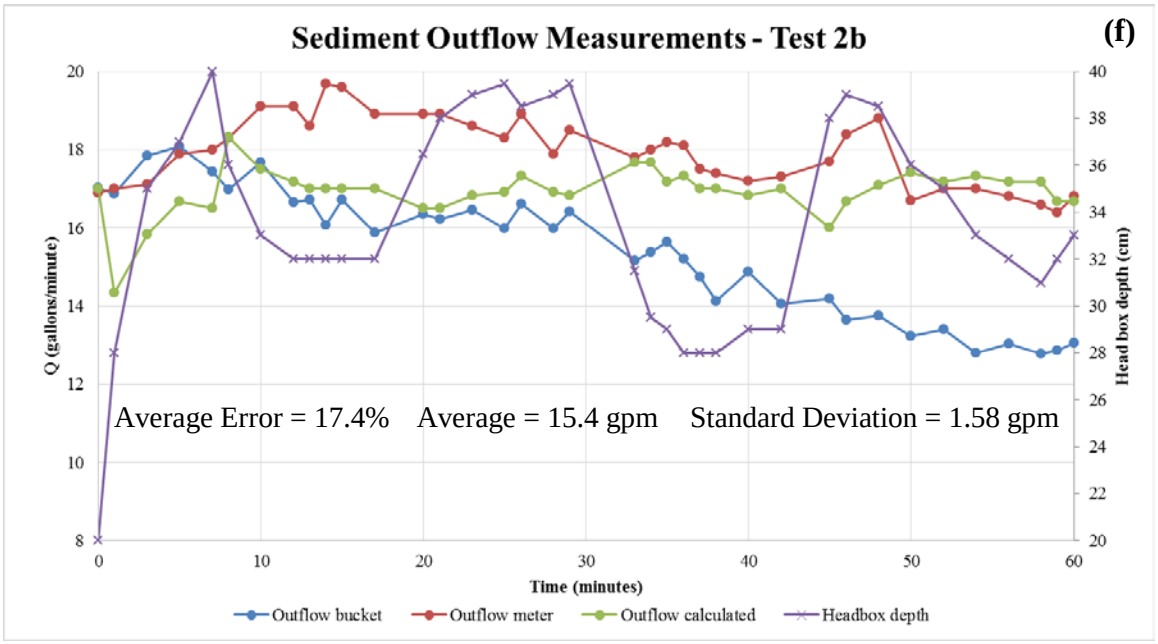

Figure 4.2. Continued.

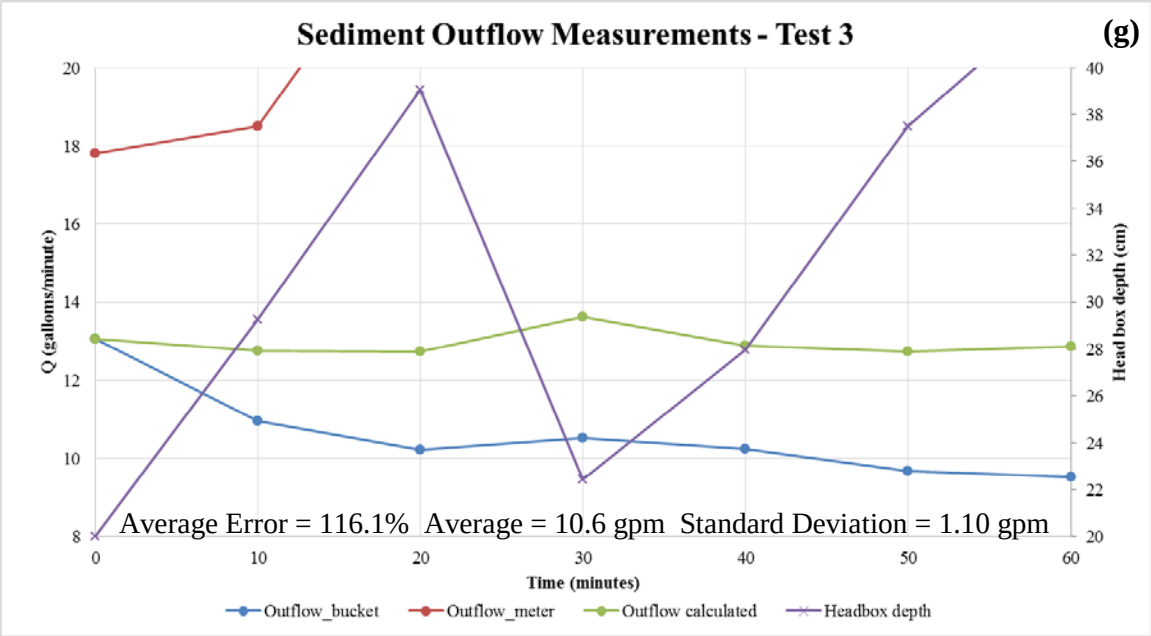

Figure 4.2. Continued.

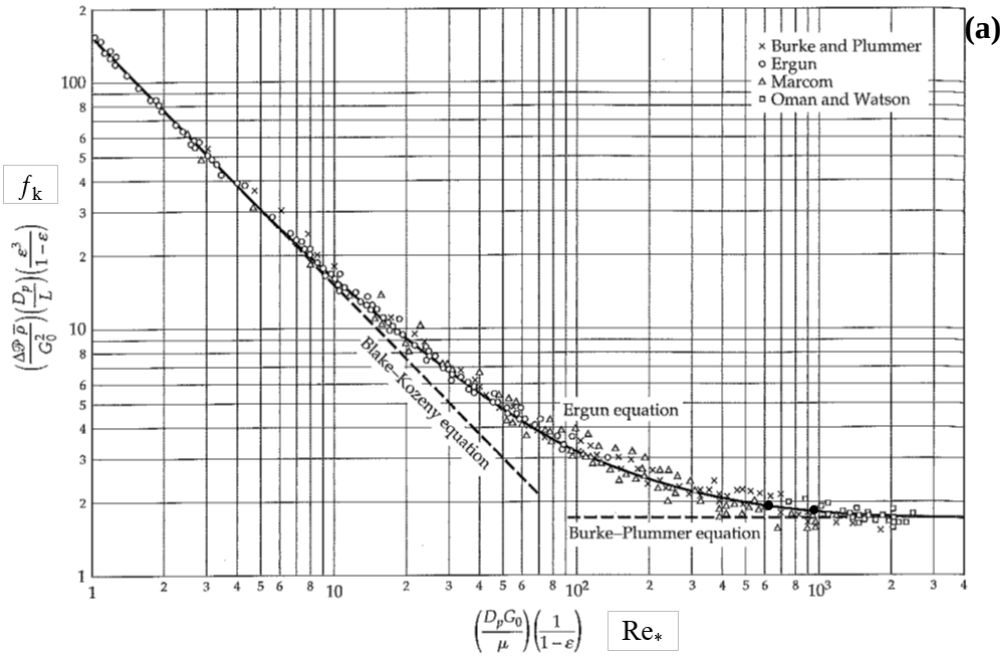

Figure 4.3. Graph of the Ergun equation. (a) With values computed for this study between black circles. (b) and (c) Magnified Ergun plot: values for clear-water (blue) and sediment runs (red).

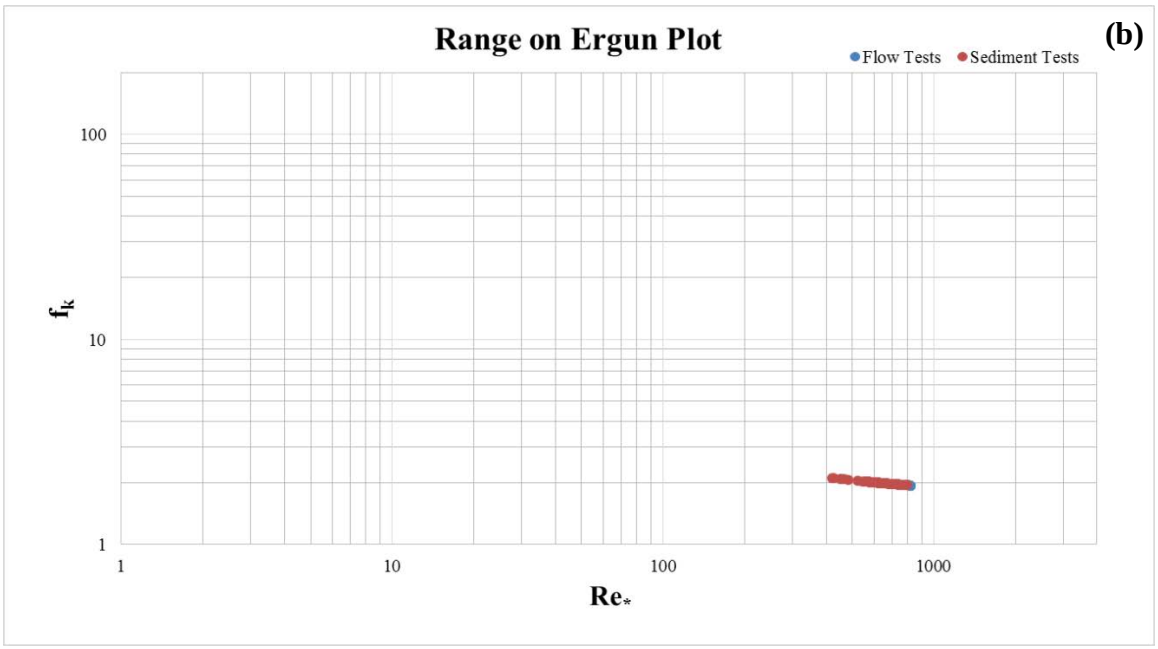

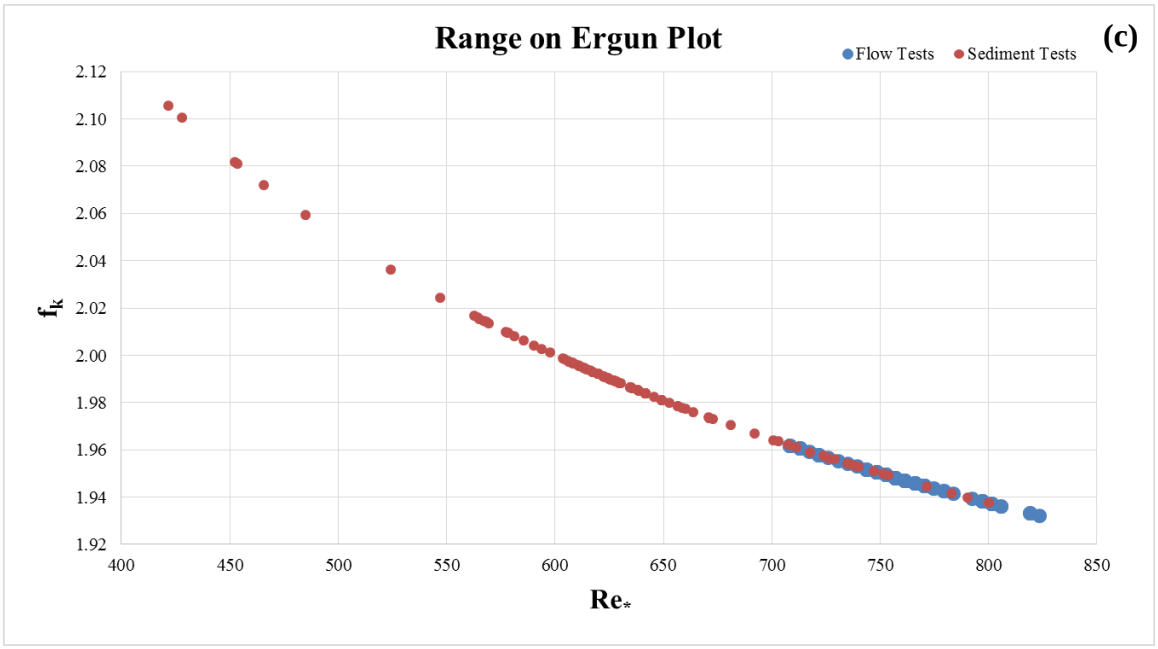

Figure 4.3. Continued.

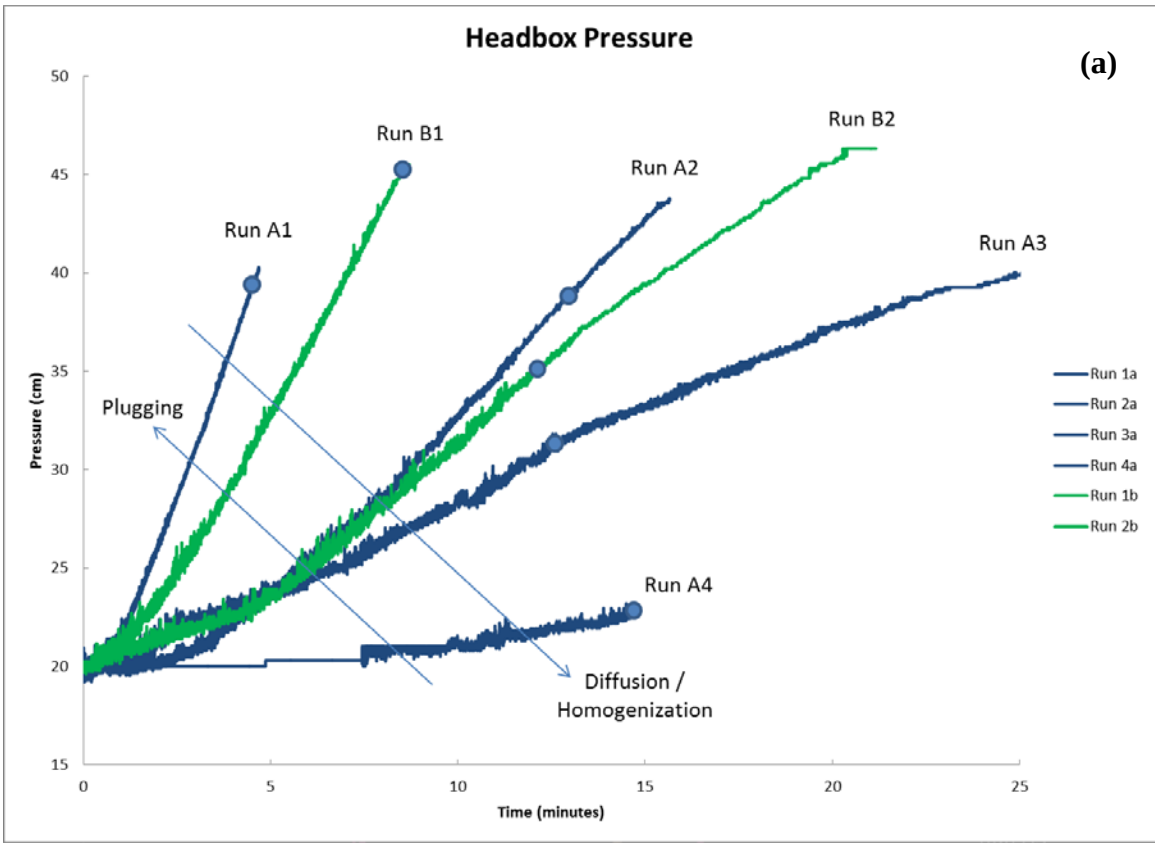

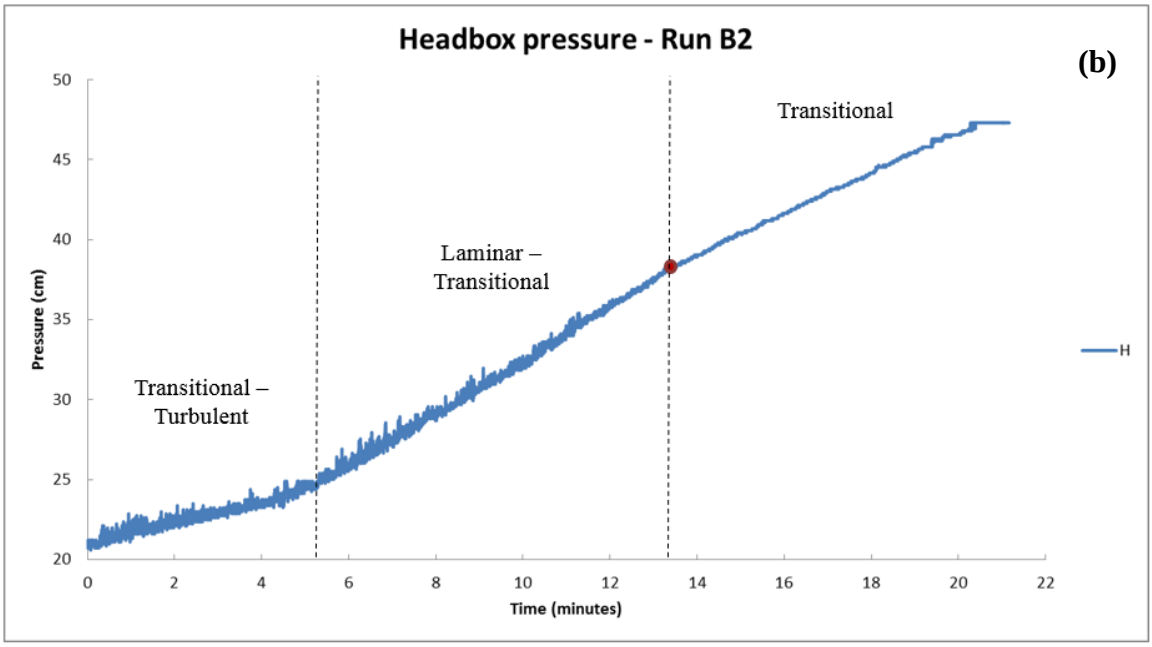

Figure 4.4. Head box pressure (a) and an example of the estimated flow regime (b).

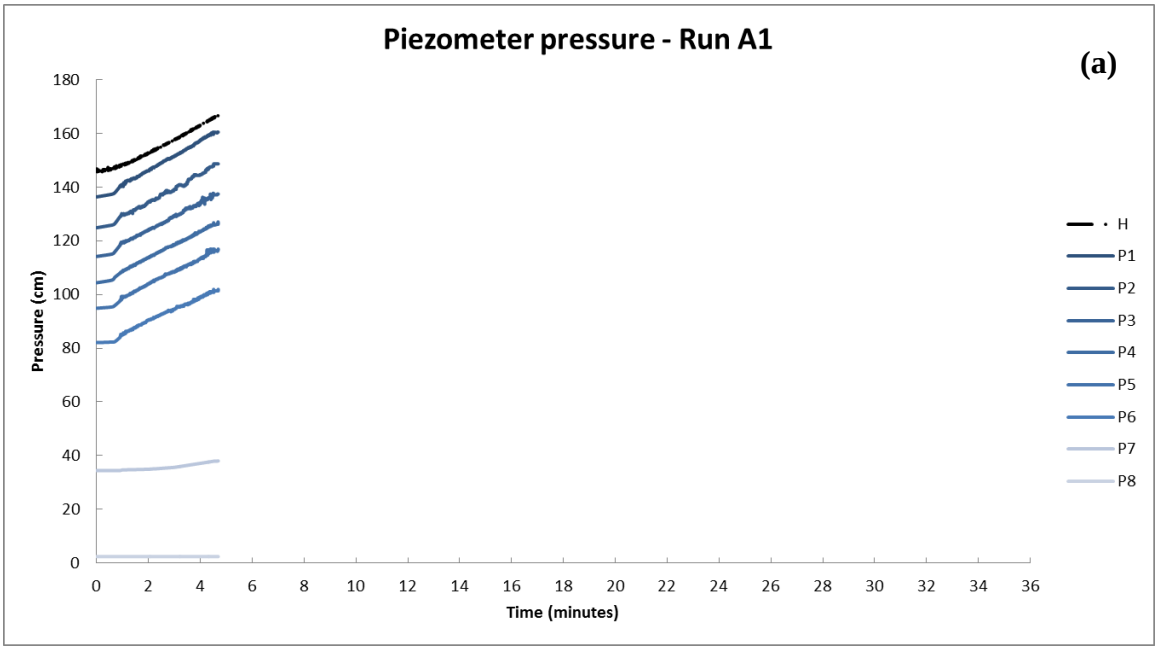

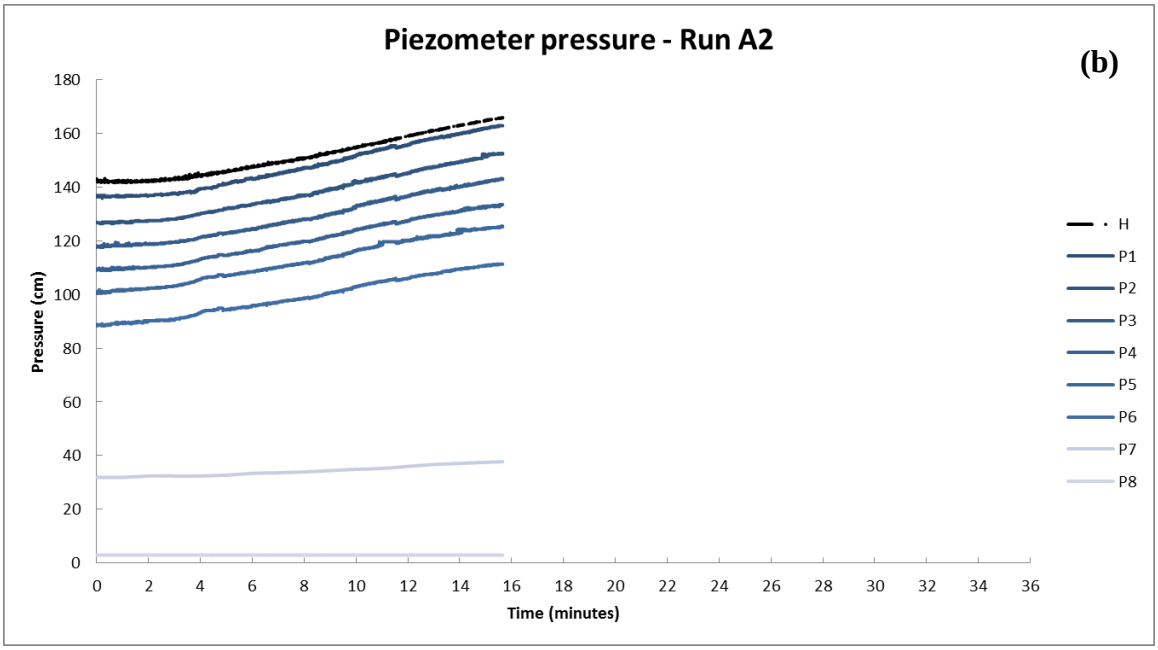

Figure 4.5. Piezometer pressure, where the total head in the permeameter is H; piezometer P1 is at the top (15 cm below the surface) and is P8 at the bottom of the permeameter (120 cm below the surface). Piezometer pressure for Runs: (a) A1; (b) A2; (c) A3; (d) B1; and (e) B2.

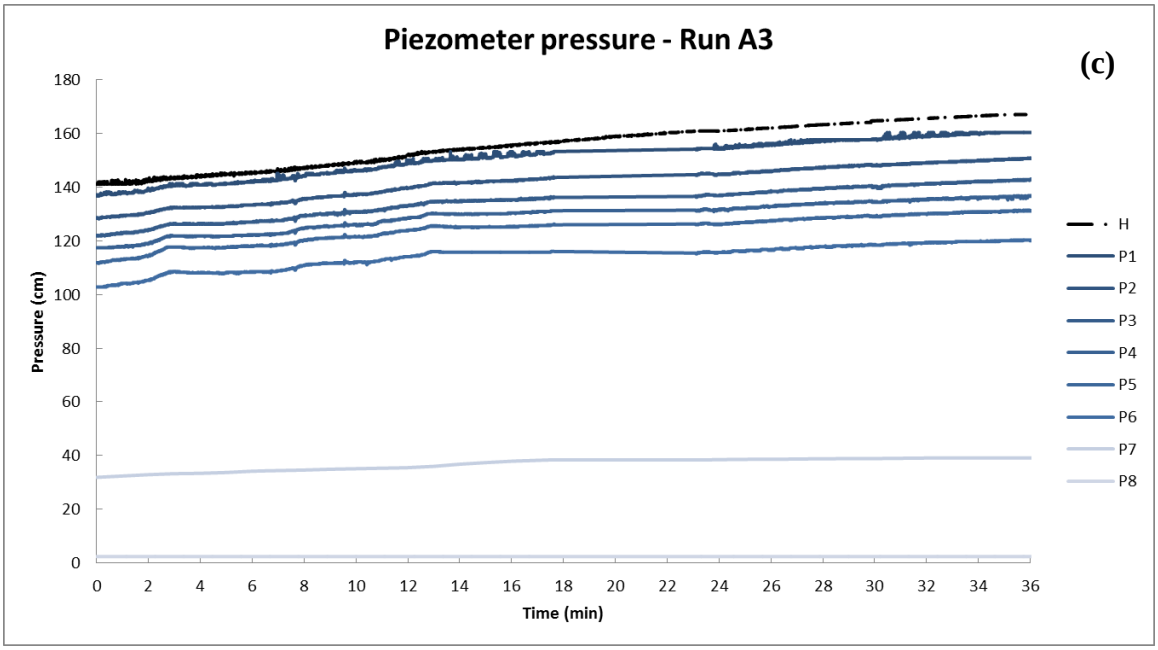

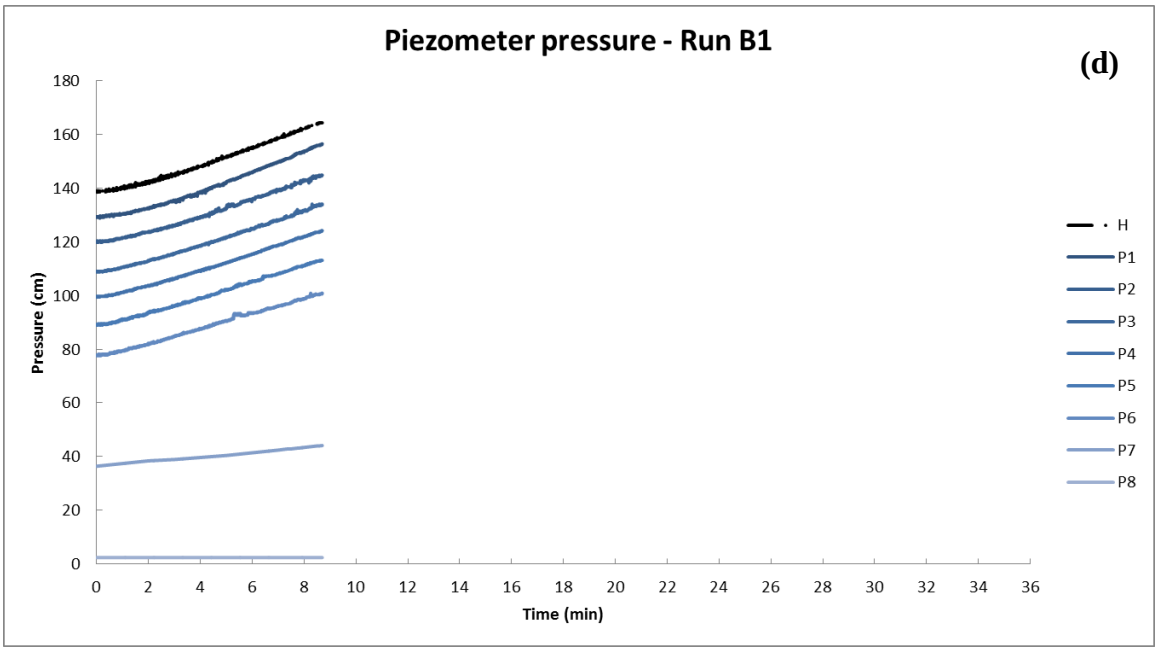

Figure 4.5. Continued.

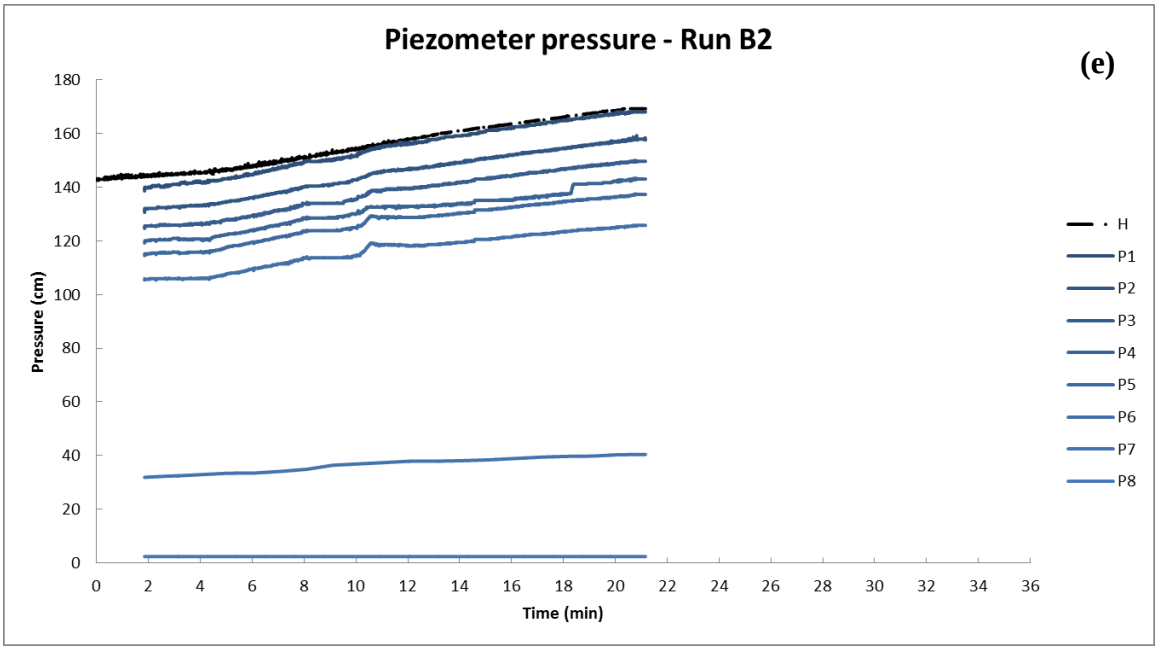

Figure 4.5. Continued.

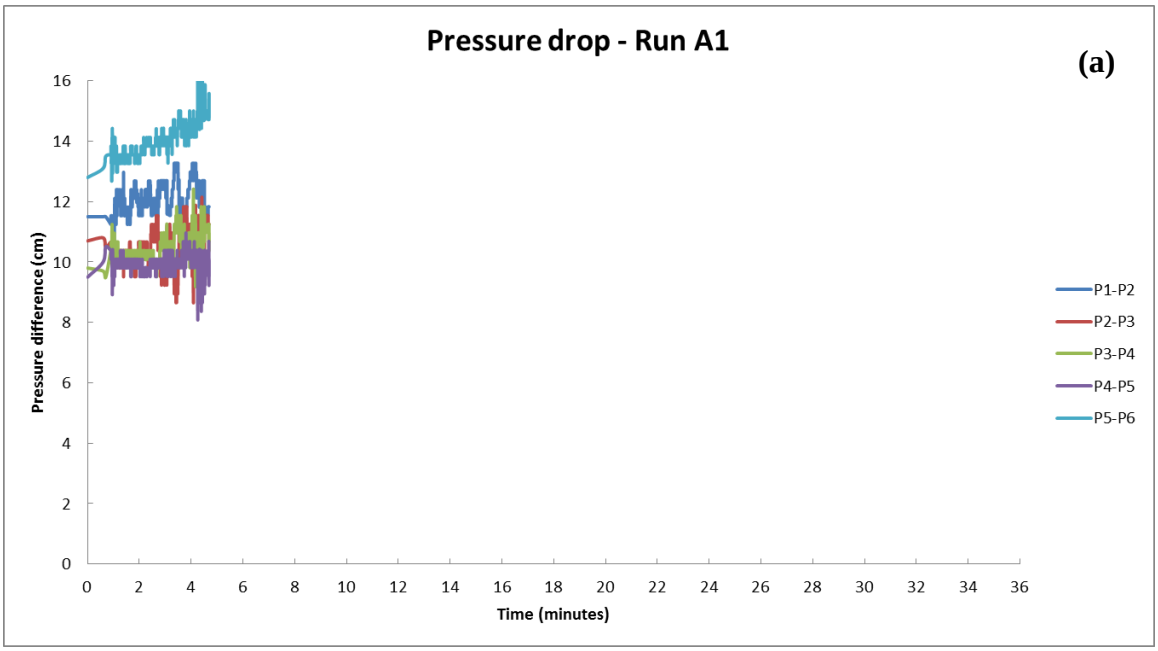

Figure 4.6. Pressure difference between neighboring piezometers shown for Runs: (a) A1; (b) A2; (c) A3; (d) B1; and (e) B2.

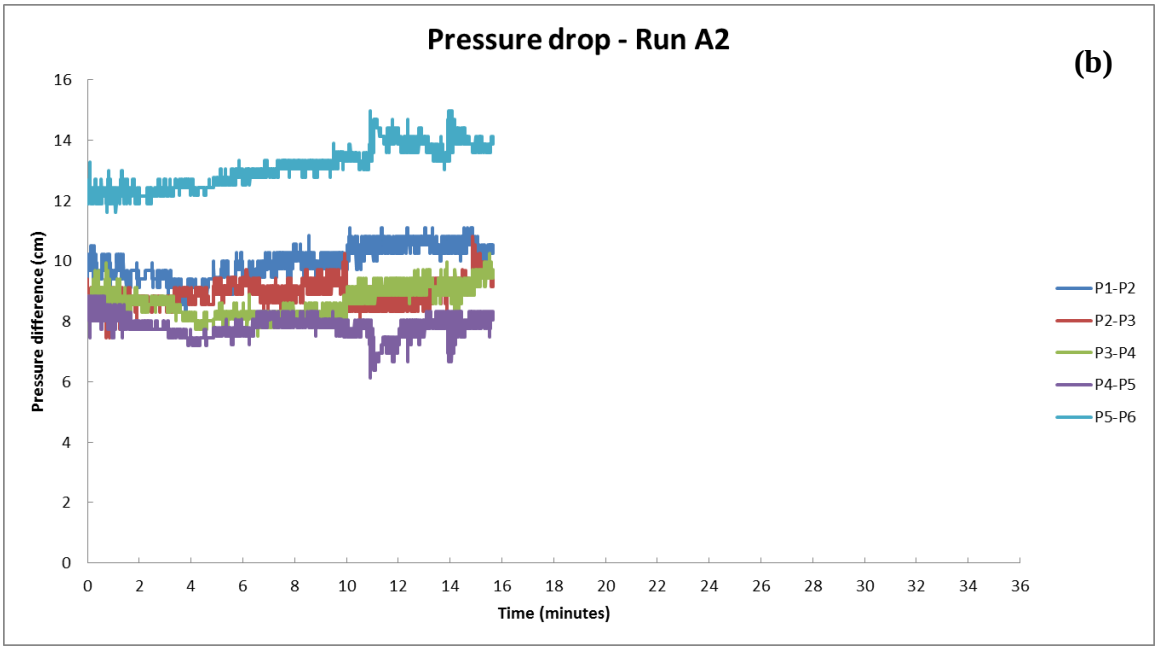

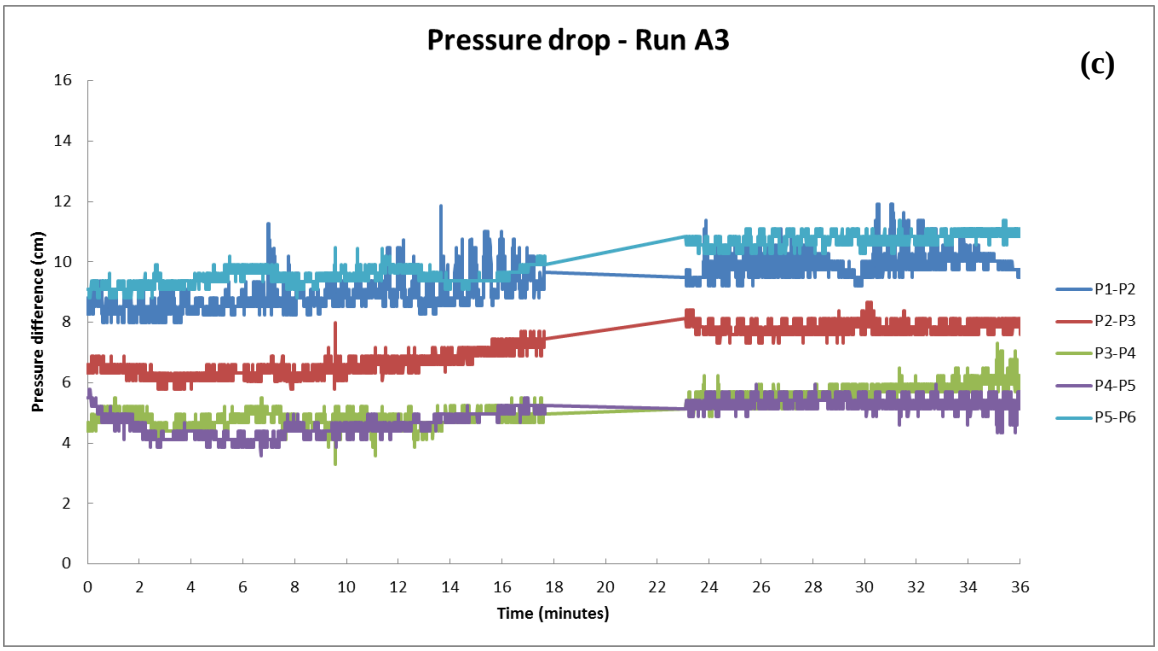

Figure 4.6. Continued.

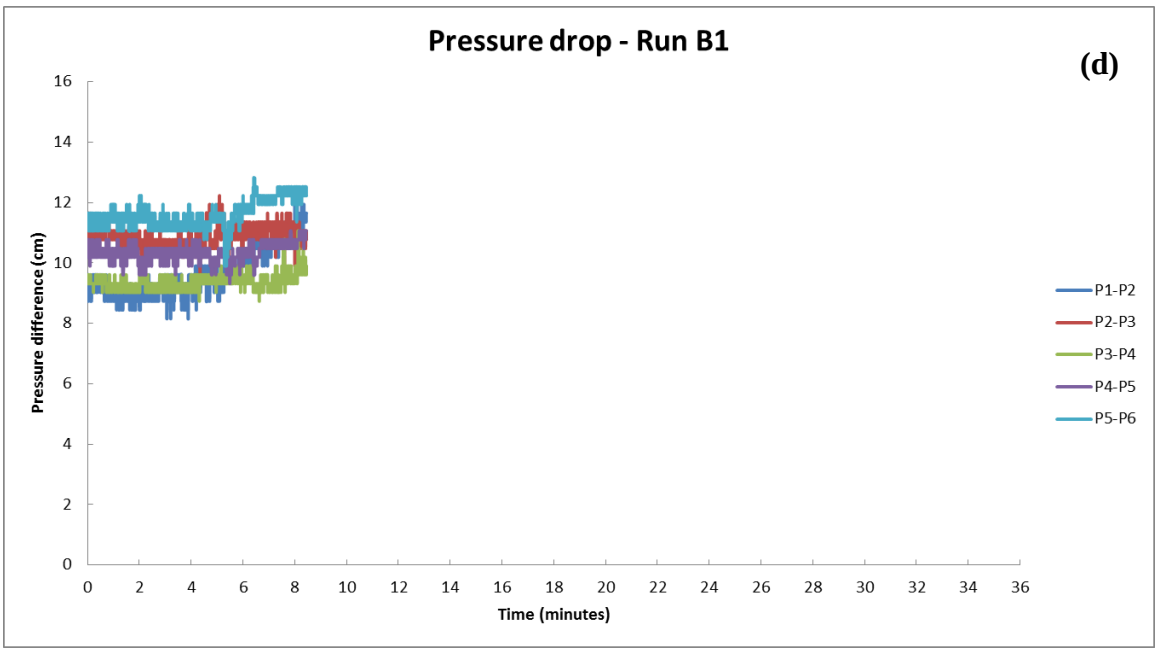

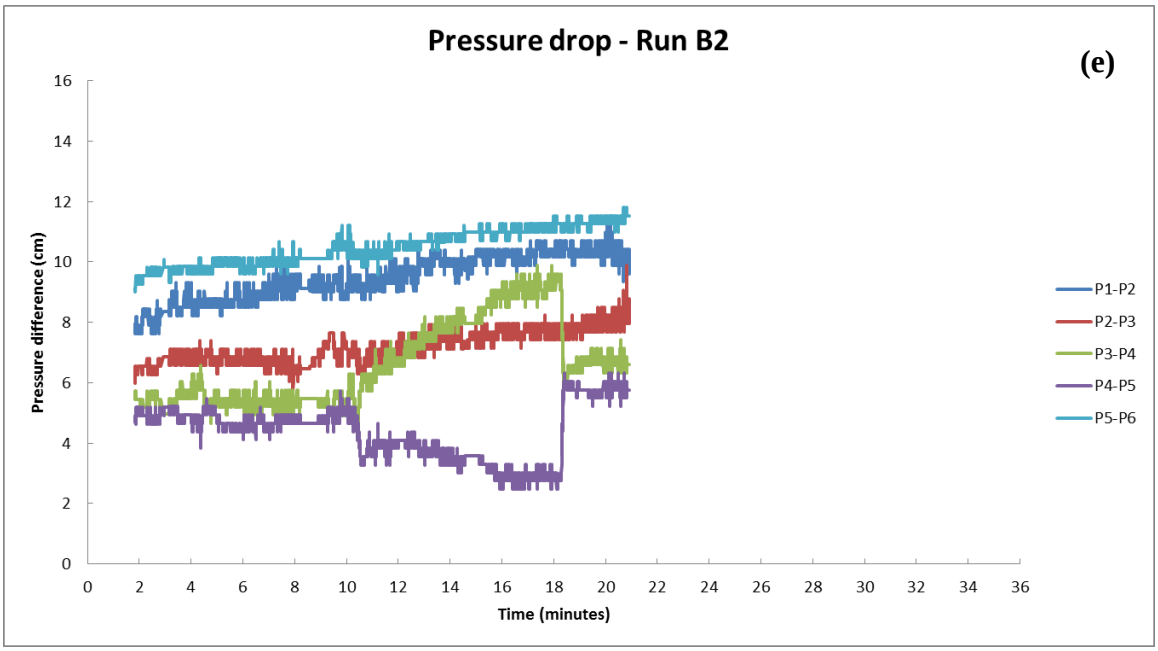

Figure 4.6. Continued.

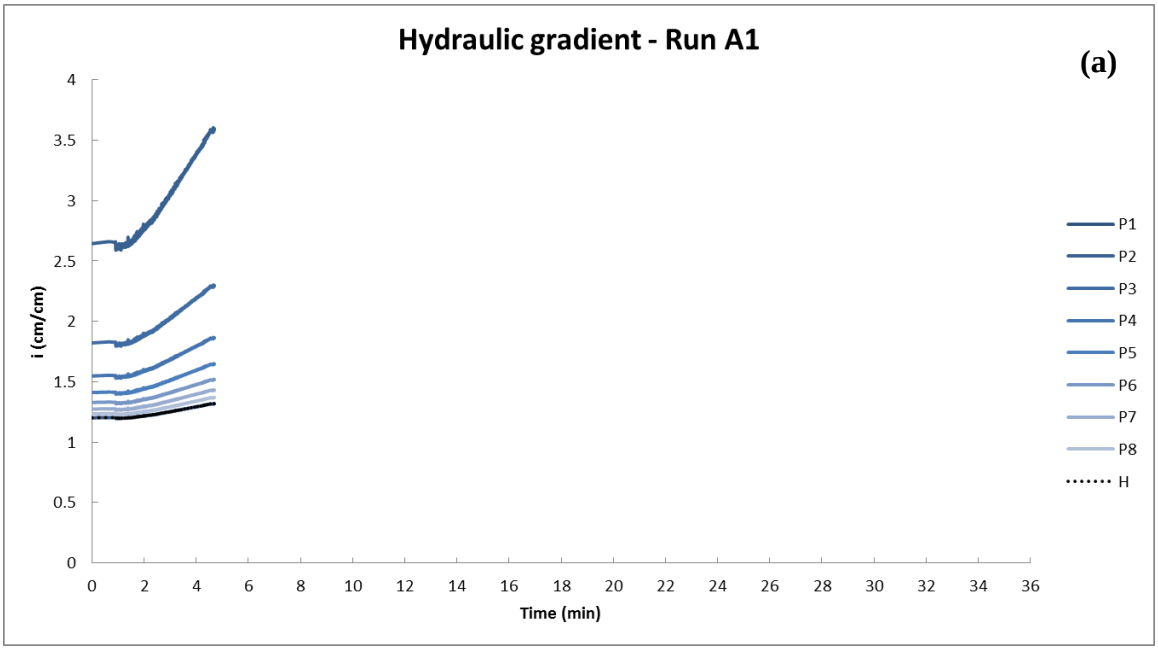

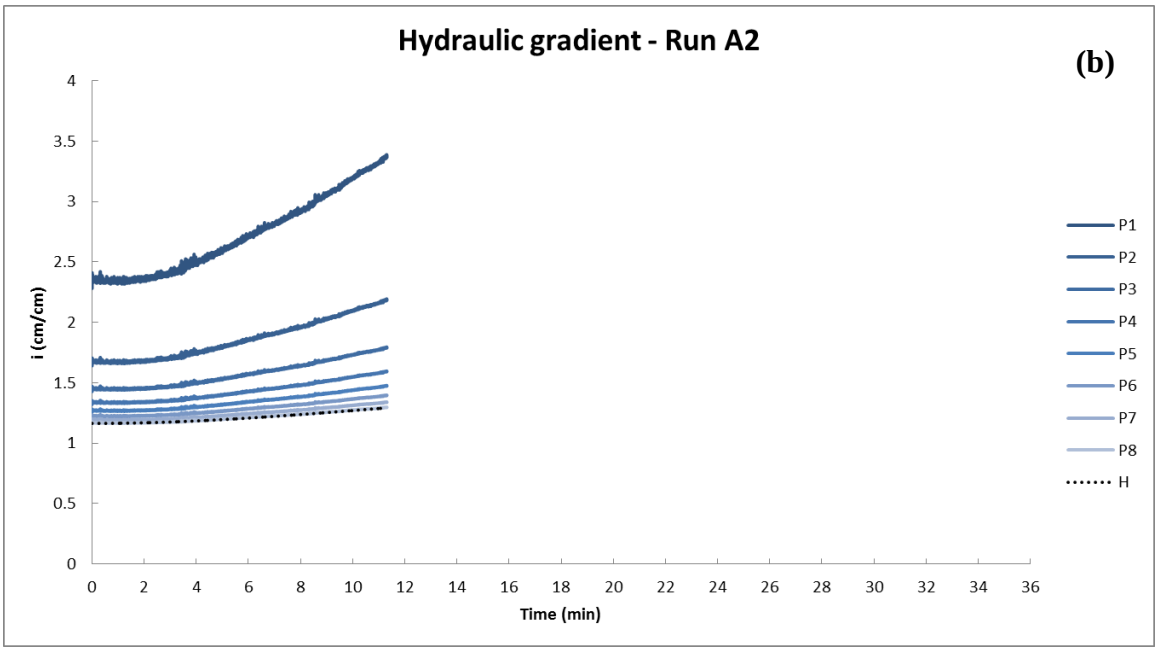

Figure 4.7. Time-series of hydraulic gradient for Runs: (a) A1; (b) A2; (c) A3; (d) A4; (e) B1; and (d) B2.

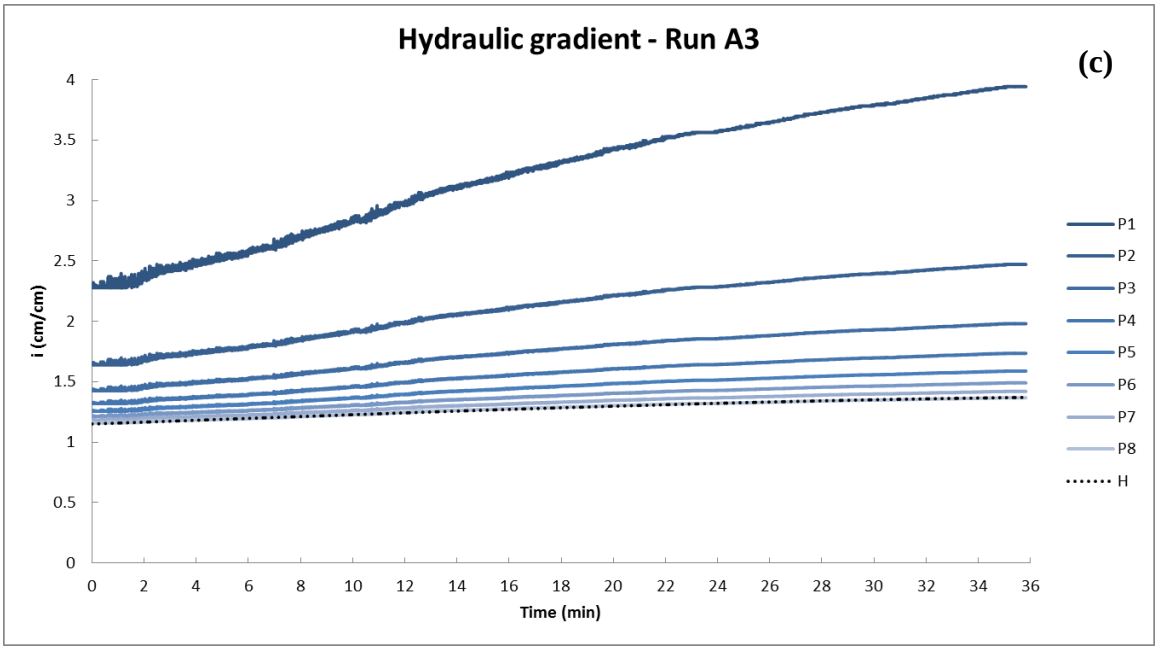

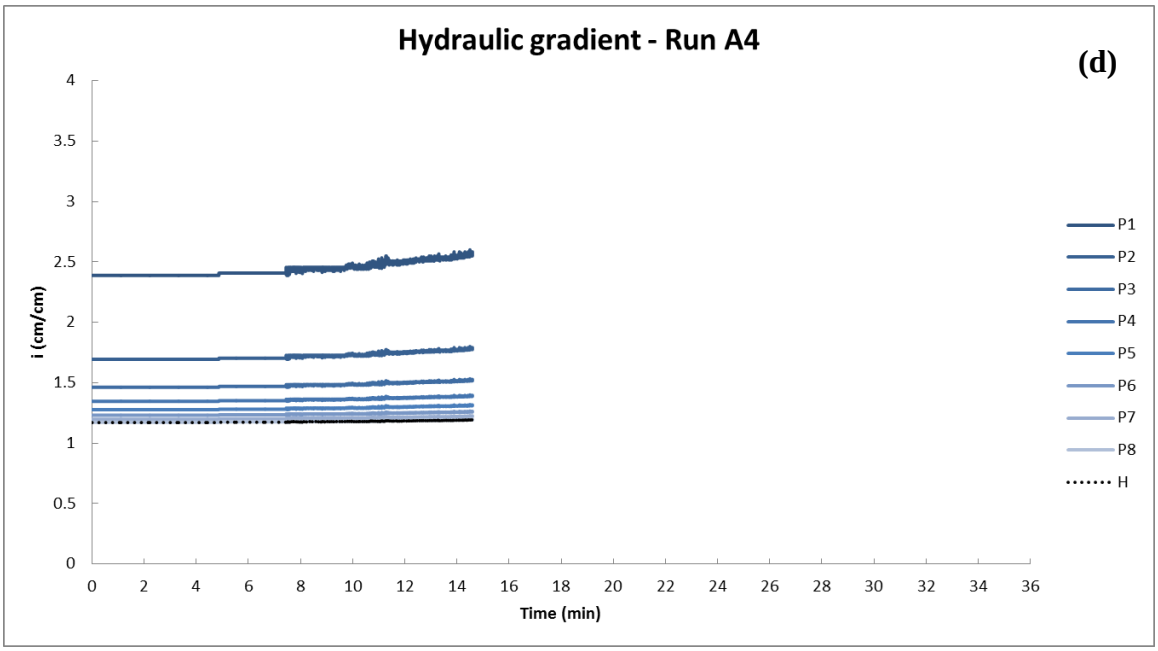

Figure 4.7. Continued.

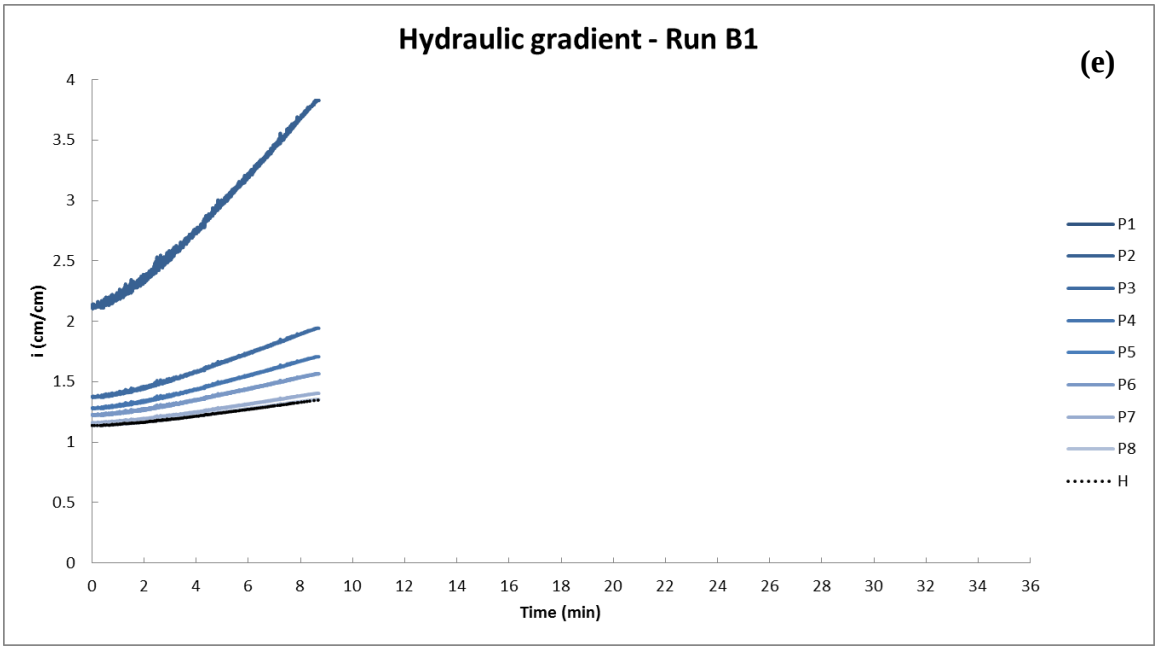

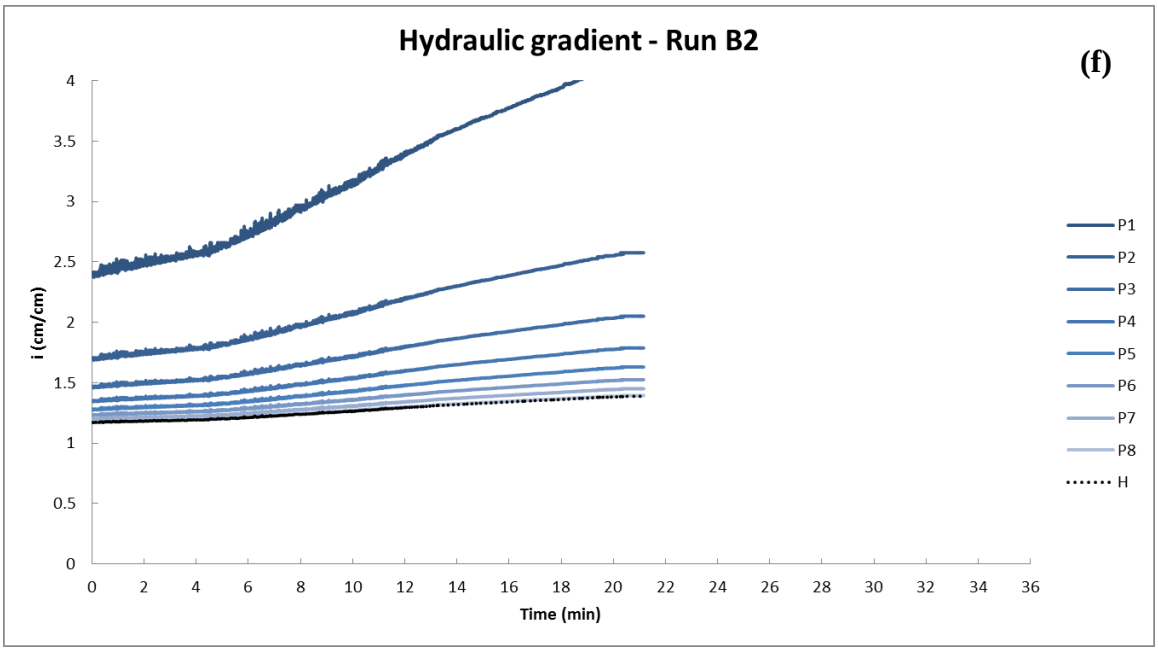

Figure 4.7. Continued.

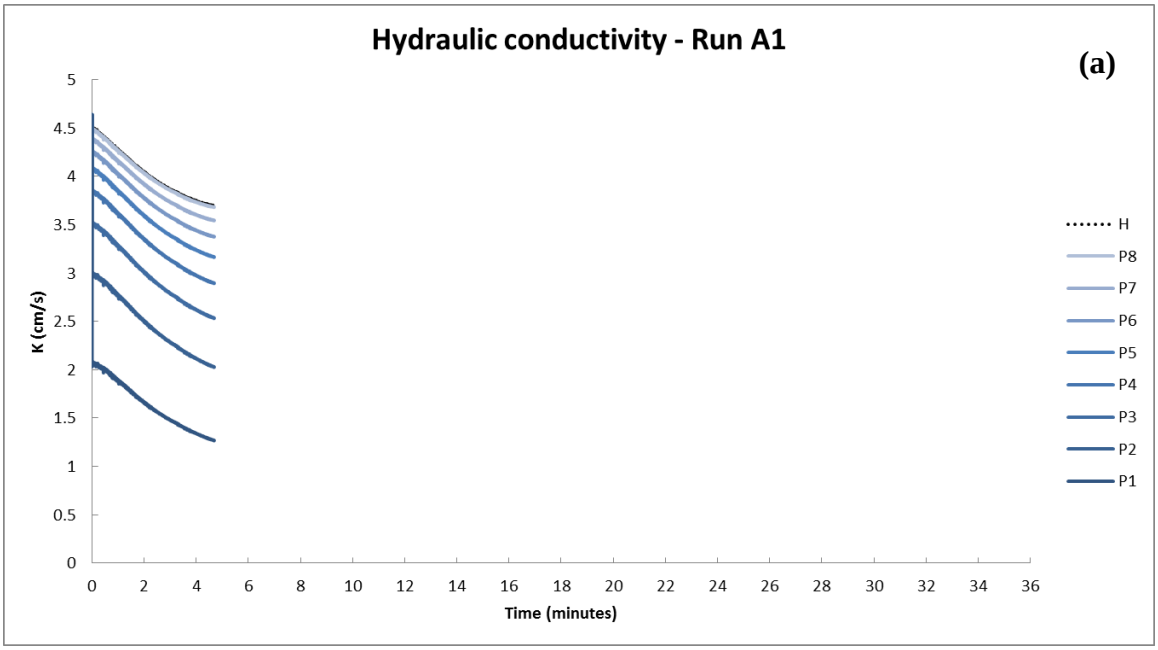

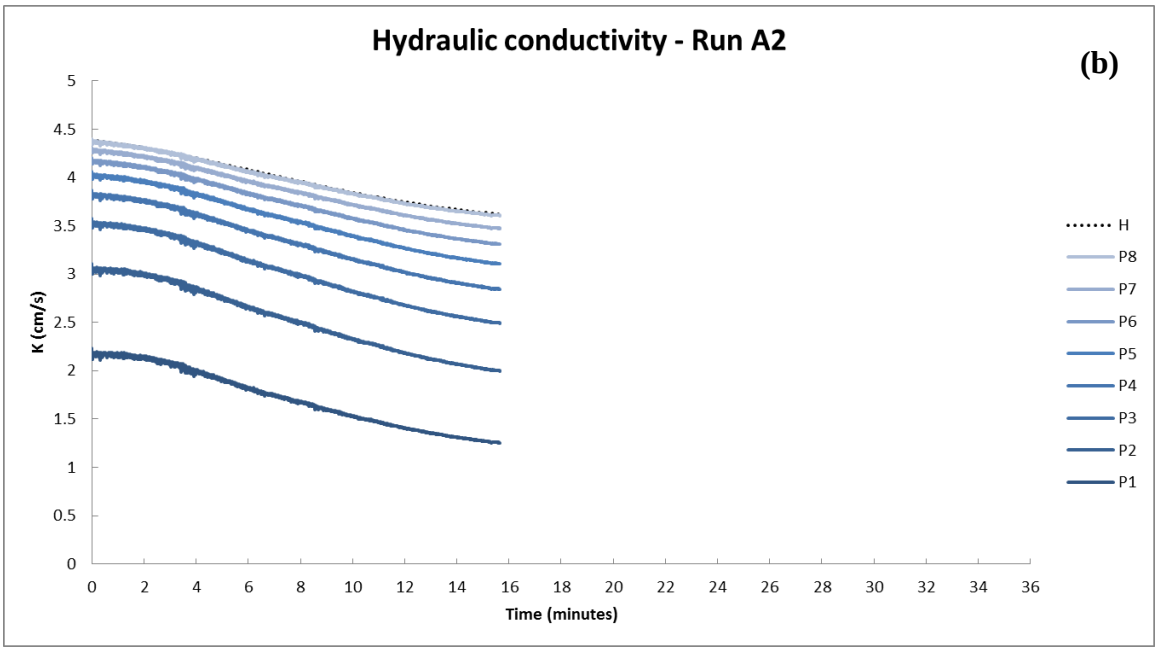

Figure 4.8. Time-series of hydraulic conductivity for Runs: (a) A1; (b) A2; (c) A3; (d) A4; (e) B1; and (f) B2.

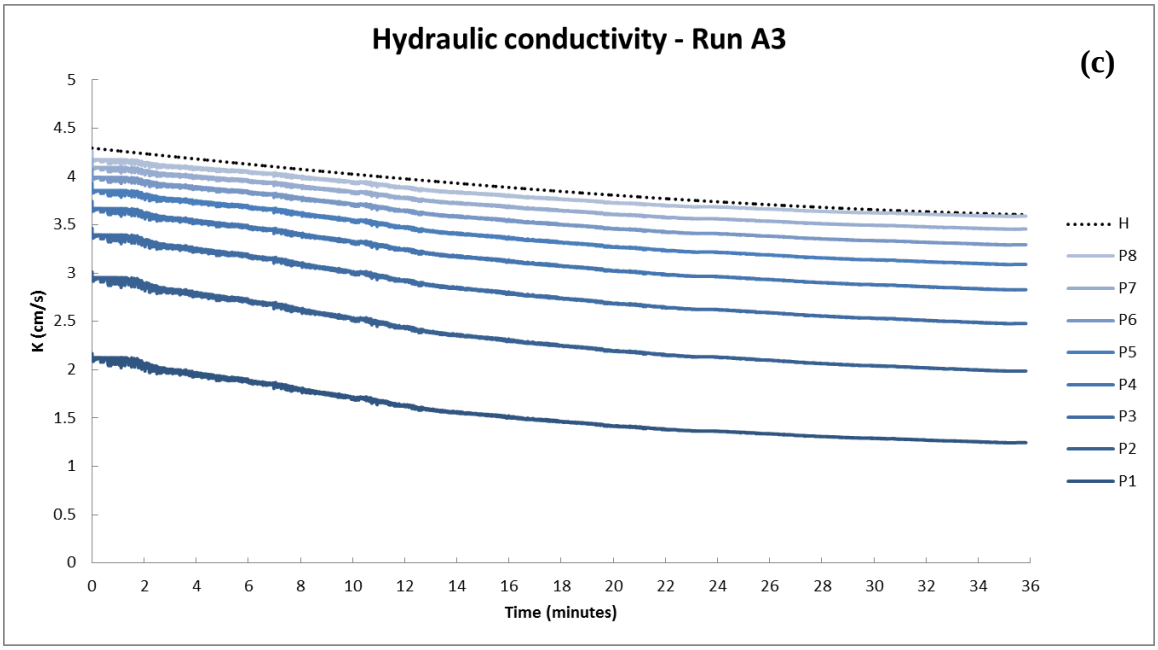

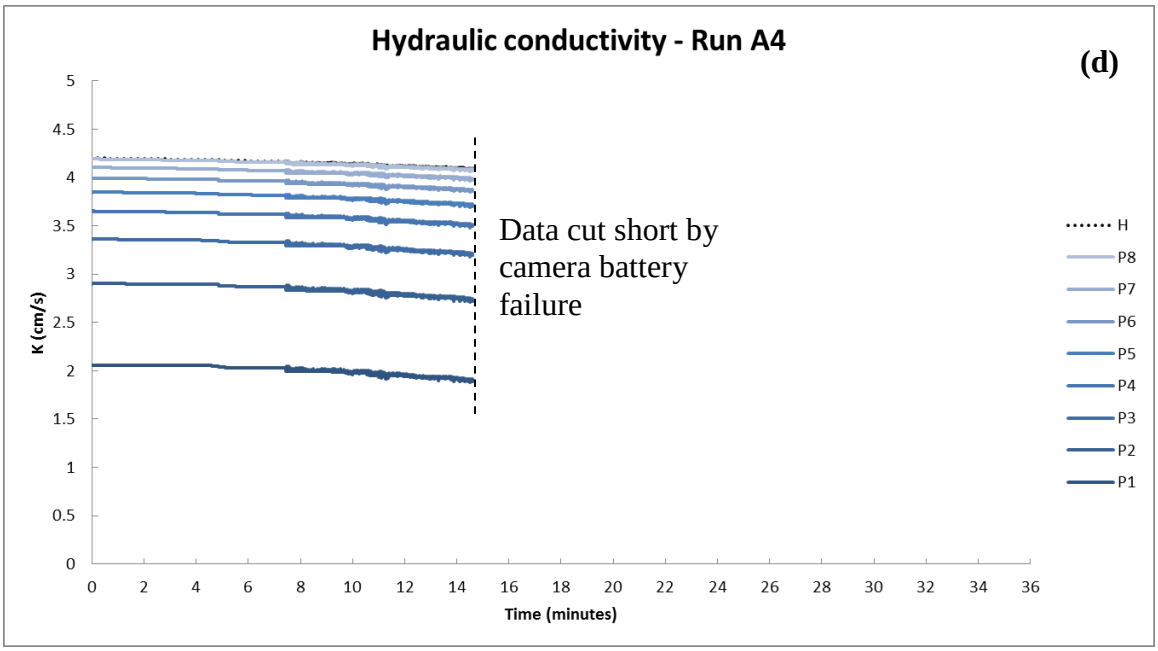

Figure 4.8. Continued.

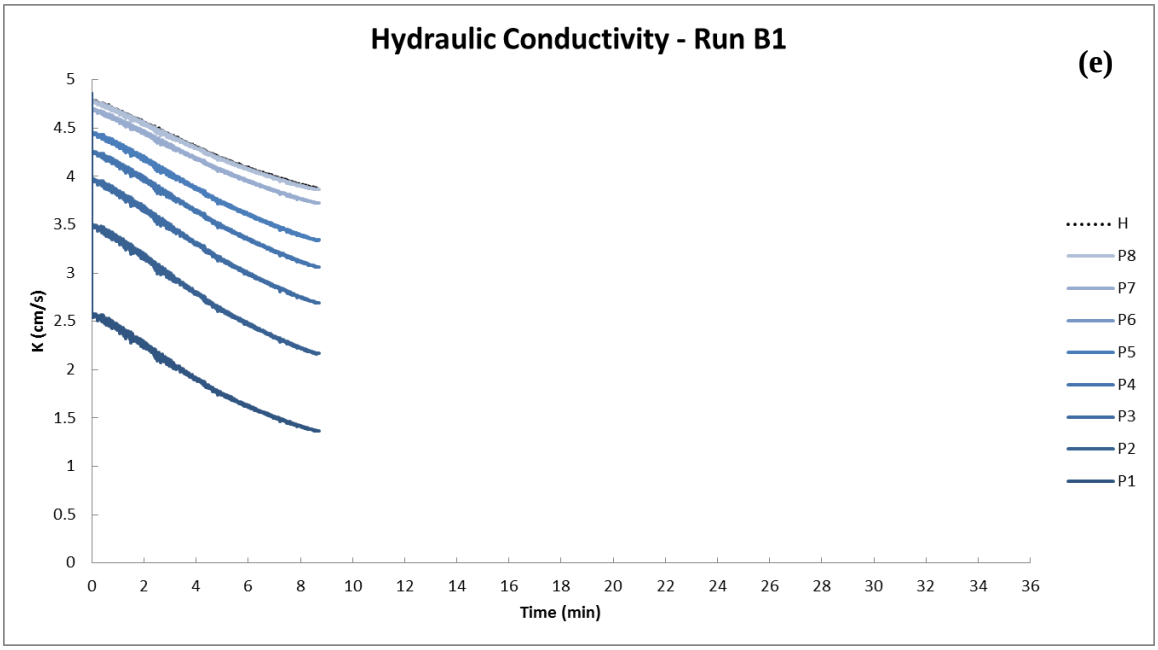

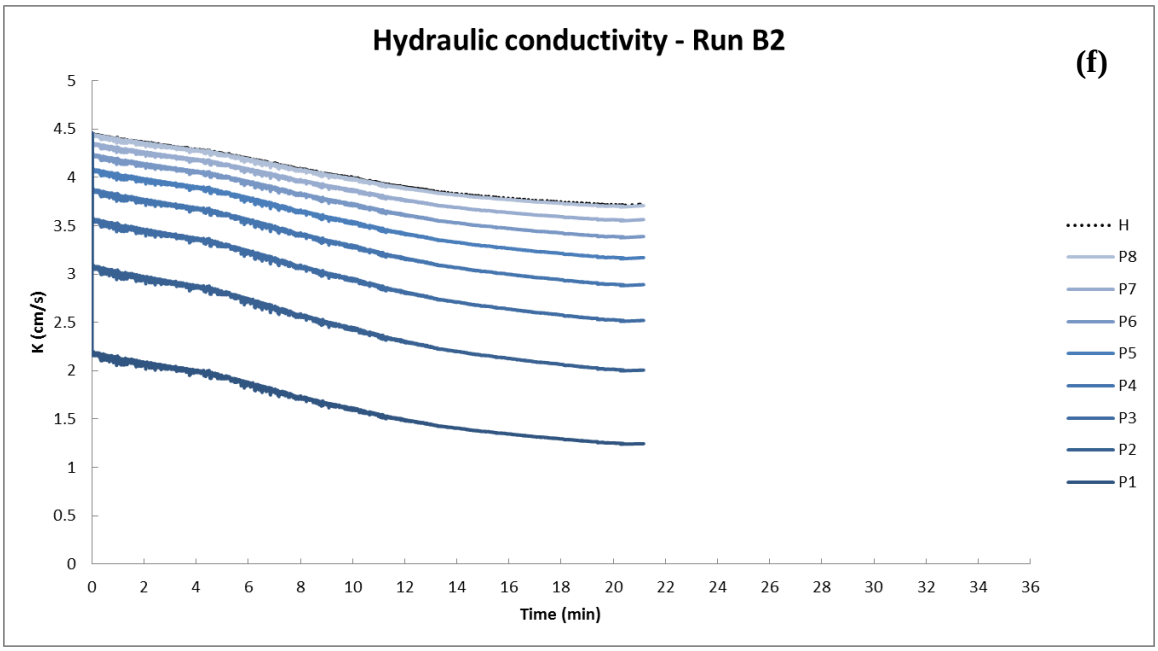

Figure 4.8. Continued.

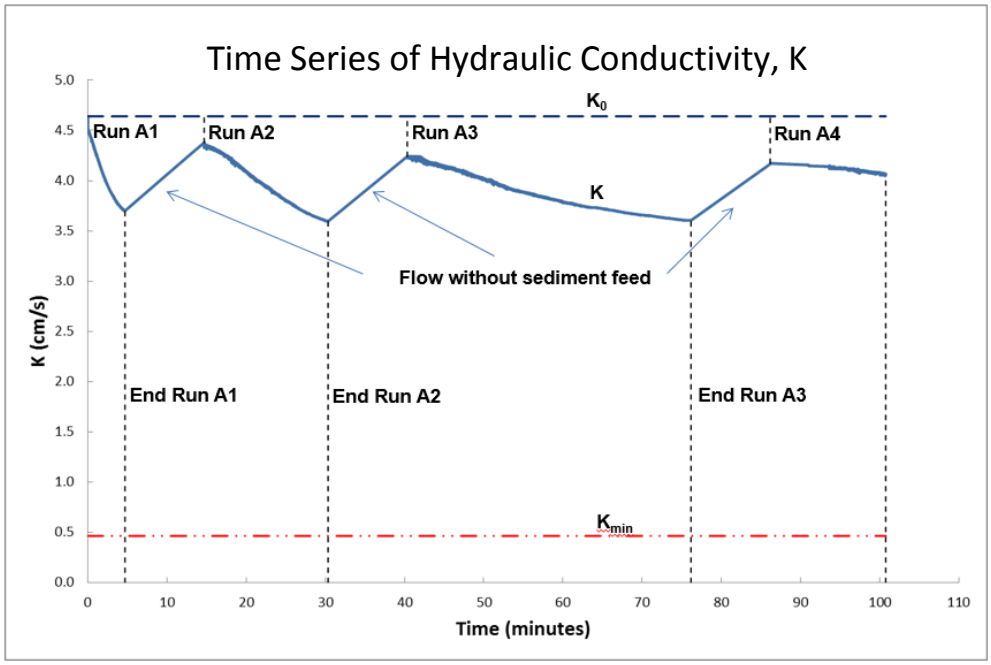

Figure 4.9. Time-series of global hydraulic conductivity, K, showing consecutive runs.

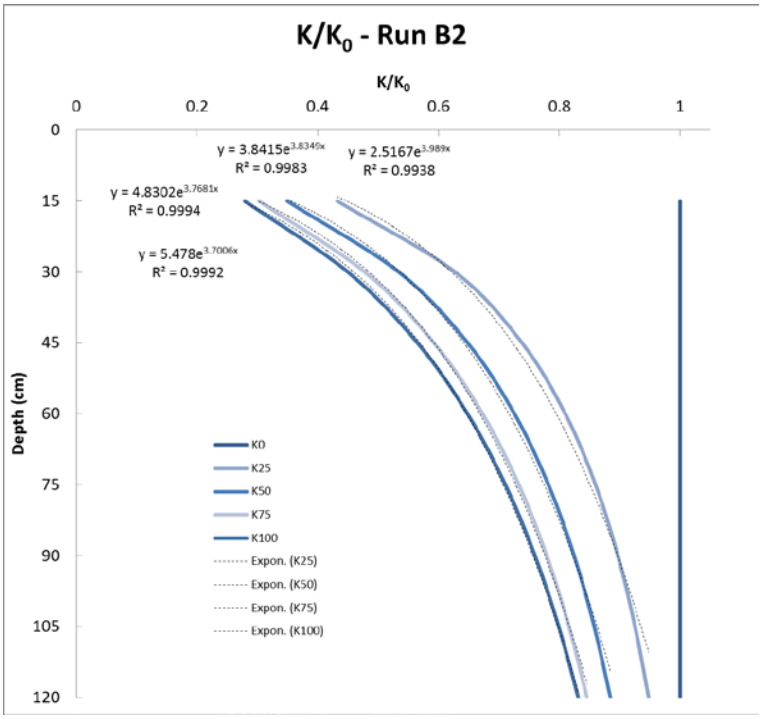

Figure 4.10. Stages of the relative hydraulic conductivity, K/K_0, for Run B2.

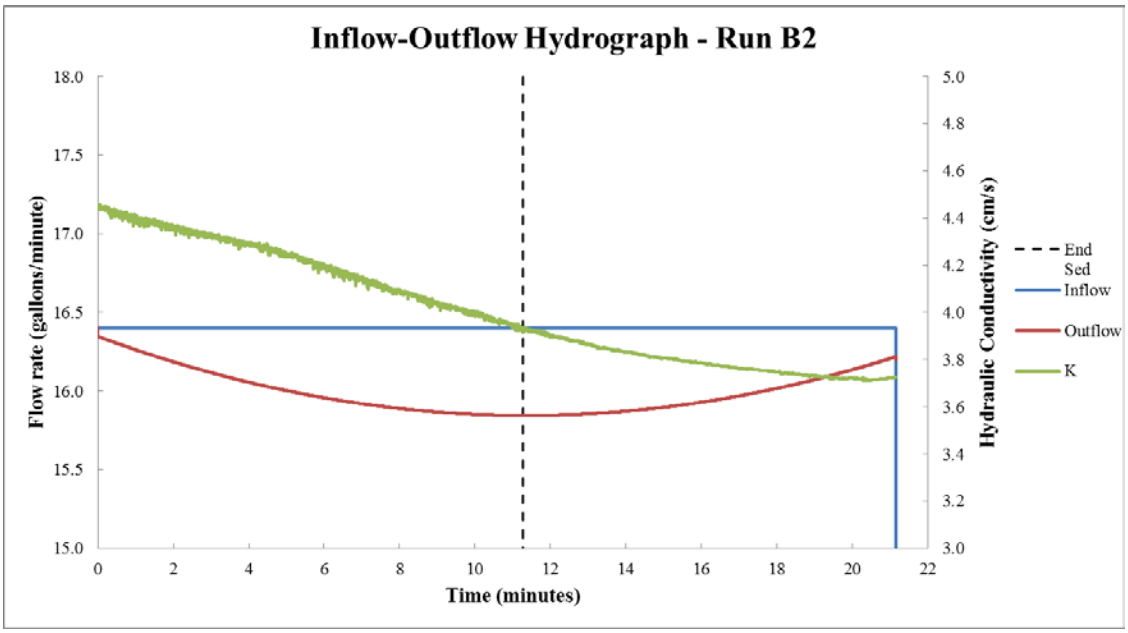

Figure 4.11. Example inflow-outflow hydrograph determined from Run B2. The blue line is the inflow rate, the red line is the outflow rate, the green line is the hydraulic conductivity, and the dashed, black line is the time at which the sediment inflow was cut-off.

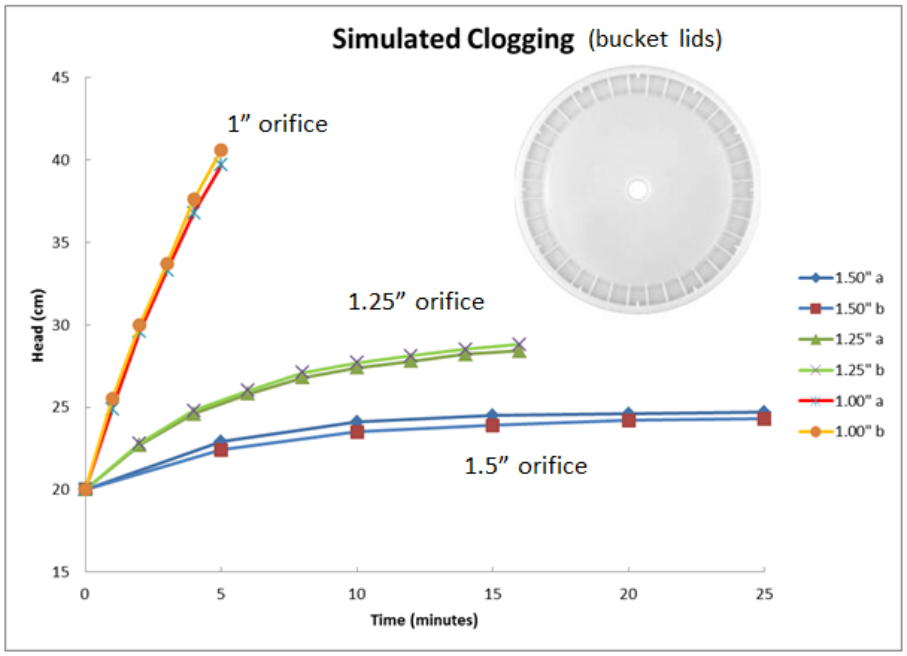

Figure 4.12. Simulated clogging using bucket lids.

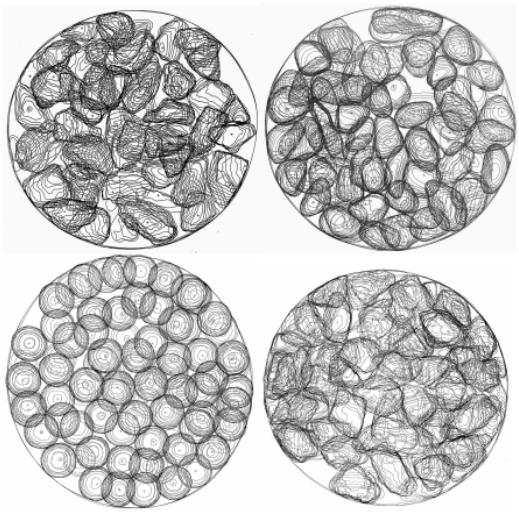

Figure 4.13. Potential pathways for wormholes illustrated by digitized slices of the top 25 mm of different types of media (Barton, 2004).

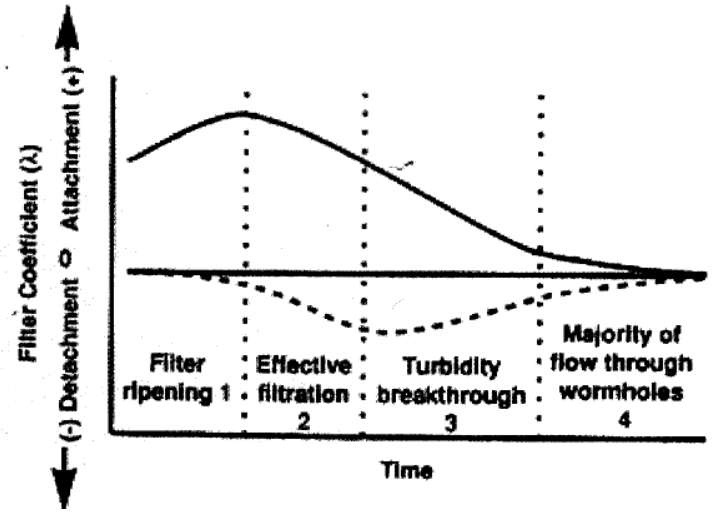

Figure 4.14. Filter cycle as proposed by Amirthararah and Ginn (1992). Attachment occurs at the same time as detachment.

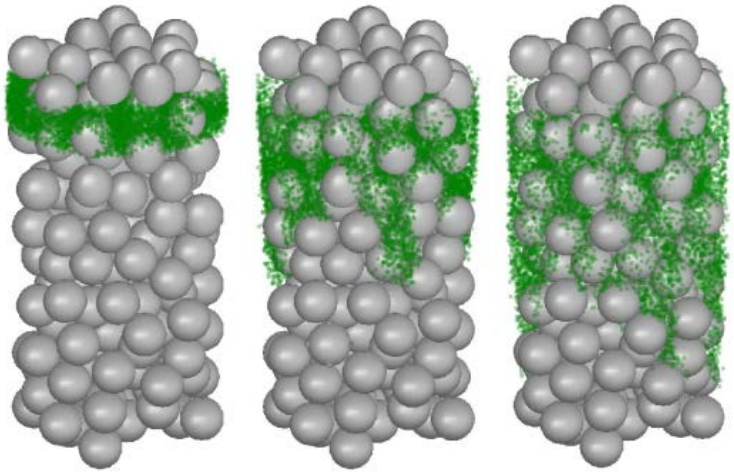

Figure 4.15. Diffusion / dispersion. Simulated dispersion in a bead pack. Courtesy of The Victoria University of Wellington, 2011.

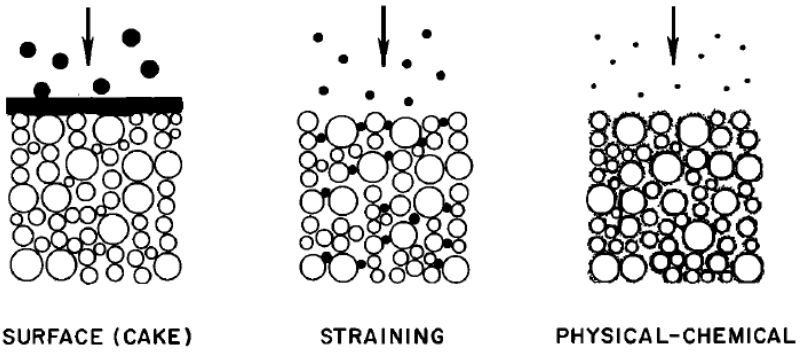

Figure 4.16. The three filtration mechanisms. Note the particle size dependence and difference in deposit morphology (McDowell-Boyer et al, 1986).

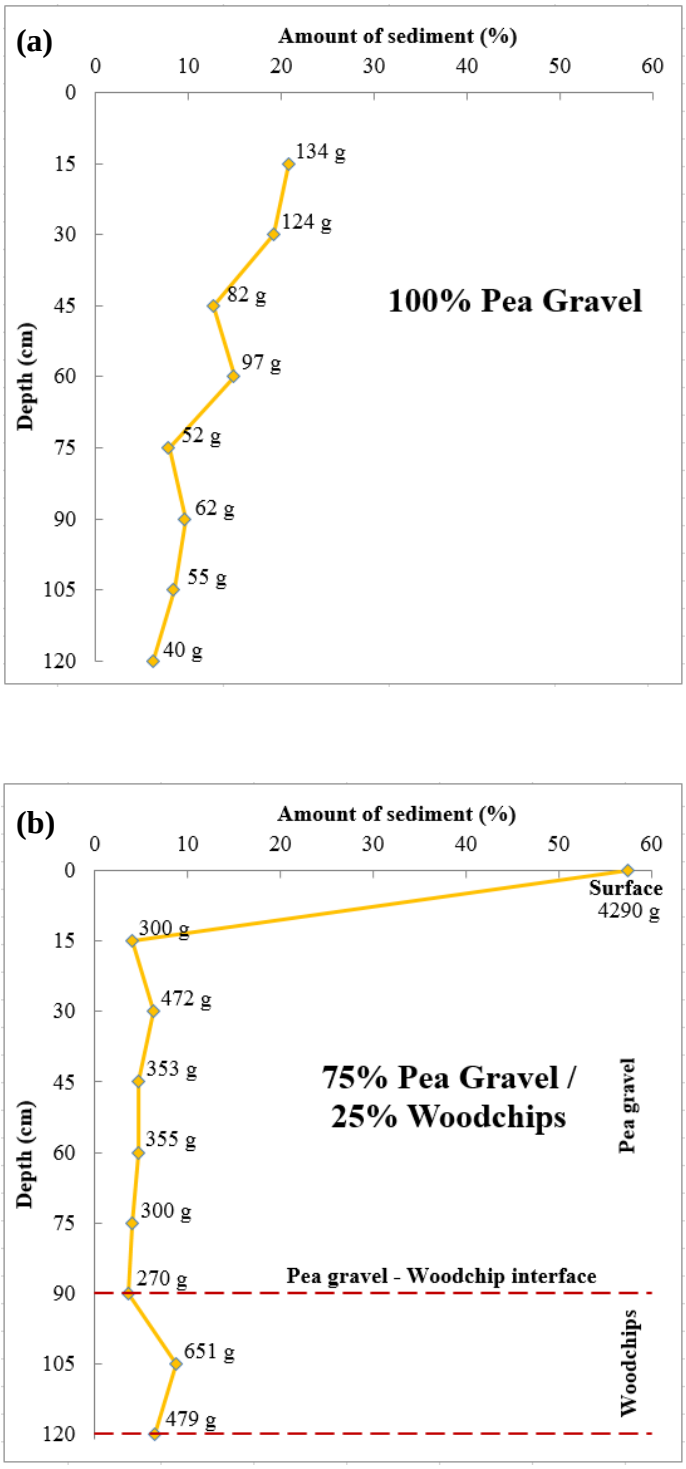

Figure 4.17. Mass of deposited sediment in the permeameter after all runs: 100% gravel shows most clogging occurring higher in the permeameter. Also the migration of a sediment front at two locations: from 0 to 30 cm and from 45 to 60 cm (a); 75% pea gravel / 25% woodchips shows a similar trend to the 100% gravel in (a) for the pea gravel section (b).

Figure 4.18. Visible intrusion of sediment from the surface at the end of Run A4. The maximum infiltration depth of fine sediments into a stable gravel bed has been reported to be between 10 and 30 cm (Beschta and Jackson, 1979; Diplas and Parker, 1984).

Figure 4.19. Observed bridging of sediment across grains of pea gravel in the permeameter.

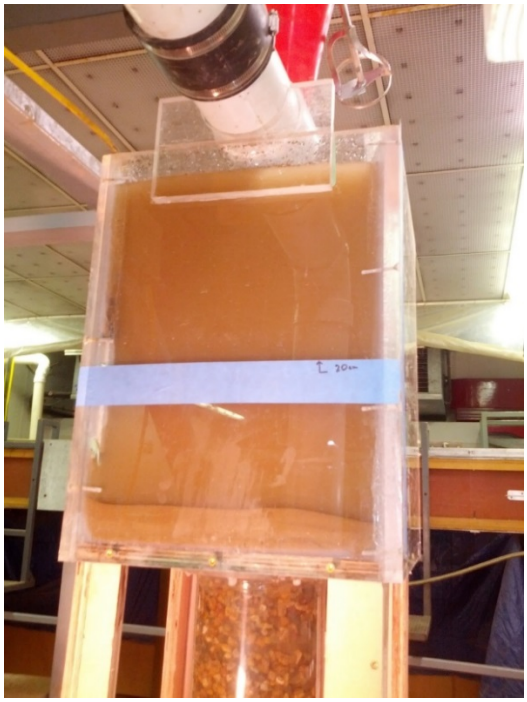

Figure 4.20. Sediment deposited in the head box during an experiment.

Figure 4.21. Sediment being drawn into the top section of the permeameter due to a lack of hydrostatic pressure holding the sediment in place. Top: (a) seconds after the water has drained from the headbox; and bottom: (b) after several minutes, the rate of sediment intrusion slows to a sluggish pace.

Figure 4.22. Dried sediment at the surface of the permeameter.

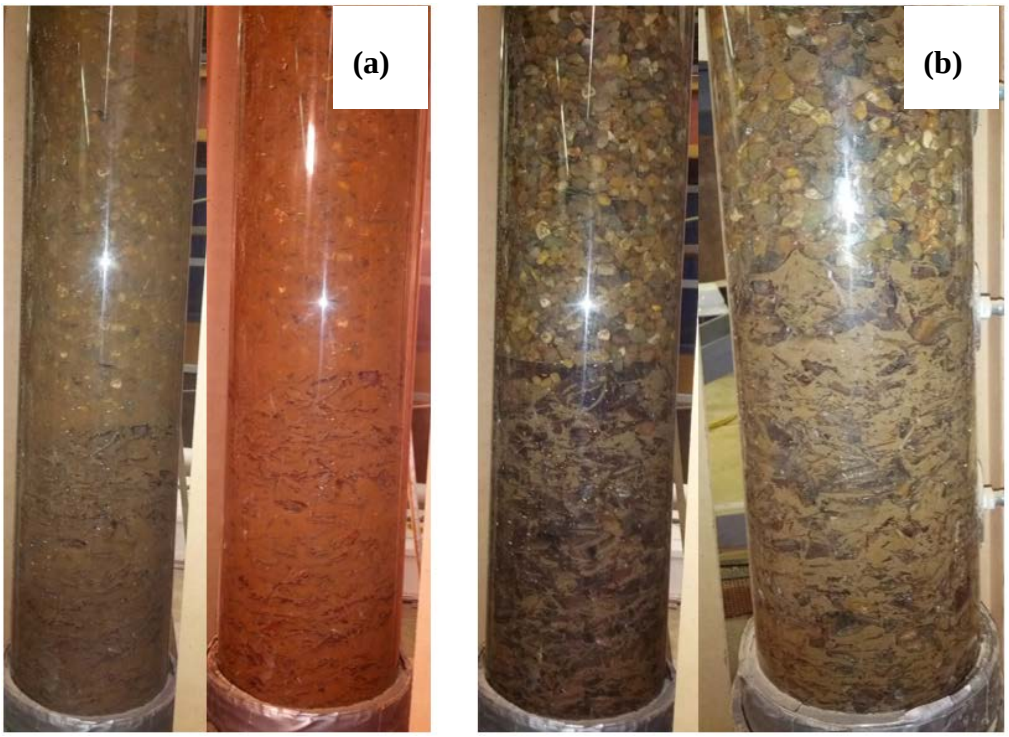

Figure 4.23. Sediment "cloud" at interface between pea gravel and woodchips with different flow patterns in pea gravel and woodchips (a); and visibly higher amounts of sediment deposition in the woodchip layer (b).

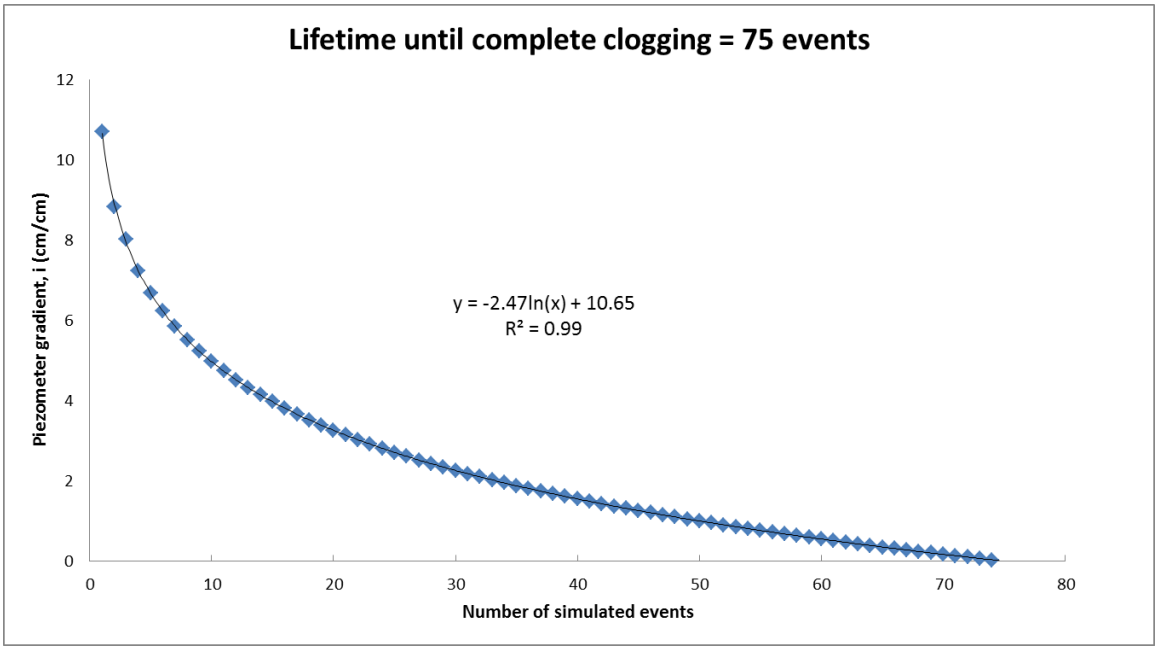

Figure 4.24. Lifetime curve. On average, the ATI will last 75 events with high concentrations of suspended sediment in the runoff.

CHAPTER 5. CONCLUSIONS

5.1 Brief Summary

The overall goal of this study was to determine the effectiveness of an Alternative Tile Intake (ATI) at reducing sediment and nutrient loads associated with runoff from storm events in an intensively managed agricultural watershed. ATIs are potentially an effective best-management practice for farm fields in this and other watersheds in the Midwest. The porous media in an ATI also acts to attenuate high flow rates generated from intense rainfalls. The gravel medium in an ATI filters out sediment and attached nutrients from the runoff, while the woodchip medium enables the denitrification of runoff flow. The ATI must be designed with an effective hydraulic retention time to optimize the processing of nutrients while having the performance a tile drainage system should. The present study involved a test site at the Clear Creek watershed in Iowa. It also involved extensive laboratory experimentation using a permeameter model that simulated a typical ATI, and provide useful insights into ATI performance. The main conclusions from these experiments are presented here, along with several recommendations for further research.

5.2 Conclusions

The study led to the following conclusions:

1. Back-up of inflow is a common feature of ATI performance. For the permeameter (simulated ATI) in the laboratory, and the ATI prototype observed in the field, flow back-up is due to five mechanisms: roughness of the gravel and woodchip media; entrance loss; sediment clogging the surface of the pea gravel; sediment clogging pore spaces within the pea gravel and woodchips; and, sediment settled-out in the outflow pipe. Of these causes, the laboratory experiments showed that sediment clogging is the major mechanism.

2. Laboratory experiments with the permeameter fitted with pea gravel and a layer of woodchips were effective in simulating the performance of an ATI as a drainage intake, subject to flows transporting high concentrations of suspended sediment. The D_{50} of the pea gravel (10.3 mm) classifies it as a medium more suitable for drainage than a separating gravel or filter sand. The permeameter trapped sediment, and showed how sediment trapping efficiency increased with time as sediment accumulated in the permeameter. However, as sediment trapping increased, the permeameter's drainage capacity decreased, because pores within the permeameter's gravel and woodchip layers accumulated sediment.
3. The experiments show that initial storms are critical, because they provide the initial shock of sediment to an ATI. Thereafter inflow rates tended to decrease, because the permeameter's drainage capacity decreased. Values of concentration of sediment in flows entering a representative ATI were found, using numerical simulations (with Water Erosion Prediction Project (WEPP) software), to be governed heavily by the initial field conditions (e.g., ground/crop cover and antecedent moisture conditions), significantly more than the intensity and duration of a rainfall event.
4. The layered media of pea gravel and woodchips in the permeameter were difficult to completely clog with sediment. The high concentrations of sediment needed to clog the permeameter support suggestions in the literature that the working life of an ATI is in the range of 10 to 20 years (e.g. Ranaivoson, 2004). The permeameter proved difficult to clog because the smallness of the ratio, D_p / D_m, or the D_{50} of the sediment influx to the D_{50} of the porous media. For this study, $D_m >> D_p$. At the field site, the ATI prototypes have continued to function from June, 2011 to present time (October, 2014) without noticeable problems.
5. The relative hydraulic conductivity never dropped to 10% of the permeameter's clean conductivity, a lower limit that prior studies (i.e. Wilson, 1999) suggest as

indicating the end of the permeameter, or ATI, effectiveness; the lowest value for this study was about 25%. The hydraulic conductivity, K, reduced at a decreasing rate with each consecutive run (simulated storm event), as would occur in the field. Consequently, the flow rate through the porous media decreased with each run with sediment-laden flow, and less sediment was transported to the permeameter with each subsequent run. The permeameter's hydraulic conductivity rebounded once clear-water flow returned and flushed some of the deposited sediment out of the permeameter.

6. Cycles of sediment sealing, then downward dispersion of sediment, occurred in the permeameter. Eventually, after many storm events, a terminal phase would be reached as the permeameter clogged; i.e., when K/K0 = 0.1. Zones of localized-clogging may occur due to preferential flow paths. The results suggest that the pressure will ultimately become equal at all points along the depth of the ATI. The permeameter experienced an increasingly homogenized infilling of sediment. Such homogenization increases the working life of an ATI as it enables flow to continue more steadily through it.
7. The tops of each layer experienced the greatest concentrations of sediment accumulation. The top of the woodchip medium experienced the overall highest deposition of sediment for the entire permeameter. Also, the top of the pea gravel medium experienced the highest mass of deposited sediment for the pea gravel section, reflecting the initial shock of sediment load that accompanied the first storm event.
8. For flow with sediment, the vs and Re* decreased below the range found for clear water flow, which was in the transitional regime. This is due to the added friction generated by the infilling sediment. Viewed in terms of macroscopic flow behavior and increased head loss, depositing sediment dampened flow turbulence during steady inflow of sediment-laden water.

9. For consecutive runs sediment using the same batch of media, the rate at which the flow backs-up decreased. Because the flow through the permeameter was lower due to partial clogging, the inflow rate had to be reduced to maintain continuity in the system. However, in reality, the opposite may be true (the rate that flow backs-up increases), since the inflow rate will depend on the intensity and duration of a rainfall event. Therefore water ponding around the intake will increase the amount of sediment that settles-out at the surface, thereby increasing the general trapping efficiency of the intake. The trend of decreased flow back-up occurs because of a re-distribution of sediment through the permeameter owing to more efficient flow paths developing each subsequent run; and deposited sediment moving down and dispersing in the permeameter.
10. The piezometer pressures increased with each consecutive run with sediment-laden flow, while the pressure difference between neighboring piezometers decreased with each consecutive run. These pressure trends reflect patterns of sediment accumulation within the permeameter. Further, non-linearity in piezometer pressures were noted as the infilling of sediment developed non-uniformly through the permeameter.
11. The highest trapping efficiency was with 75% pea gravel and 25% woodchips as expected than 100% pea gravel. For 75% pea gravel and 25% woodchips, the largest accumulations of sediment occurred in the woodchips, with the second greatest amount at or near the top of the gravel bed. For the 2 runs with 100% pea gravel in the permeameter, 68.8% (462 grams) of the accumulated sediment was within the top 60 cm of the column and 31.2% (209 grams) in the bottom 60 cm of the column. For the 8 runs with 75% pea gravel and 25% woodchips, the top of the permeameter had 46.6% of the accumulated sediment in the top 60 cm and 53.4% in the bottom 60 cm. If the deposited sediment in the head box (above the permeameter) is included, there was 57.4% (4290 grams) at the surface, 19.8%

(1480 grams) in the top 60 cm and 22.7% (1699 grams) in the bottom 60 cm. Over time, sediment plugs will migrate deeper into the column. For a single medium (100% pea gravel), results shown in the form of relative conductivity, K/K_0, revealed an exponential profile with decreasing K looking up-section. This is, in part, supported by the results of the mass of accumulated sediment in the permeameter (**Figure 4.17 (a)**).

12. The ATI must be designed with an effective hydraulic retention time to optimize denitrification in the woodchips layer. However, it must also have the performance a tile intake should have. Clogging of the woodchip layer will increase the retention time due to its reduced hydraulic conductivity. Compaction or decomposition of the woodchip layer will be a potential issue over time. Under constant pressure the flow through decreases during compression.

5.3 Recommendations for Future Research

This study also led to a recommended set of aspects for future research:

1. Select a well sorted (poorly graded) medium for longer lifespan.
2. Grass filter strips may help increase the lifetime of an ATI, acting as a frontline defense for filtering out sediment by decreasing the velocity of runoff flow.
3. From the constant head tests, it was found that the addition of woodchips slightly lowered K (less than 1 cm/s). Moreover, newly installed woodchip media will decrease in K over time due to compaction and possible swelling of the wood grains, which shrink the pore spaces. Conversely, gravel medium should be washed of fine sediment that has inevitably accumulated from the rock-fill source, otherwise the initial $K = K_0$ will not be at its maximum potential starting value.

4. Loading rates of suspended solids determined from field work and/or a hillslope scale model such as WEPP may be used to predict associated amounts of nutrients such as phosphates and nitrates from the hillslope.
5. When the ATI is completely plugged, suggested options for maintenance are: (1) clear-off dried sediment as the surface of the ATI; (2) dig out top layer and replace with fresh gravel; (3) put woodchip layer at shallower depth. This is because it (may) trap most of the sediment and adversely affect the desired hydraulic residence time;
6. An effective and economical method of reducing runoff and sediment losses is by retaining crop residue from the previous year's crop (e.g. Ranaivoson, 2005). An important extension of this study would be to develop a rigorous comparison of the sediment loads produced by land management practices that remove and retain crop residue and how this affects the lifespan of an ATI. Based on a historical climatic context it has been estimated that untilled gravel filters will last at least ten years because tilling through gravel filters greatly increases the rate of sediment deposition (Ranaivoson, 2005).

REFERENCES

Abaci, O., & Papanicolaou, A.N., 2009. Long-term effects of management practices on water-driven soil erosion in an intense agricultural sub-watershed: monitoring and modelling. Hydrological processes, 23(19), 2818-2837.

Beschta, R.L., and Jackson W.L., 1979. The intrusion of fine sediments into a stable gravel bed. *J. Fish Res. Bd Can*., 36, pp: 285-294.

Bird R.B., Stewart, W.E., Lightfoot E.N., 1960. Transport Phenomena. Chapter 6: Interphase Transport in Isothermal Systems. John Wiley & Sons, Inc. pp: 180-196.

Christianson, L., Castelló, A., Christianson, R., Helmers, M., and Bhandari, A., 2010. Hydraulic property determination of denitrifying bioreactor fill media. Applied Engineering in Agriculture. 26(5): 849-854.

Chun J.A., Cooke, R.A., Eheart, J.W., and M.S. Kang, 2009. Estimation of flow and transport parameters for woodchip-based bioreactors: I. Laboratory-scale bioreactor. *Biosystems Eng.* 104(3): 384-395

Dermisis, D., Abaci, O., Papanicolaou, A.N., and Wilson, C.G., 2010. Evaluating grassed waterway efficiency in southeastern Iowa using WEPP. Soil Use and Management.

Einstein, H.A., 1968. Deposition of suspended particles in a gravel bed. Journal of the Hydraulics Division. 5:1197-1205.

Ergun, S., 1952. Fluid flow through packed columns. Vol. 48, No. 2. Pp: 89-94.

Haan, C.T., Barfield, B.J., and Hayes, J.C., 1994. Design Hydrology and Sedimentology for Small Catchments. Academic Press Inc., New York, NY.

Hillel, D., 1998. Environmental Soil Physics. San Diego, California: Academic Press.

Joy, D.M., Lennox, W.C., & Kouwen, N., 1991. Particulate transport in a porous media under non-linear flow conditions. Journal of Hydraulic Research, 29(3), 373-385.

Karlen, D.L., Tomer, M.D., Neppel, J., & Cambardella, C.A. 2008. A preliminary watershed scale soil quality assessment in north central Iowa, USA. Soil and Tillage Research, 99(2), 291-299.

Loperfido, J.V., Just, C.L., Papanicolaou, A.N., & Schnoor, J.L., 2010. In situ sensing to understand diel turbidity cycles, suspended solids, and nutrient transport in Clear Creek, Iowa. Water Resources Research, 46(6).

Mays, D.C., Hunt, J.R., 2003. Fluid velocity, particle penetration and permeability reduction in clogging porous media.

McDowell-Boyer, L.M., Hunt, J.R., & Sitar, N., 1986. Particle transport through porous media. Water Resources Research, 22(13), 1901-1921.

Minnesota Pollution Control Agency, 2012. 2012 impaired waters list. Minnesota Pollution Control Agency: Division of Water Quality.

Nicks, A.D., Lane L.J., Gander, G.A., 1995. Chapter 2 – Weather generator. In USDA-Water Erosion Prediction Project: Hillslope Profile and Watersned Model Documentation, NSERL Report No. 10, Flanagan, D.C., Nearing, M.A. (eds). USDA-ARS National Soil Erosion Research Laboratory: West Lafayette.

Papanicolaou, A. N., & Abaci, O., 2008. Upland erosion modeling in a semihumid environment via the water erosion prediction project model. Journal of irrigation and drainage engineering, 134(6), 796-806.

Ranaivoson A.Z.H., 2004. Effect of fall tillage following soybeans and the presence of gravel filters on runoff losses of solids, organic matter, and phosphorus on a field scale. PhD Thesis, The University of Minnesota.

Ranaivoson, A.Z., Moncrief, J.F., Dittrich, M.A., 2005. Field evaluation of gravel filters for depressional areas in farm fields. Proceedings of the 2nd Agricultural Drainage Field Day. University of Minnesota Southwest Research and Outreach Center. Contributed paper.

Robertson W.D., N. Yeung, P.W. VanDriel, and P.S. Lombardo, 2005. High-permeability layers for remediation of ground water; go wide, not deep. Ground Water 43(4): 574-581.

Sakthivadivel, R., and Einstein, H.A., 1970. Clogging of porous column of spheres by sediment. *Journal of Hydraulic Division*, ASCE, 96 (2), pp: 461 – 472.

Schälchli, U., 1995. Basic equations for siltation of beds. Journal of Hydraulic Engineering. 121(3):274-287.

Sutarto, T., Papanicolaou, A.N., Wilson, C.G., & Langendoen, E.J., 2014. Stability Analysis of Semicohesive Streambanks with CONCEPTS: Coupling Field and Laboratory Investigations to Quantify the Onset of Fluvial Erosion and Mass Failure. Journal of Hydraulic Engineering.

Van Driel, P.W., W.D. Robertson, and L.C. Merkley, 2006. Denitrification of agricultural drainage using wood-based reactors. Trans. ASABE 49(2): 565-573.

Wilson, B.N., Nguyen, H.V., Singh, U.B., Morgan, S., Van Buren, P., Mickelson, D., Jahnke, E., and Hansen, B., 1999. Evaluations of Alternative Designs for Surface Tile Inlets Using Prototype Studies. *Final Report: Minnesota Department of Agriculture*. Biosystems and Agricultural Engineering Department and St. Anthony Falls Laboratory, University of Minnesota.

Wilson, C.G., Papanicolaou, A.T., & Denn, K.D., 2012. Partitioning fine sediment loads in a headwater system with intensive agriculture. Journal of Soils and Sediments, 12(6), 966-981.

Wu, F.C., & Huang, H.T., 2000. Hydraulic resistance induced by deposition of sediment in porous medium. Journal of Hydraulic Engineering, 126(7), 547-551.